Study on the Changes in Cellulose Crystal Structures Through Low-Concentration Alkali Treatments and Its Application for Controlling Mechanical Properties

Yuki Kugo

Hokkaido University

2024

CONTENTS

Chapter 1.

General Introduction

1.1. Over View of Cellulose

Currently, there is a strong demand to replace petroleum-based products with biodegradable and bio-based products. As a renewable resource, cellulose has the potential to provide solutions to many problems, including carbon dioxide emissions from the massive consumption of petroleum resources, environmental damage from petroleum-based non-biodegradable plastics, global warming and climate change from carbon dioxide and other greenhouse gases, and unsustainability in a linear economy [1]. Cellulose is a linear biopolymer composed of glucose residues via β1,4-glycosidic bonds, as shown in Fig 1-1. Cellulose is synthesized by most plants as a component of cell walls and is the most abundant biopolymer on Earth [2]. The above-mentioned growing awareness of the significant negative impact on the global environment based on the massive consumption of petroleum has led to a sharp increase in interest in cellulose, which is renewable and has a low environmental impact. Cellulose has long been used as paper and clothing by taking advantage of its intact structure and physical properties, and is also widely used in the form of regenerated cellulose and cellulose derivatives for clothing, films, dialysis membranes, and other applications. Furthermore, cellulose nanofibers (CNFs) [3], [4] and cellulose nanocrystals (CNCs) [5] have been developed in recent years, and new applications of cellulose are being promoted, such as composite materials with polymers [6], [7] and natural rubber [8], and catalytic nanocomposite materials [9], [10].

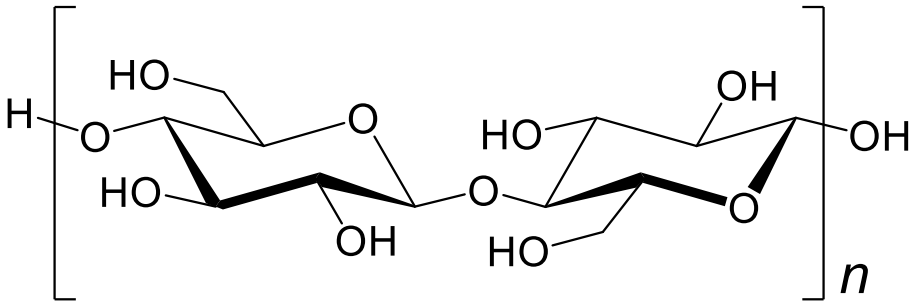

Fig. 1-1. The structural formula of cellulose

1.2. Crystal Forms of Cellulose and Crystal Transition from Cellulose I to II

The mechanical and chemical properties of cellulose materials are affected by their crystal form. Gaining a detailed understanding of the cellulose crystal contributes to the development of novel applications for cellulose. Typical crystal forms of cellulose include cellulose I, II, III, and IV. Native cellulose, found in plants, algae, and bacteria, is cellulose I crystal. Native cellulose from nature is a mixture of two crystalline forms, I_α and I_β, in varying proportions [11]. The cellulose found in algae and bacteria is rich in I_α, while cellulose found in plants and tunicates is rich in I_β. Cellulose I_α irreversibly transitions to I_β when treated at temperatures above 200 °C [12]. Recrystallization from dissolved cellulose I or alkali treatment with concentrated sodium hydroxide (NaOH) solution, called mercerization [13], causes a crystal transition from cellulose I to II. The crystalline system of cellulose is mainly classified into the cellulose I family (cellulose I, III_I, and IV_I) and cellulose II family (cellulose II, III_{II}, and IV_{II}), as shown in Fig 1-2. Cellulose III_I and III_{II} are obtained by treating cellulose I or cellulose II with liquid ammonia [14], [15], or ethylenediamine [16], respectively. Cellulose IV_I and IV_{II} are obtained by thermal treatment at 260 °C on cellulose III_I and III_{II} and cannot

be prepared directly from cellulose I [17]. Cellulose III_I reverts to cellulose I or II [18], while cellulose IV_I reverts exclusively to cellulose I and cellulose III_{II} and IV_{II} revert exclusively to cellulose II [19]. Furthermore, the cellulose II family, once formed from the cellulose I family, no longer reverts to the cellulose I family [20], and artificial production of cellulose I from cellulose II has not yet been successful. These suggest that there are specific structural differences between cellulose I and II. In other words, detailed studies on cellulose I and II will greatly contribute to the development of insights into the crystal structure of cellulose.

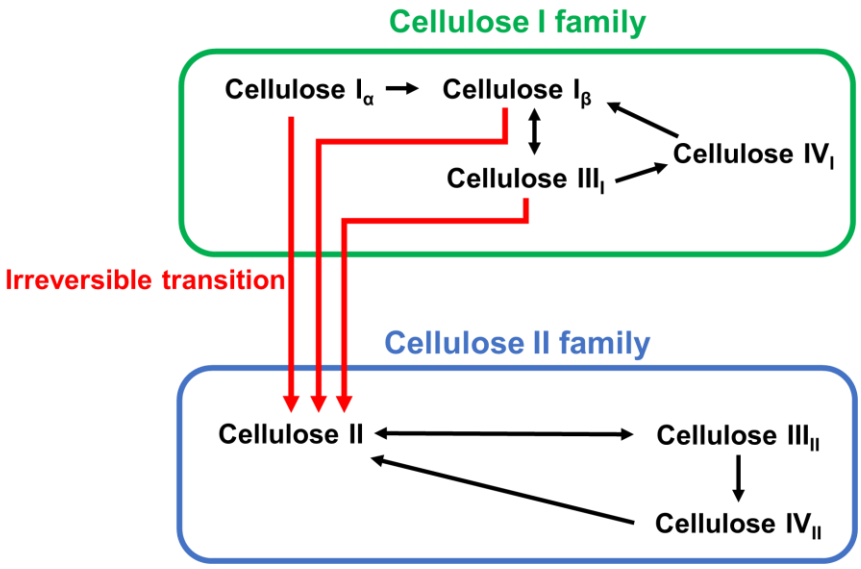

Fig. 1-2. The crystalline system of cellulose I family and cellulose II family [21]

The mercerization process was established in the 19th century by John Mercer [22]. In this treatment, cellulose I undergoes several intermediates called Na-cellulose (alkali cellulose) to become cellulose II [23], [24]. When cellulose I is soaked in a 12-20 % NaOH solution, it transitions to Na-cellulose I [23], [25], [26]. Furthermore, a concentrated alkaline solution of more than 32 % transforms

to Na-cellulose II [24], [27]. Na-cellulose III is obtained by vacuum drying Na-cellulose I [23]. In addition, Na-cellulose I transformed into Na-cellulose IV in low-temperature washing, whereas Na-cellulose I is reconverted to cellulose I in high-temperature washing [28]. Na-cellulose IV, a hydrated form of cellulose II without sodium content, is also obtained by washing Na-cellulose II or III with water [29]; drying Na-cellulose IV yields cellulose II [30], and the crystal transition from cellulose I to II is completed during the mercerization process as described above. Although lithium chloride/*N*, *N*-dimethylacetamide (DMAc/LiCl) [31], *N*-methylmorpholine-*N*-oxide monohydrate (NMMO) [32], and ionic liquids [33]–[35] are known as regeneration solvents for cellulose I, low-concentration aqueous NaOH solutions have attracted attention due to their advantages of low cost, low toxicity, and no pretreatment required. Alkaline treatments with 7-10 wt% NaOH solutions at room temperature [36]–[38] do not complete the crystal transition from cellulose I to II. Nevertheless, cellulose is dissolved when using these low-concentration NaOH solutions at low temperatures (–20 °C) [39], [40], and the crystal transition of cellulose I to II also proceeds in the insoluble portions [40]. Furthermore, the addition of urea [41], thiourea [42], [43], and zinc oxide (ZnO) [44] to the NaOH solution enhanced the solubility and promoted the crystal transition at higher temperatures than when treated with the alkaline solution alone; in the NaOH treatment; below 0 °C and at a NaOH concentration of about 8 wt%, the alkaline cellulose, a transition to Na-Cellulose Q occurs, Q of Quellung (“swelling” in German) [45], [46]. In other words, a detailed study of alkali cellulose is crucial in discussing the

crystal transition. However, the mechanism of the crystal transition from cellulose I to II, including the formation of alkali cellulose, remains unclear, and if it can be clarified, it may lead to the development of new applications of cellulose, such as the creation of innovative cellulose materials.

One of the differences between cellulose I and II is thought to lie in the packing mode of the cellulose molecular chain, as described in the X-ray diffraction structural analysis [47]–[49]. The ends of the cellulose molecular chain can be divided into non-reducing (O4-terminus) and reducing (O1-terminus) ends. These two types of ends give rise to molecular orientation. In cellulose I, cellulose molecular chains are thought to pack parallel, while in cellulose II, cellulose molecular chains are thought to pack antiparallel. As a mechanism for the change in packing mode from parallel to antiparallel, it has been proposed that NaOH infiltrates from the amorphous region, causing cellulose to swell, and within the swollen region, the cellulose chains move between crystalline regions arranged in opposite directions, causing cellulose chains to reorient antiparallel [27], [36]. Another proposed mechanism is that the cellulose molecular chain folds back on itself [50]. Recently, Sawada et al. suggested that cellulose molecular chains are likely to be packed antiparallel by folding, based on the results of neutron diffraction experiments [51]. However, there is no direct evidence that cellulose II is antiparallel, and the debate on the packing mode of cellulose II is still ongoing.

The conformation of the hydroxymethyl group at the C6 position is one of the guidelines for observing the crystal form and the mode of the intrachain hydrogen bonds. Nuclear magnetic

resonance (NMR) measurements [52] can distinguish that the conformation of the hydroxymethyl group for *tg* (trans-gauche), *gt* (gauche-trans), and *gg* (gauche-gauche), respectively, as shown in Fig 1-3. The torsion angles (O5-C5-C6-O6) and (C4-C5-C6-O6) of the side chain are trans and gauche for *tg*, gauche and trans for *gt*, and gauche and gauche for *gg* conformation. These differences are due to the different networks of inter- and intra-chain hydrogen bonds in the molecular chains of cellulose I and II. The crystals of cellulose I and II have hydrophilic and hydrophobic planes [53]. In the solid state, the O6 hydroxyl groups on the equatorial plane of glucose residues form intra- and intermolecular chain hydrogen bonds with adjacent residues and cellulose chains, forming hydrophilic planar sheets. Similarly, hydrogen atoms in the axial planes of glucose residues form hydrophobic planes between molecular chain sheets. In cellulose I, the intramolecular chain hydrogen bonds consist of O3-O5 and O6-O2. Furthermore, the O6-O2 hydrogen bond has two network patterns: one in which a proton on O2 is donated to O6 to make an intrachain hydrogen bond, and the other in which O6 donates a proton to O2 to make an intrachain hydrogen bond [54]. In cellulose II crystals, on the other hand, the intrachain hydrogen bond in the molecular chain consists of O6-O3 and O5-O3 [47]. Furthermore, the conformation at the C6 position in surface regions and dissolved cellulose is gg conformation [55]–[57]. The difference in the C6 position between cellulose I and II suggests that the cleavage of intra-molecular chain hydrogen bonds and the formation of new hydrogen bonds occur during the crystal transition. In our laboratory, Nomura et al. reported calculations showing that in

both of the two network patterns of cellulose I, the *tg* structure changes to the *gt* structure rather than returning to its original structure after changing to the *gg* structure [58], which may contribute to the crystal transition from cellulose I to cellulose II This may contribute to the irreversible crystal transition from cellulose I to cellulose II. Therefore, it is important to focus on the structural change at the C6 position in the crystal transition from cellulose I to II to elucidate this crystal transition mechanism.

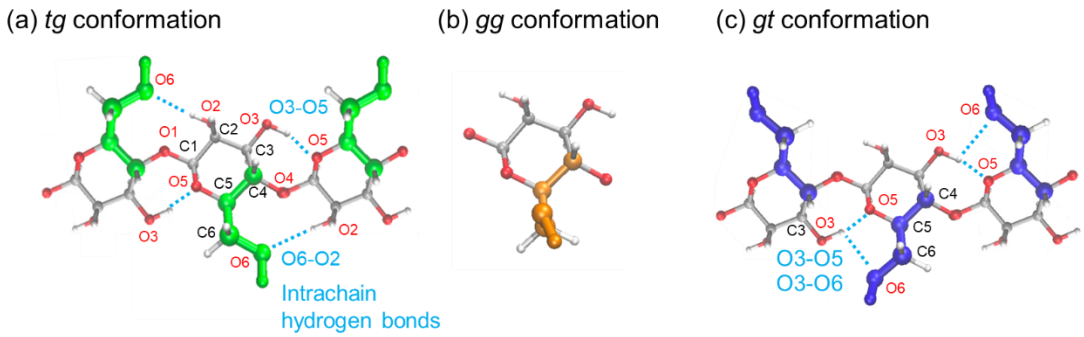

Fig. 1-3. The confirmation of the C6 hydroxymethyl group and intrachain hydrogen bonds: (a) *tg* (trans-gauche), (b) *gg* (gauche-gauche), and (c) *gt* (gauche-trans).

1.3. Preparation of Cellulose II Materials with High Crystallinity

The mercerization process can improve the mechanical and chemical properties of cellulose fibers, such as dimensional stability, dyeability, reactivity, gloss, and fabric smoothness [59]. It has been reported that disordered regions coexist in cellulose microfibrils in addition to crystalline regions [60]. Cellulose I exhibits high crystallinity and consequently excellent mechanical properties, while cellulose II is less crystalline and thereby has lower mechanical properties [61]. In fact, typical Young's modulus of cellulose I and II have been reported to be 138 GPa and 88 GPa, respectively [62]. As

mentioned above, cellulose II has excellent properties, and the preparation of cellulose II materials with excellent mechanical properties would lead to an expansion of its industrial applications. Many efforts have been made to prepare high-strength cellulose II materials, including saponification of cellulose acetate and more ordered cellulose regeneration processes using more polar coagulation media (acetone < EtOH < MeOH < aqueous solutions of Na_2SO_4 and H_2SO_4) [63], [64] and ionic liquids [65]. In addition to that, it has been reported that the crystallinity of cellulose II can be enhanced by post-treatment with low concentrations of aqueous alkaline solutions [66]–[71].

In a previous report from our laboratory [72], we showed that post-treatment of cellulose II powder with 10 wt% NaOH solution promoted the highest crystallinity enhancement among the post-treatments with 0–25 wt% NaOH solution, and proposed a mechanism for the enhancement of crystallinity. The secondary structure of cellulose consists of structures with diameters of approximately 3.5 nm called microfibril [73], which contain crystals. Microfibrils are directly observed by scanning electron microscope, transmission electron microscope, and atomic force microscopy [74]–[77]. Microfibrils self-organize and twist to form ribbons. Fig 1-4 shows a schematic cross-sectional view of a cellulose ribbon. Surfaces are classified into accessible surfaces, which are accessible to water and other solvents, and inaccessible surfaces, which are inaccessible to solvents [78], [79]. The outermost surface of the cellulose ribbon is always accessible to the surrounding solvent and is called an accessible surface. On the other hand, the microfibril crystal surfaces inside

the ribbon formed by the accumulation of microfibrils are no longer accessible from the surrounding solvent and are called inaccessible surfaces. These surface regions can be distinguished by solid-state ^{13}C NMR [78], [79], and confirmed by dynamic nuclear polarized solid-state NMR spectroscopy [80]. In our previous report [72], the percentage of accessible surfaces remained almost the same, but as the crystallinity increased, the percentage of inaccessible surfaces decreased and the crystal size increased after post-processing. Furthermore, solid-state ^{13}C CP/MAS NMR spectra showed that the cellulose II sample soaked in a low-concentration NaOH solution is a mixture of cellulose II crystal and Na-Cellulose. These results support the crystallinity enhancement mechanism, as shown in Fig 1-5, in which the rearrangement of cellulose molecules on the inaccessible surface converts these regions into a crystalline region and enhances the crystal size. The important aspects of this mechanism are that the NaOH does not penetrate the crystalline region, but only the inaccessible surface/amorphous region, and that the rearrangement of the cellulose molecules occurs only at this inaccessible surface. This post-treatment with a 10 wt% NaOH solution is expected to be effective in the preparation of highly crystalline cellulose II materials.

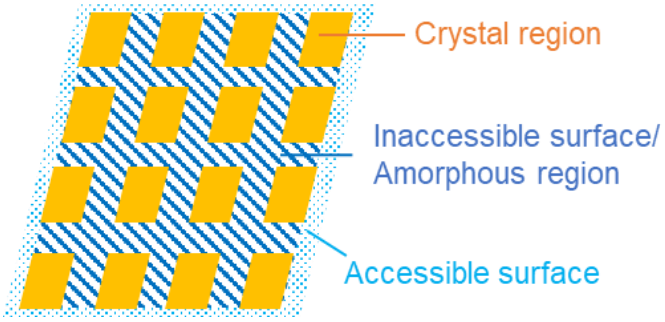

Fig. 1-4. Schematic image of cellulose ribbon consisting of crystal region (microfibril), accessible surface, and inaccessible surface/amorphous region [66].

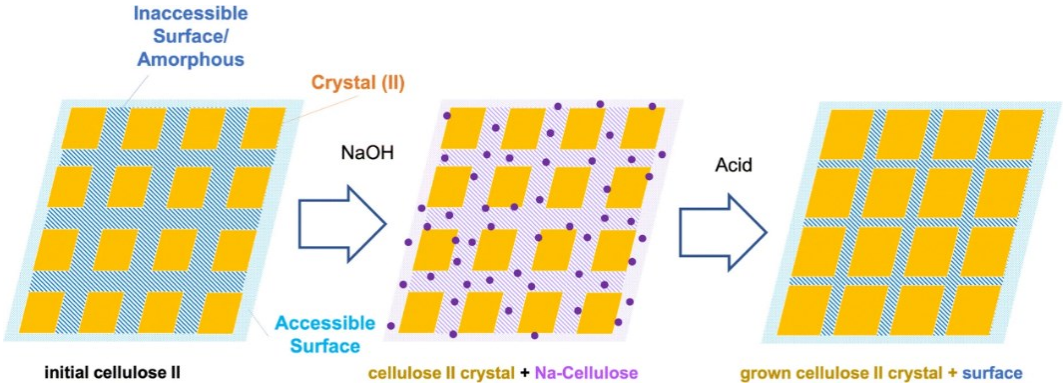

Fig. 1-5. Schematic images of the crystallinity improvement mechanism in the post-treatment on cellulose II powder using a 10 wt% NaOH solution [72].

1.4. All-cellulose composites

All-cellulose composites composed solely of cellulose have been investigated over the past two decades as another way to produce mechanically strong cellulose materials. Fiber-reinforced polymer composites have many applications, but their nature as two components (reinforcement and outer matrix) makes their reuse and recycling quite difficult [81]. In recent years, the demand for environmentally friendly bio-composites [82], [83] has led to renewed interest in all-cellulose composites, which are composed entirely of cellulose. Since the first report on all-cellulose composites by Nishino et al [84], many studies on these composites have been conducted. Many review articles

[85]–[87] explain that two approaches, impregnation and surface dissolution, have been mainly utilized to fabricate these composites, as shown in Fig 1-6.

The impregnation method requires two steps: first, a cellulose solution is prepared, and then the composite material is prepared by impregnating this cellulose solution with the cellulose material that will be used as reinforcement. On the other hand, in the surface dissolution method, composite materials are prepared in a single step. In this method, the cellulose material is soaked in a solvent to partially dissolve the outer layer, allowing the undissolved core to serve as the reinforcement. In this method, the cellulose in the material serves as the raw material for both the outer matrix and the reinforcing fibers. In the impregnation method, the morphological properties of the reinforcement and the cellulose concentration are the main determinants of the mechanical properties of the all-cellulose composite [88], [89]. In the surface dissolution method, dissolution time, cellulose orientation, and cellulose crystal form are the main determinants of mechanical properties [90]–[94]. Thus, the properties of the reinforcement correlate with the properties of the all-cellulose composite, and in the case of cellulose I and II composites, cellulose I is expected to have a significant influence on the mechanical properties of the composite [95]. Therefore, in the formation of cellulose I and II composites with excellent mechanical properties, it is important to control the distribution and proportion of cellulose I, which has high mechanical strength, and cellulose II, which acts as the matrix.

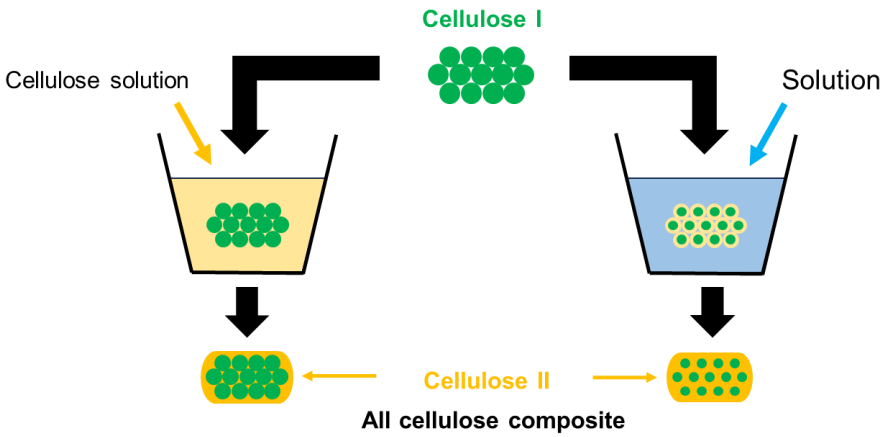

Fig. 1-6. Scheme of the preparation of all-cellulose composite in impregnation approach and surface dissolution approach.

1.5. Objective and Outline of This Thesis

The objective of this study is to create new cellulose-based materials that combine the properties of cellulose II with controllable and excellent mechanical properties, such as cellulose II materials with high crystallinity and all-cellulose composites composed of both cellulose I and II. The creation of cellulose materials with such excellent properties will lead to further development of cellulose applications. In order to create such promising cellulose materials, it is essential to have a deep understanding of cellulose I and II crystals. In this study, I investigated the mechanism of crystal transition from cellulose I to II in low-temperature and low-concentration alkali treatment and the enhancement of crystallinity of cellulose II in low-concentration alkali treatment, and based on these findings, I created a new cellulose-based material with both excellent mechanical properties.

To elucidate the mechanism of this crystal transition, I focused on low-concentration NaOH treatment at low temperatures. The crystal transition from cellulose I to II does not proceed in room

temperature treatment with low-concentration NaOH solution. Furthermore, it was observed that NaOH did not penetrate the cellulose crystal region in the low-concentration NaOH post-treatment of cellulose II. These results suggest that regardless of cellulose I and II, NaOH does not penetrate the crystalline region in the room temperature treatment with a low concentration of NaOH solution. On the contrary, crystal transition progresses at low temperatures, suggesting that NaOH may affect the crystalline region in low-concentration NaOH treatment at low temperatures. The clarification of the dynamics of NaOH at various temperatures and the accompanying structural changes of cellulose crystals, as shown in Fig 1-7, will contribute to the elucidation of the mechanism of crystal transition of cellulose.

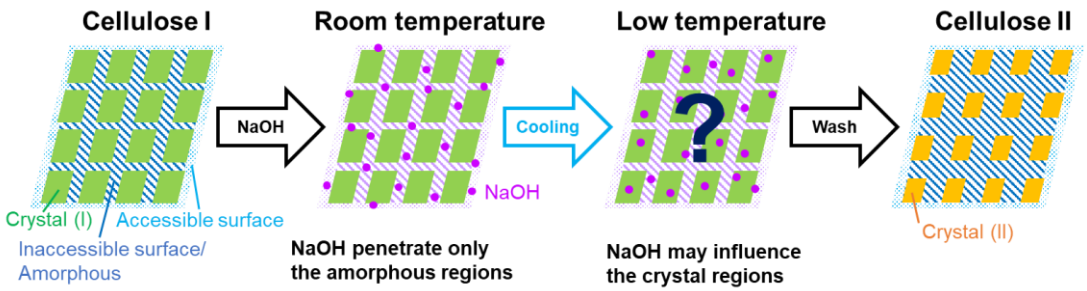

Fig. 1-7. The anticipated crystal transition and penetration of NaOH due to temperature changes in the cellulose soaked in a low-concentration NaOH solution

This doctoral dissertation consists of the following five chapters. In Chapter 1, an overview of cellulose as a material and its crystal morphology was introduced, and in particular, the differences between cellulose I and II, which provide clues for clarifying the crystal transition mechanism, were explained. In addition, the fabrication method of high-strength cellulose materials with the properties

of cellulose II was also introduced.

In Chapter 2, the mechanism of crystal transition from cellulose I to II in low-temperature, low-concentration NaOH treatment is discussed. The structural changes of cellulose molecules were traced by temperature-dependent NMR and WAXS measurements of cellulose immersed in low-concentration NaOH solutions. In addition, ^{23}Na NMR relaxation time NMR measurements with various concentrations of NaOH solutions were used to trace the Na ion dynamics of various concentrations of NaOH solutions. Based on the obtained results, the crystal transition mechanism was discussed.

In Chapter 3, the enhancement of crystallinity of cellulose II and the control of mechanical properties of cellulose II fibers by post-treatment with low concentrations of NaOH solutions were discussed. The crystallinity of samples obtained by long-term single and multiple post-treatment was analyzed. The mechanism of crystallinity improvement was discussed based on the changes in the ratio of crystalline, surface, and amorphous regions. Based on this mechanism, the duration of the post-treatment cycle was optimized. Furthermore, cellulose II fibers with high crystallinity were prepared and their mechanical properties were analyzed.

In Chapter 4, I attempted to fabricate new cellulose materials with high mechanical properties. The crystal transition during quenching with liquid nitrogen was traced by solid-state ^{13}C NMR measurements. Based on the obtained results, I created a new cellulose material whose

mechanical properties can be controlled by crystal transition.

Chapter 5 summarized the results of this study.

REFERENCES

[1] O. Nechyporchuk, M. N. Belgacem, and J. Bras, "Production of cellulose nanofibrils: A review of recent advances," *Ind Crops Prod*, vol. 93, pp. 2–25, 2016, doi: 10.1016/j.indcrop.2016.02.016.

[2] D. Klemm, B. Heublein, H. P. Fink, and A. Bohn, "Cellulose: Fascinating biopolymer and sustainable raw material," *Angewandte Chemie – International Edition*, vol. 44, no. 22, pp. 3358–3393, 2005, doi: 10.1002/anie.200460587.

[3] R. Kose, I. Mitani, W. Kasai, and T. Kondo, "'Nanocellulose' as a single nanofiber prepared from pellicle secreted by *Gluconacetobacter xylinus* using aqueous counter collision," *Biomacromolecules*, vol. 12, no. 3, pp. 716–720, 2011, doi: 10.1021/bm1013469.

[4] A. Isogai, T. Saito, and H. Fukuzumi, "TEMPO-oxidized cellulose nanofibers," *Nanoscale*, vol. 3, no. 1, pp. 71–85, 2011, doi: 10.1039/c0nr00583e.

[5] Y. Habibi, L. A. Lucia, and O. J. Rojas, "Cellulose nanocrystals: Chemistry, self-assembly, and applications," *Chem Rev*, vol. 110, no. 6, pp. 3479–3500, 2010, doi: 10.1021/cr900339w.

[6] A. Iwatake, M. Nogi, and H. Yano, "Cellulose nanofiber-reinforced polylactic acid," *Compos Sci Technol*, vol. 68, no. 9, pp. 2103–2106, 2008, doi: 10.1016/j.compscitech.2008.03.006.

[7] J. Dlouhá, L. Suryanegara, and H. Yano, "Cellulose nanofibre-poly(lactic acid) microcellular foams exhibiting high tensile toughness," *React Funct Polym*, vol. 85, pp. 201–207, 2014, doi: 10.1016/j.reactfunctpolym.2014.07.016.

[8] P. M. Visakh, S. Thomas, K. Oksman, and A. P. Mathew, "Crosslinked natural rubber nanocomposites reinforced with cellulose whiskers isolated from bamboo waste: Processing and mechanical/thermal properties," *Compos Part A Appl Sci Manuf*, vol. 43, no. 4, pp. 735–741, 2012, doi: 10.1016/j.compositesa.2011.12.015.

[9] H. Wei, K. Rodriguez, S. Renneckar, and P. J. Vikesland, "Environmental science and engineering applications of nanocellulose-based nanocomposites," *Environ Sci Nano*, vol. 1, no. 4, pp. 302–316, 2014, doi: 10.1039/c4en00059e.

[10] W. Wang *et al.*, "Synthesis of mesoporous TiO2 induced by nano-cellulose and its photocatalytic properties," *Bioresources*, vol. 11, no. 2, pp. 3084–3093, 2016, doi: 10.15376/biores.11.2.3084-3093.

[11] M. Jarvis, "Cellulose stacks up," *Nature*, vol. 426, no. 6967, pp. 611–612, Dec. 2003, doi: 10.1038/426611a.

[12] H. Yamamoto, F. Horii, and H. Odani, "Structural changes of native cellulose crystals induced by annealing in aqueous alkaline and acidic solutions at high temperatures," *Macromolecules*, vol.

22, no. 10, pp. 4130–4132, 1989, doi: 10.1021/ma00200a058.

[13] A. C. O'sullvian, "Cellulose: the structure slowly unravels," *Cellulose*, vol. 4, no. 3, pp. 173–207, 1997, doi: 10.1023/A:1018431705579.

[14] M. Wada, L. Heux, A. Isogai, Y. Nishiyama, H. Chanzy, and J. Sugiyama, "Improved structural data of cellulose IIII prepared in supercritical ammonia," *Macromolecules*, vol. 34, no. 5, pp. 1237–1243, 2001, doi: 10.1021/ma001406z.

[15] M. Wada, L. Heux, Y. Nishiyama, and P. Langan, "X-ray crystallographic, scanning microprobe X-ray diffraction, and cross-polarized/magic anglespinning 13C NMR studies of the structure of cellulose III II," *Biomacromolecules*, vol. 10, no. 2, pp. 302–309, 2009, doi: 10.1021/bm8010227.

[16] Y. Numata, H. Kono, S. Kawano, T. Erata, and M. Takai, "Cross-polarization/magic-angle spinning 13C nuclear magnetic resonance study of cellulose I–ethylenediamine complex," *J Biosci Bioeng*, vol. 96, no. 5, pp. 461–466, Dec. 2003, doi: 10.1016/S1389-1723(03)70132-7.

[17] M. Wada, L. Heux, and J. Sugiyama, "Polymorphism of cellulose I family: Reinvestigation of cellulose Ivl," *Biomacromolecules*, vol. 5, no. 4, pp. 1385–1391, 2004, doi: 10.1021/bm0345357.

[18] M. Wada, "In situ observation of the crystalline transformation from cellulose IIII to Iβ," *Macromolecules*, vol. 34, no. 10, pp. 3271–3275, 2001, doi: 10.1021/ma0013354.

[19] S. W. J.Hayashi, A.Sufoka, J. Ohkita, "The Conformation of Existences of Cellulose IIII, IIIII, IVI, and IVII by The X-Ray Method," *Journal of Polymer Science: Polmer Letters Edition*, vol. 13, pp. 23–27, 1975, doi: https://doi.org/10.1002/pol.1975.130130104.

[20] A. Isogai and M. Usuda, "Solid-State CP/MAS 13C NMR Study of Cellulose Polymorphs," *Macromolecules*, vol. 22, no. 7, pp. 3168–3172, 1989, doi: 10.1021/m100197a045.

[21] A. Sarkar and S.Pérez, Discover Polysaccharides Cellulose, A Database of Polysachharide 3D structures, Cermav, https://polysac3db.cermav.cnrs.fr/discover_cellulose.html, (Accessed December 9, 2023)

[22] I. Holme and R. S. Blackburn, "John Mercer FRS, FCS, MPhS, JP: the Father of Textile Chemistry," *Coloration Technology*, vol. 135, no. 3, pp. 171–182, 2019, doi: 10.1111/cote.12398.

[23] T. Okano and A. Sarko, "Mercerization of cellulose. I. X-ray diffraction evidence for intermediate structures," *J Appl Polym Sci*, vol. 29, no. 12, pp. 4175–4182, 1984, doi: 10.1002/app.1984.070291247.

[24] F. Porro, O. Bedue, H. Chanzy, and L. Heux, "Solid-state 13 C NMR study of Na -cellulose complexes," *Biomacromolecules*, vol. 8, no. 8, pp. 2586–2593, 2007, doi: 10. 1021/bm0702657.

[25] H. Yokota, T. Sei, F. Horii, and R. Kitamaru, “13C CP/MAS NMR study on alkali cellulose,” *J Appl Polym Sci*, vol. 41, no. 3–4, pp. 783–791, 1990, doi: 10.1002/app.1990.070410325.

[26] J. Schoeck, R. J. Davies, A. Martel, and C. Riekel, “Na-cellulose formation in a single cotton fiber studied by synchrotron radiation microdiffraction,” *Biomacromolecules*, vol. 8, no. 2, pp. 602–610, 2007, doi: 10.1021/bm060844w.

[27] T. Okano and A. Sarko, “Mercerization of Cellulose. II. Intermediates and a Possible Mercerization Mechanism,” *J Appl Polym Sci*, vol. 30, no. 1, pp. 325–332, 1985, doi: 10.1002/app.1985.070300128.

[28] N. H. Kim, J. Sugiyama, and T. Okano, “X-ray and electron diffraction study of Na-cellulose I: The effect of washing temperature on the structure of Na-cellulose I,” *Mokuzai Gakkaishi*, vol. 37, no. 7, pp. 637–643, 1991.

[29] H. Nishimura, T. Okano, and A. Sarko, “Mercerization of Cellulose. 6. Crystal and Molecular Structure of Na-Cellulose IV,” *Macromolecules*, vol. 24, no. 3, pp. 771–778, 1991, doi: 10.1021/ma00003a021.

[30] K. Kobayashi, S. Kimura, E. Togawa, and M. Wada, “Crystal transition from Na-cellulose IV to cellulose II monitored using synchrotron X-ray diffraction,” *Carbohydr Polym*, vol. 83, no. 2, pp. 483–488, 2011, doi: 10.1016/j.carbpol.2010.08.006.

[31] T. Bikova and A. Treimanis, “Problems of the MMD analysis of cellulose by SEC using DMA/LiCl: A review,” *Carbohydr Polym*, vol. 48, no. 1, pp. 23–28, 2002, doi: 10.1016/S0144-8617(01)00207-7.

[32] H. P. Fink, P. Weigel, H. J. Purz, and J. Ganster, “Structure formation of regenerated cellulose materials from NMMO-solutions,” *Progress in Polymer Science*, vol. 26, no. 9. Pp. 1473–1524, 2001. Doi: 10.1016/S0079-6700(01)00025-9.

[33] R. P. Swatloski, S. K. Spear, J. D. Holbrey, and R. D. Rogers, “Dissolution of cellulose with ionic liquids,” *J Am Chem Soc*, vol. 124, no. 18, pp. 4974–4975, 2002, doi: 10.1021/ja025790m.

[34] D. A. Fort, R. C. Remsing, R. P. Swatloski, P. Moyna, G. Moyna, and R. D. Rogers, “Can ionic liquids dissolve wood? Processing and analysis of lignocellulosic materials with 1-n-butyl-3-methylimidazolium chloride,” *Green Chemistry*, vol. 9, no. 1, pp. 63–69, 2007, doi: 10.1039/b607614a.

[35] Y. Cao, J. Wu, J. Zhang, H. Li, Y. Zhang, and J. He, “Room temperature ionic liquids (RTILs): A new and versatile platform for cellulose processing and derivatization,” *Chemical Engineering*

Journal, vol. 147, no. 1, pp. 13–21, 2009, doi: 10.1016/j.cej.2008.11.011.

[36] H. Shibazaki, S. Kuga, and T. Okano, "Mercerization and acid hydrolysis of bacterial cellulose," *Cellulose*, vol. 4, no. 2, pp. 75–87, 1997, doi: 10.1023/A:1024273218783.

[37] E. Dinand, M. Vignon, H. Chanzy, and L. Heux, "Mercerization of primary wall cellulose and its implication for the conversion of cellulose I → cellulose II," *Cellulose*, vol. 9, no. 1, pp. 7–18, 2002, doi: 10.1023/A:1015877021688.

[38] H. Wang, H. Kataoka, S. Tsuchikawa, and T. Inagaki, "Terahertz time-domain spectroscopy as a novel tool for crystallographic analysis in cellulose: Cellulose I to cellulose II, tracing the structural changes under chemical treatment," *Cellulose*, vol. 29, no. 6, pp. 3143–3151, 2022, doi: 10.1007/s10570-022-04493-x.

[39] K. Kamide, K. Okajima, T. Matsui, and K. Kowsaka, "Study on the solubility of cellulose in aqueous alkali solution by deuteration IR and ^{13}C NMR," *Polym J*, vol. 16, no. 12, pp. 857–866, 1984, doi: 10.1295/polymj.16.857.

[40] A. Isogai and R. H. Atalla, "Dissolution of cellulose in aqueous NaOH solutions," *Cellulose*, vol. 5, no. 4, pp. 309–319, 1998, doi: 10.1023/A:1009272632367.

[41] J. Cai and L. Zhang, "Unique gelation behavior of cellulose in NaOH/urea aqueous solution," *Biomacromolecules*, vol. 7, no. 1, pp. 183–189, 2006, doi: 10.1021/bm0505585.

[42] D. Ruan *et al.*, "A rapid process for producing cellulose multi-filament fibers from a NaOH/thiourea solvent system," *Macromol Rapid Commun*, vol. 27, no. 17, pp. 1495–1500, 2006, doi: 10.1002/marc.200600232.

[43] Z. Jiang *et al.*, "Dissolution and metastable solution of cellulose in NaOH/thiourea at 8 °C for Construction of nanofibers," *Journal of Physical Chemistry B*, vol. 121, no. 8, pp. 1793–1801, 2017, doi: 10.1021/acs.jpcb.6b10829.

[44] W. Liu, T. Budtova, and P. Navard, "Influence of ZnO on the properties of dilute and semi-dilute cellulose-NaOH-water solutions," *Cellulose*, vol. 18, no. 4, pp. 911–920, 2011, doi: 10.1007/s10570-011-9552-9.

[45] Sobue, H., Kiessig. H., & Hess. K. (1939). Das System Cellulose–Natriumhydroxyd–Wasser in Abhängigkeit von der Temperatur. *Zeitschrift für Physikalische Chemie*, 43B(1), 309-328. https://doi.org/10.1515/zpch-1939-4324.

[46] T. Budtova and P. Navard, "Cellulose in NaOH–water based solvents: a review," *Cellulose*, vol. 23, no. 1, pp. 5–55, 2016, doi: 10.1007/s10570-015-0779-8.

[47] P. Langan, Y. Nishiyama, and H. Chanzy, "A revised structure and hydrogen-bonding system in cellulose II from a neutron fiber diffraction analysis," *J Am Chem Soc*, vol. 121, no. 43, pp. 9940–9946, 1999, doi: 10.1021/ja9916254.

[48] Y. Nishiyama, J. Sugiyama, H. Chanzy, and P. Langan, "Crystal Structure and Hydrogen Bonding System in Cellulose Iβ from Synchrotron X-ray and Neutron Fiber Diffraction," *J Am Chem Soc*, vol. 124, no. 31, pp. 9074–9082, 2002, doi: 10.1021/ja037055w.

[49] Y. Nishiyama, J. Sugiyama, H. Chanzy, and P. Langan, "Crystal Structure and Hydrogen-Bonding System in Cellulose I_α from Synchrotron X-ray and Neutron Fiber Diffraction," *J Am Chem Soc*, vol. 125, no. 47, pp. 14300–14306, 2003, doi: https://doi.org/10.1021/ja0257319.

[50] A. Buleon, H. Chanzy, and E. Roche, "Shish Kebab-Like Structures of Cellulose.," *J Polym Sci Part B Polym Lett*, vol. 15, no. 5, pp. 265–270, 1977, doi: 10.1002/pol.1977.130150502.

[51] D. Sawada *et al.*, "Untangling the threads of cellulose mercerization," *Nat Commun*, vol. 13, no. 1, pp. 1–6, 2022, doi: 10.1038/s41467-022-33812-w.

[52] F. Horii, A. Hirai, and R. Kitamaru, "Solid-state 13C-NMR study of conformations of oligosaccharides and cellulose: Conformation of CH2OH group about the exo-cyclic C-C bond," *Polymer Bulletin*, vol. 10, no. 7–8, pp. 357–361, 1983, doi: 10.1007/BF00281948.

[53] B. Medronho and B. Lindman, "Competing forces during cellulose dissolution: From solvents to mechanisms," *Curr Opin Colloid Interface Sci*, vol. 19, no. 1, pp. 32–40, 2014, doi: 10.1016/j.cocis.2013.12.001.

[54] Y. Nishiyama, G. P. Johnson, A. D. French, V. T. Forsyth, and P. Langan, "Neutron crystallography, molecular dynamics, and quantum mechanics studies of the nature of hydrogen bonding in cellulose Iβ," *Biomacromolecules*, vol. 9, no. 11, pp. 3133–3140, 2008, doi: 10.1021/bm800726v.

[55] R. H. Newman and T. C. Davidson, "Molecular conformations at the cellulose-water interface," *Cellulose*, vol. 11, no. 1, pp. 23–32, 2004, doi: 10.1023/B:CELL.0000014778.49291.c6.

[56] J. Cai and L. Zhang, "Rapid dissolution of cellulose in LiOH/urea and NaOH/urea aqueous solutions," *Macromol Biosci*, vol. 5, no. 6, pp. 539–548, 2005, doi: 10.1002/mabi.200400222.

[57] P. Phyo, T. Wang, Y. Yang, H. O'Neill, and M. Hong, "Direct determination of hydroxymethyl conformations of plant cell wall cellulose using 1 H polarization transfer solid-state NMR," *Biomacromolecules*, vol. 19, no. 5, pp. 1485–1497, 2018, doi: 10.1021/acs.biomac.8b00039.

[58] S. Nomura, S. Sato, and T. Erata, "DFT approach to the pathway of conformational changes of

cellulose C6-hydroxymethyl group with simple cellotetraose model involving the mechanism of mercerization process," *Chem Phys Lett*, vol. 742, no. October 2019, p. 137154, 2020, doi: 10.1016/j.cplett.2020.137154.

[59] P. Goswami, R. S. Blackburn, J. Taylor, and P. White, "Sorption of dyes on cellulose II: Effect of alkali treatment of fibreand dye structure," *Cellulose*, vol. 18, no. 4, pp. 1063–1072, 2011, doi: 10.1007/s10570-011-9540-0.

[60] P. Chen, C. Terenzi, I. Furó, L. A. Berglund, and J. Wohlert, "Quantifying Localized Macromolecular Dynamics within Hydrated Cellulose Fibril Aggregates," *Macromolecules*, vol. 52, no. 19, pp. 7278–7288, 2019, doi: 10.1021/acs.macromol.9b00472.

[61] C. Djahedi, L. A. Berglund, and J. Wohlert, "Molecular deformation mechanisms in cellulose allomorphs and the role of hydrogen bonds," *Carbohydr Polym*, vol. 130, pp. 175–182, 2015, doi: 10.1016/j.carbpol.2015.04.073.

[62] T. Nishino, K. Takano, and K. Nakamae, "Elastic modulus of the crystalline regions of cellulose polymorphs," *J Polym Sci B Polym Phys*, vol. 33, no. 11, pp. 1647–1651, 1995, doi: 10.1002/polb.1995.090331110.

[63] N. Isobe, U. J. Kim, S. Kimura, M. Wada, and S. Kuga, "Internal surface polarity of regenerated cellulose gel depends on the species used as coagulant," *J Colloid Interface Sci*, vol. 359, no. 1, pp. 194–201, 2011, doi: 10.1016/j.jcis.2011.03.038.

[64] Å. Östlund, A. Idström, C. Olsson, P. T. Larsson, and L. Nordstierna, "Modification of crystallinity and pore size distribution in coagulated cellulose films," *Cellulose*, vol. 20, no. 4, pp. 1657–1667, Aug. 2013, doi: 10.1007/s10570-013-9982-7.

[65] Z. Liu, X. Sun, M. Hao, C. Huang, Z. Xue, and T. Mu, "Preparation and characterization of regenerated cellulose from ionic liquid using different methods," *Carbohydr Polym*, vol. 117, pp. 99–105, 2015, doi: 10.1016/j.carbpol.2014.09.053.

[66] B. R. Manjunath and A. Venkataraman, "Fibrillar aggregation in cotton cellulose subjected to multiple swelling treatments with alkali," *Journal of Polymer Science: Polymer Chemistry Edition*, vol. 18, pp. 1407–1424, 1980, doi: 10.1002/pol.1980.170180424.

[67] P. Langan, Y. Nishiyama, and H. Chanzy, "X-ray structure of mercerized cellulose II at 1 Å resolution," *Biomacromolecules*, vol. 2, no. 2, pp. 410–416, 2001, doi: 10.1021/bm005612q.

[68] X. Colom and F. Carrillo, "Crystallinity changes in lyocell and viscose-type fibres by caustic treatment," *Eur Polym J*, vol. 38, no. 11, pp. 2225–2230, 2002, doi: 10.1016/S0014-

3057(02)00132-5.

[69] J. Široký, R. S. Blackburn, T. Bechtold, J. Taylor, and P. White, “Attenuated total reflectance Fourier-transform Infrared spectroscopy analysis of crystallinity changes in lyocell following continuous treatment with sodium hydroxide,” *Cellulose*, vol. 17, no. 1, pp. 103–115, Feb. 2010, doi: 10.1007/s10570-009-9378-x.

[70] M. Hirota, N. Tamura, T. Saito, and A. Isogai, “Cellulose II nanoelements prepared from fully mercerized, partially mercerized and regenerated celluloses by 4-acetamido-TEMPO/NaClO/NaClO2 oxidation,” *Cellulose*, vol. 19, no. 2, pp. 435–442, 2012, doi: 10.1007/s10570-011-9642-8.

[71] K. Daicho, S. Fujisawa, and T. Saito, “Linear correlation between True density and crystallinity of regenerated and mercerized celluloses,” *Biomacromolecules*, vol. 24, no. 2, pp. 661–666, 2023, doi: 10.1021/acs.biomac.2c01067.

[72] S. Nomura, Y. Kugo, and T. Erata, “13C NMR and XRD studies on the enhancement of cellulose II crystallinity with low concentration NaOH post-treatments,” *Cellulose*, vol. 27, no. 7, pp. 3553–3563, May 2020, doi: 10.1007/s10570-020-03036-6.

[73] G. Chinga-Carrasco, “Cellulose fibres, nanofibrils and microfibrils: The morphological sequence of MFC components from a plant physiology and fibre technology point of view,” *Nanoscale Res Lett*, vol. 6, pp. 1–7, 2011, doi: 10.1186/1556-276X-6-417.

[74] J. Sugiyama, H. Harada, Y. Fujiyoshi, and N. Uyeda, “Lattice images from ultrathin sections of cellulose microfibrils in the cell wall of Valonia macrophysa Kütz.,” *Planta*, vol. 166, no. 2, pp. 161–168, 1985, doi: 10.1007/BF00397343.

[75] J. Sugiyama, R. Vuong, and H. Chanzy, “Electron Diffraction Study on the Two Crystalline Phases Occurring in Native Cellulose from an Algal Cell Wall,” *Macromolecules*, vol. 24, no. 14, pp. 4168–4175, 1991, doi: 10.1021/ma00014a033.

[76] T. Imai, J. L. Putaux, and J. Sugiyama, “Geometric phase analysis of lattice images from algal cellulose microfibrils,” *Polymer (Guildf)*, vol. 44, no. 6, pp. 1871–1879, 2003, doi: 10.1016/S0032-3861(02)00861-3.

[77] S. J. Hanley, J. F. Revol, L. Godbout, and D. G. Gray, “Atomic force microscopy and transmission electron microscopy of cellulose from Micrasterias denticulata; evidence for a chiral helical microfibril twist,” *Cellulose*, vol. 4, no. 3, pp. 209–220, 1997, doi: 10.1023/A:1018483722417.

[78] P. T. Larsson, K. Wickholm, and T. Iversen, “A CP/MAS 13C NMR investigation of molecular

ordering in celluloses," *Carbohydr Res*, vol. 302, no. 1–2, pp. 19–25, 1997, doi: 10.1016/S0008-6215(97)00130-4.

[79] G. Zuckerstätter, N. Terinte, H. Sixta, and K. C. Schuster, "Novel insight into cellulose supramolecular structure through 13C CP-MAS NMR spectroscopy and paramagnetic relaxation enhancement," in *Carbohydrate Polymers*, 2013, pp. 122–128. Doi: 10.1016/j.carbpol.2012.05.019.

[80] A. Kirui *et al.*, "Atomic resolution of cotton cellulose structure enabled by dynamic nuclear polarization solid-state NMR," *Cellulose*, vol. 26, no. 1, pp. 329–339, Jan. 2019, doi: 10.1007/s10570-018-2095-6.

[81] A. Conroy, S. Halliwell, and T. Reynolds, "Composite recycling in the construction industry," *Compos Part A Appl Sci Manuf*, vol. 37, no. 8, pp. 1216–1222, 2006, doi: 10.1016/j.compositesa.2005.05.031.

[82] M. A. Dweib, B. Hu, A. O'Donnell, H. W. Shenton, and R. P. Wool, "All natural composite sandwich beams for structural applications," *Compos Struct*, vol. 63, no. 2, pp. 147–157, 2004, doi: 10.1016/S0263-8223(03)00143-0.

[83] A. K. Mohanty, A. Wibowo, M. Misra, and L. T. Drzal, "Effect of process engineering on the performance of natural fiber reinforced cellulose acetate biocomposites," *Compos Part A Appl Sci Manuf*, vol. 35, no. 3, pp. 363–370, 2004, doi: 10.1016/j.compositesa.2003.09.015.

[84] T. Nishino, I. Matsuda, and K. Hirao, "All-Cellulose Composite," *Macromolecules*, vol. 37, no. 20, pp. 7683–7687, 2004, doi: 10.1021/ma049300h.

[85] T. Huber, J. Müssig, O. Curnow, S. Pang, S. Bickerton, and M. P. Staiger, "A critical review of all-cellulose composites," *J Mater Sci*, vol. 47, no. 3, pp. 1171–1186, 2012, doi: 10.1007/s10853-011-5774-3.

[86] B. Baghaei and M. Skrifvars, "All-Cellulose Composites: A Review of Recent Studies on Structure, Properties and Applications," *Molecules*, vol. 25, no. 12, 2020, doi: 10.3390/molecules25122836.

[87] S. Tanpichai, A. Boonmahitthisud, N. Soykeabkaew, and L. Ongthip, "Review of the recent developments in all-cellulose nanocomposites: Properties and applications," *Carbohydr Polym*, vol. 286, no. February, p. 119192, 2022, doi: 10.1016/j.carbpol.2022.119192.

[88] C. Qin, N. Soykeabkaew, N. Xiuyuan, and T. Peijs, "The effect of fibre volume fraction and mercerization on the properties of all-cellulose composites," *Carbohydr Polym*, vol. 71, no. 3, pp.

458–467, 2008, doi: 10.1016/j.carbpol.2007.06.019.

[89] J. M. Spörl *et al.*, "Ionic Liquid Approach Toward Manufacture and Full Recycling of All-Cellulose Composites," *Macromol Mater Eng*, vol. 303, no. 1, pp. 1–8, 2018, doi: 10.1002/mame.201700335.

[90] W. Gindl and J. Keckes, "Drawing of self-reinforced cellulose films," *J Appl Polym Sci*, vol. 103, no. 4, pp. 2703–2708, 2007, doi: 10.1002/app.25434.

[91] T. Nishino and N. Arimoto, "All-cellulose composite prepared by selective dissolving of fiber surface," *Biomacromolecules*, vol. 8, no. 9, pp. 2712–2716, 2007, doi: 10.1021/bm0703416.

[92] H. Yousefi, M. Faezipour, T. Nishino, A. Shakeri, and G. Ebrahimi, "All-cellulose composite and nanocomposite made from partially dissolved micro-and nanofibers of canola straw," *Polym J*, vol. 43, no. 6, pp. 559–564, 2011, doi: 10.1038/pj.2011.31.

[93] S. Fujisawa, E. Togawa, and N. Hayashi, "Orientation control of cellulose nanofibrils in all-cellulose composites and mechanical properties of the films," *Journal of Wood Science*, vol. 62, no. 2, pp. 174–180, 2016, doi: 10.1007/s10086-015-1533-4.

[94] N. C. Hildebrandt, P. Piltonen, J. P. Valkama, and M. Illikainen, "The effect of calendaring on the mechanical properties of paper-based, self-reinforcing composites," *Cellulose*, vol. 25, no. 7, pp. 4001–4010, 2018, doi: 10.1007/s10570-018-1831-2.

[95] W. Gindl and J. Keckes, "All-cellulose nanocomposite," *Polymer (Guildf)*, vol. 46, no. 23, pp. 10221–10225, 2005, doi: 10.1016/j.polymer.2005.08.040.

Chapter 2.

Elucidation of the Mechanism of the Crystal Transition of Cellulose I to II in Low-Concentration Alkali Treatments at Low Temperature

2.1. Introduction

It is important to have a deep understanding of the crystal structures of cellulose I and II to create novel cellulose materials. In particular, elucidation of the crystal transition mechanism from cellulose I to II is an important issue concerning the crystal structure of cellulose. Cellulose I crystals transition to cellulose II crystals by a process called mercerization using a concentrated NaOH solution. This transition does not occur at low NaOH concentrations (8-10 wt%) at room temperature [1], [2]. On the other hand, this transition proceeds at low temperatures in a low concentration of NaOH solution [3], [4]. However, the structural changes of cellulose molecules accompanying the crystal transition and their driving force have remained unclear. In this chapter, I aimed to clarify the structural changes in the cellulose molecular chain associated with the crystal transition, especially the hydroxymethyl group at the C6 position.

It has been proposed that the disruption of intrachain hydrogen bonds [5] and hydrophobic interactions [6], [7] are important for the crystal transition from cellulose I to II. Cellulose I has intrachain O2-O6 and O3-O5 hydrogen bonds [8], and cellulose II has intrachain O3-O6 and O3-O5 hydrogen bonds [9], as shown in Fig 1-3. Cellulose I and II have different conformations of C6 hydroxymethyl groups, due to different intrachain hydrogen bonds (O2-O6 in cellulose I and O3-O6 in cellulose II). Therefore, the change in hydrogen bonding may be involved in the crystal transition. Our previously reported calculations indicate that the *tg* structure does not return to its original structure when it experiences a change, but rather changes to the *gt* structure [10], which may

contribute to the crystal transition from cellulose I to cellulose II. Therefore, the conformation at the C6 position is one of the guidelines for observing the crystal structures and intrachain hydrogen bonds, and the elucidating the conformational changes at the C6 position may further our understanding of the crystal transition.

The purpose of this chapter is to elucidate the mechanism of crystal transition from cellulose I to cellulose II in low-concentration NaOH treatments at low temperatures. In addition, the ultimate goal is to utilize the findings obtained in this chapter for the creation of new cellulose materials.

Firstly, the NaOH treatments at low temperatures with a low-concentration NaOH solution were conducted at various temperatures to track the progression of crystal transition. Next, the in situ solid-state ^{13}C cross-polarization magic angle spinning (CP/MAS) NMR measurement and the in situ wide-angle X-ray scattering (WAXS) measurement were performed to evaluate the conformational changes during crystal transition. Additionally, in order to anticipate the structure of cellulose molecules during crystal transition, the computational calculations were performed on the cello-oligomers which have no hydrogen bonds between glucose residues. Furthermore, the dynamics of Na ions were evaluated via ^{23}Na NMR relaxation time measurement. The crystal transition mechanism from cellulose I to II was discussed from the results obtained by these experiments.

2.2. Methods

2.2.1. Materials

Filter paper powder (100-200 mesh, cellulose > 99%) derived from cotton linter with DP (degrees of polymerization) 250, and kraft pulp paper (bleached hardwood kraft pulp, cellulose ca. 80 % and hemicellulose ca. 20 %) with DP 650-840 purchased from Advantech Co., Ltd (Tokyo, Japan) and Nippon Paper Industries (Tokyo, Japan), respectively, were used as the cellulose materials. Cellobiose was purchased from FUJIFIRM Wako Pure Chemical Corporation (Osaka, Japan) and used as prepared. NaOH (> 97.0 %) and H_2SO_4 (> 95.0 %) were purchased from FUJIFILM Wako Pure Chemical Corporation (Osaka, Japan). Deionized water (Elix®Essential3, Merck KgaA, Darmstadt, Germany) was used to prepare aqueous solutions of NaOH and H_2SO_4 and to wash the cellulose samples.

2.2.2. Nuclear Magnetic Resonance (NMR) Measurements

All NMR measurements, including the NMR relaxation time measurements, were performed using a Bruker AVANCE NEO 500 spectrometer (Bruker, Germany) at Instrumental Analysis Support Office, the Frontier Chemistry Center, Faculty of Engineering, Hokkaido University, Japan. Solid-state ^{13}C CP/MAS NMR spectra were recorded at 125 MHz. The samples were packed in a 3.2 mm rotor and spun at a frequency of 10 kHz. All the CP/MAS high-resolution spectra were recorded with a 1H 90° pulse with a pulse length of 4.0 μs, a contact time of 1.5 ms, and a repetition time of 4 s. The ramp and tppm-15 sequences were used for the contact pulse and decoupling,

respectively. The chemical shift was calibrated using the carbonyl carbon of glycine (176.46 ppm) as the reference.

^{23}Na NMR relaxation time measurements were performed at 133 MHz. The samples were packed into the MAS rotor; however, no MAS conditions were applied during the temperature control and relaxation time measurements. Spin lattice relaxation time (T_1) measurements were performed using the inversion recovery method with a 90° pulse length of 3.1 μs. The T_1 values were obtained using the fitting program of the TOPSPIN NMR software developed by Bruker Inc.

2.2.3. Low-Concentration NaOH Treatments at Various Temperatures

Cellulose powder was added to an 8 wt% NaOH solution at room temperature (24 °C) and centrifuged at 1,000 × g for 5 min. The supernatant was removed, and the precipitate was used for NaOH treatment. The centrifuge tubes with 8 wt% NaOH-soaked cellulose were chilled at –30 °C, –25 °C, –20 °C, –18 °C, –17 °C, –16 °C, –15 °C, –10 °C, and –5 °C in a cryostat (EYELA PFR-1000, TOKYO RIKAKIKAI Co., Ltd, Tokyo, Japan) for up to 90 min. The temperature was controlled by cooling ethanol in this instrument. Immediately after the sample was removed from the low temperature to room temperature (24 °C), a 10 vol% H_2SO_4 solution was added in sufficient volume to bring the pH below 7.0. These samples were washed with deionized water, and air-dried at room temperature (24 °C). These dried samples were analyzed via solid-state ^{13}C CP/MAS NMR. The C6 resonance lines of solid-state ^{13}C CP/MAS NMR spectra were deconvoluted using the Dmfit2017 line-

fitting program [10]. A Lorentzian shape was used for each line. The C6 resonance lines were deconvoluted based on the chemical shifts for the *tg* (64–66 ppm), *gt* (62–63 ppm), and *gg* (60–62 ppm) conformations [12] as shown in Fig 2-1 [13], [14]. Additionally, the *gg* lines were divided into two categories: accessible surfaces which can be accessed by solvents such as water, and inaccessible surfaces which cannot be accessed by solvents but can be accessible by solute ions [15]. The proportion of cellulose II in the crystal region was calculated using the following equation:

$$\text{Proportion of cellulose II in crystal region} = \frac{A_{gt}}{A_{tg} + A_{gt}} \times 100$$

where A_{tg} is the integrated area of *tg* lines at 66.0, 65.5, and 65.2 ppm, and A_{gt} is the integrated area of *gt* lines at 63.3 and 62.6 ppm.

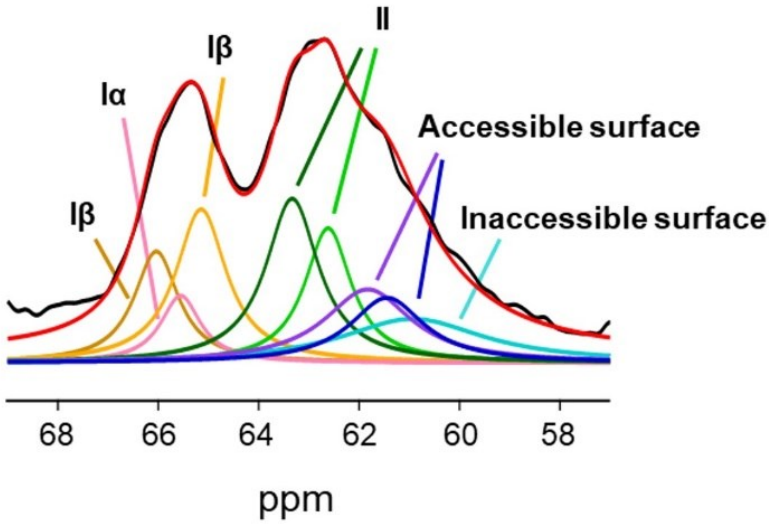

Fig. 2-1. C6 line fitting model in the solid-state ^{13}C CP/MAS NMR spectrum.

2.2.4. In situ Solid-State ^{13}C Cross-Polarization Magic Angle Spinning (CP/MAS) NMR Measurement

Cellulose powder was added to a 10 wt% NaOH solution at room temperature (24 °C) and centrifuged 1,000 × g for 5 min. The supernatant was removed, and the precipitate was analyzed via in situ solid-state ^{13}C CP/MAS NMR. As a complete crystal transition could not be observed with 8 wt% NaOH-soaked cellulose powder, a 10 wt% NaOH solution was used, which does not induce crystal transition at 24 °C. The sample was packed in a 3.2 mm rotor, and the rotor was set in the probe inside the NMR instrument. Solid-state ^{13}C CP/MAS NMR measurements were performed as the temperature was lowered from 24 °C to –25 °C and increased from –25 °C to 24 °C. A variable-temperature instrument system was used in the experiments.

First, the measurement was conducted at 24 °C, and MAS was stopped after the measurement. The temperature in the probe was lowered from 24 °C to 20 °C while the rotor remained stationary in the probe. The temperature was changed without MAS to minimize the discrepancy between the displayed and actual temperatures. MAS was restarted 30 min after the temperature reached 20 °C and the measurements were obtained, after which MAS was stopped. The same operation was performed while decreasing the temperature down to –25 °C at intervals of 5 °C and while increasing the temperature to room temperature in increments of 5 °C.

2.2.5. In situ Wide-Angle X-ray Scattering (WAXS) Measurement

In situ WAXS measurements of the 10 wt% NaOH-soaked cellulose powder were performed at the BL-6A beamline, and measurements of the 10 wt% NaOH-soaked pulp paper were performed at the BL-10C beamline of the Photon Factory of the High-Energy Accelerator Research Organization (KEK, Tsukuba, Japan). The range of q differed between these measurements as the beamlines were different. The X-ray wavelength and exposure time were 1.50 Å (8.27 keV) and 60 s, respectively. PILATUS 100k detectors (Dectris Ltd., Switzerland) were used for the WAXS data acquisition. The sample-to-detector distance was calibrated using the scattering pattern of silver behenate (Nagara Science Co. Ltd., Japan). One-dimensional (1D) profiles were obtained as plots of scattering intensity vs. scattering vector (q), where $q = (4\pi/\lambda) \sin(\theta/2)$ (λ, wavelength; θ, scattering angle).

Variable-temperature measurements of 10 wt% NaOH-soaked cellulose samples were performed over a range from room temperature (24 °C) to low temperatures as well as from low temperature to room temperature (24 °C). The samples were prepared using the procedures described in Section 2.2.4. The sample was packed into the center hole of a 1.5-mm-thick flat washer and closed on both sides with a 1.2-mm-thick Kapton sheet. A flat washer with the samples was fixed on a stage (Linkam Scientific Instruments, UK), and the temperature was controlled by blowing air that was cooled with liquid nitrogen. In situ WAXS measurements were performed at room temperature (25 °C), 20 °C, 10 °C, 0 °C, –10 °C, –20 °C, –30 °C, and –35 °C, followed by increasing the temperature to –30 °C, –20 °C, –10 °C, 0 °C, 10 °C, and 20 °C.

The same 10 wt% NaOH-soaked cellulose samples used for in situ WAXS measurements were analyzed via solid-state ^{13}C CP/MAS NMR before neutralization. Then, the samples were neutralized with a 10 vol% H_2SO_4 solution, washed with water, and air-dried. The samples were again analyzed via solid-state ^{13}C CP/MAS NMR. These measurements were acquired to confirm the crystal transition during the in situ WAXS measurements and after neutralization.

2.2.6. Calculation to Identify Stable Structures of the Cello-oligomers

Structure optimization calculations of cellobiose, cellotriose, and cellotetraose, which have no hydrogen bonds between glucose residues, were performed using the Gaussian G16 program with the B3LYP/6-31+G (d,p) basis set. Vibrational frequency calculations were performed on the optimized structures, and the absence of negative vibrational frequencies confirms the adequacy of the results of the structure optimization calculation. The calculations were performed using a supercomputer system at the Information Initiative Center of Hokkaido University, Sapporo, Japan. Each initial structure was constructed using GaussView 6.0 software and then cleaned for creation.

2.2.7. ^{23}Na NMR Relaxation Time Measurements

Cellulose powder was added to 1, 5, 8, and 10 wt% NaOH solutions at room temperature (24 °C), and these mixtures were centrifuged at × 1,000 g for 5 min. The supernatant was removed, and the precipitate was used for ^{23}Na NMR relaxation time measurements. These samples were packed

in a 3.2 mm rotor and set in an NMR instrument. Furthermore, the relaxation times of ^{23}Na nuclei in 1 and 10 wt% NaOH solutions without cellulose powder were measured to evaluate the influence of cellulose.

First, the spin-lattice relaxation time (T_1) at 24 °C was measured. Then, the temperature inside the probe was decreased to 20 °C, and T_1 was measured after 10 min of temperature stabilization. The same operation was performed at 15 °C, 10 °C, 5 °C, 0 °C, –5 °C, –10 °C, –15 °C, –20 °C, and –25 °C. Subsequently, the temperature inside the probe was increased to –20 °C, –15 °C, –10 °C, –5 °C, 0 °C, 5 °C, 10 °C, 15 °C, 20 °C, and 24 °C, and the relaxation times were acquired. Then, solid-state ^{13}C CP/MAS NMR measurements were conducted to confirm the alkali concentration at which the crystal transition proceeded.

2.2.8. NMR Measurements of NaOH-Soaked Cellulose using a High-Concentration NaOH Solution

In situ ^{13}C CP/MAS NMR and ^{23}Na NMR relaxation time measurements of cellulose soaked in a 25 wt% NaOH solution were performed at room temperature (24 °C) to investigate mercerization in a concentrated NaOH solution. The samples were prepared as described in Sections 2.2.4 and 2.2.7, albeit with a 25 wt% NaOH solution. ^{23}Na NMR relaxation time measurements of a 25 wt% NaOH solution without cellulose powder were also performed at 24 °C for comparison.

2.3. Results and Discussions

2.3.1. Crystal Transition in Low-Concentration Alkali Treatments at Various Temperatures

Fig 2-2 shows the content rates of cellulose II in the 8 wt% NaOH-soaked cellulose powder treated at various temperatures. The crystal transition was not completed at temperatures above –16 °C but only below –17 °C. The lower the processing temperature, the shorter the time required to complete the crystal transition. This behavior indicates that the crystal transition from cellulose I to cellulose II was a non-Arrhenius-type reaction, as it occurred only at low temperatures. This suggests the importance of temperature conditions. In addition, the NaOH in NaOH solutions with concentrations where the crystal transition progressed may exhibit specific dynamic behaviors compared to those in solutions where the crystal transition did not progress. Therefore, Na ions dynamics may affect crystal transition. Hence, Na-ion dynamics must be evaluated along with the conformational changes in the cellulose molecular chains to elucidate the crystal transition. Consequently, temperature-variable in situ solid-state ^{13}C CP/MAS NMR and WAXS measurements, as well as ^{23}Na NMR relaxation time measurements, were acquired using the NaOH-soaked cellulose.

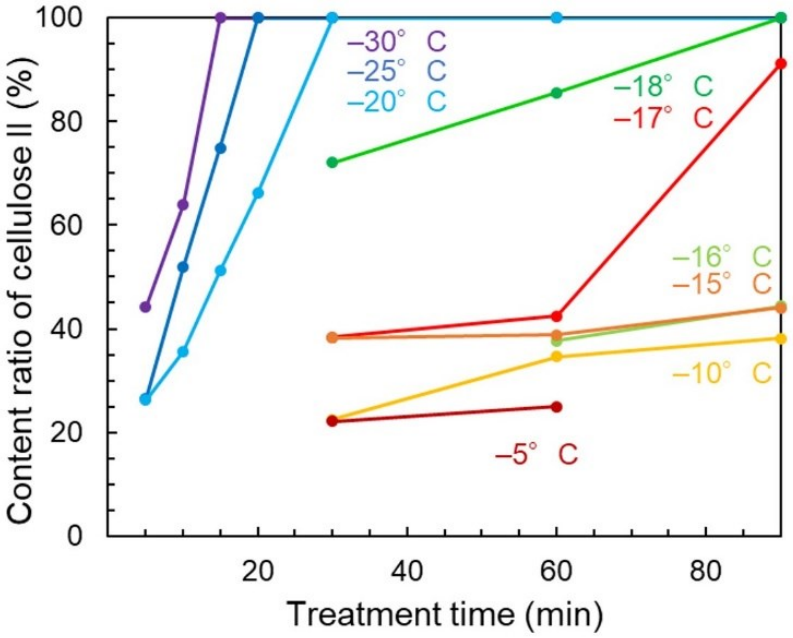

Fig. 2-2. Time-course changes for the proportion of cellulose II in the low-concentration (8 wt%) NaOH-soaked cellulose powder treated at various temperatures.

2.3.2. In situ ^{13}C Solid-State CP/MAS NMR Measurements

Fig 2-3 shows the in situ solid-state ^{13}C CP/MAS NMR spectra of 10 wt% NaOH-soaked cellulose powder as the temperature gradually decreased. The C6 line shifted from 65 to 61 ppm, indicating a change in the O6 conformation from *tg* to *gg*. Similar upfield shifts were observed for the C1 and C4 lines, indicating corresponding environmental changes. In particular, the large upfield shift of the C4 line from 89 to 80 ppm was observed. These line shifts occurred at lower temperatures than after the at C6, suggesting that the conformational changes at C1 and C4 occurred after the changes at C6. In addition, this C4 line shift indicated a reduction of crystallinity, as the C4 line at 89 ppm, which is attributed to the crystalline regions [16], had decreased. Fig 2-4 shows the solid-state ^{13}C CP/MAS

NMR spectra as the temperature was increased from –25 °C to 24 °C. The C1 and C4 lines shifted downfield, whereas the C6 line was maintained at 61 ppm, indicating that the *gg* conformation of O6 was maintained. The C4 line shifted to 86 ppm, which is attributed to the surface/amorphous region [16]. The C4 upfield shift observed at low temperatures and at 24 °C after warming is consistent with that for alkaline cellulose reported previously [17]. In summary, the in situ solid-state ^{13}C CP/MAS NMR spectra indicate that crystallinity reduction and conformational changes were observed when the temperature was decreased, and these changes were maintained when the temperature was increased. Additionally, it was shown that the crystal transition from cellulose I to alkali cellulose occurred during alkali treatment, but not to cellulose II.

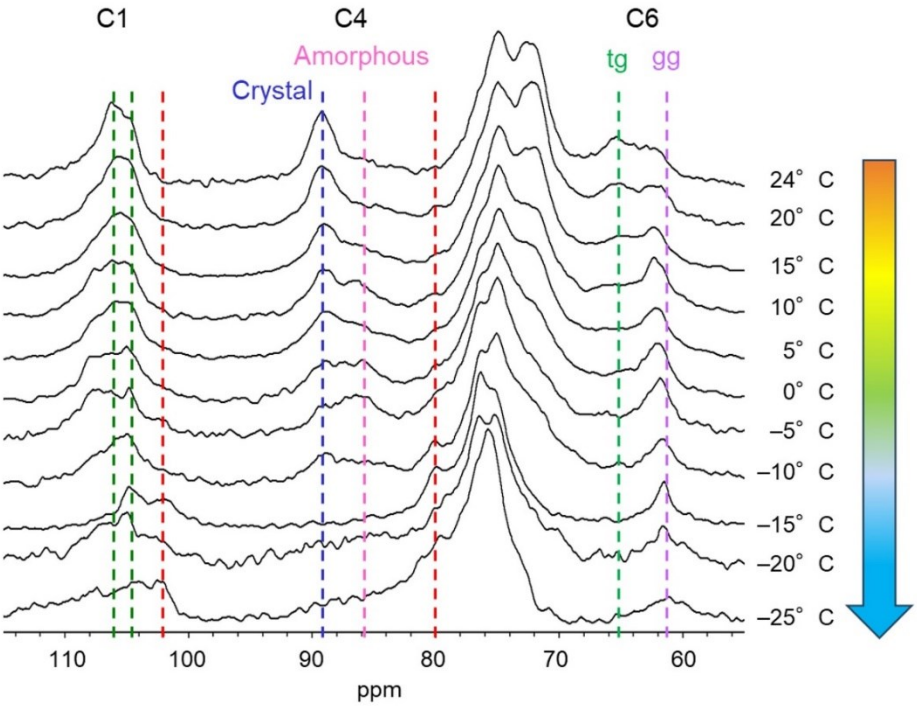

Fig. 2-3. Solid-state ^{13}C CP/MAS NMR spectra of 10 wt% NaOH-soaked cellulose powder as the temperature was lowered from 24 °C to 20 °C, 15 °C, 10 °C, 5 °C, 0 °C, –5 °C, –10 °C, –15 °C, –20 °C, and –25 °C.

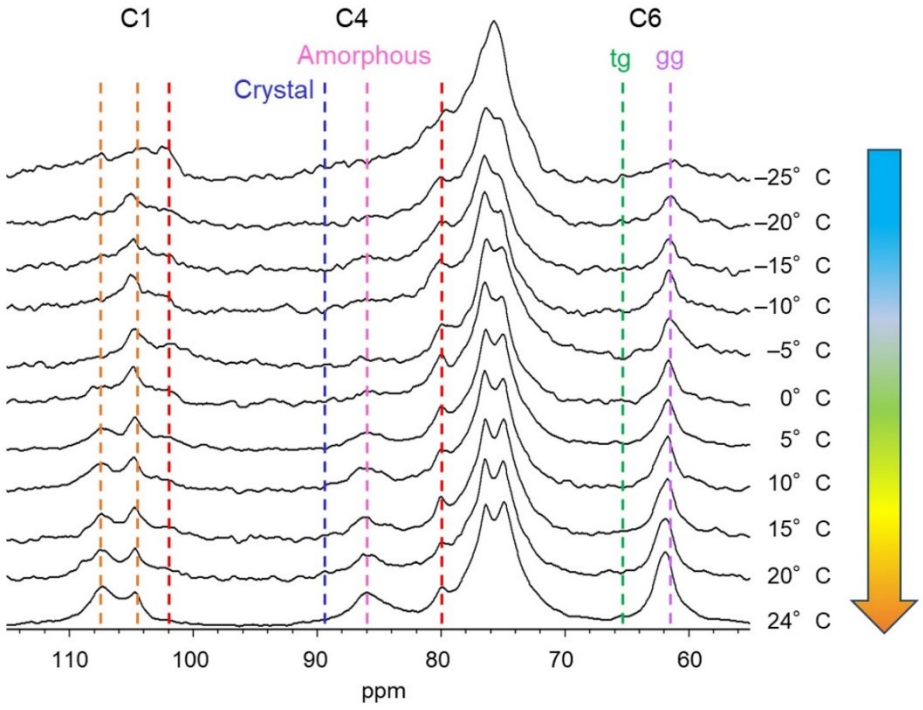

Fig. 2-4. Solid-state ^{13}C CP/MAS NMR spectra of 10 wt% NaOH-soaked cellulose powder as the temperature was increased from –25 °C to –20 °C, –15 °C, –10 °C, –5 °C, 0 °C, 5 °C, 10 °C, 15 °C, 20 °C, and 24 °C. The in situ ^{13}C NMR measurements shown in Figs 2-3 and 2-4 were conducted consecutively. The spectrum measured at –25 °C is also shown in Fig 2-4, and the sample underwent in situ NMR measurements from room temperature (24 °C) to low temperatures before obtaining this spectrum.

2.3.3. In situ WAXS Measurements

Fig 2-5(a) shows the WAXS profiles obtained from the in situ WAXS measurements of the 10 wt% NaOH-soaked cellulose powder at different temperatures. As the temperature decreased, the intensity of the cellulose I crystal peaks decreased, and the width at half maximum increased, indicating a reduction in cellulose crystallinity. These WAXS profiles are consistent with those observed for cellulose powder dissolved in a LiOH/urea solution, which indicated a decrease in crystallinity [18]. Moreover, the crystal peaks of cellulose I almost disappeared at –35 °C. This

decrease in crystallinity confirms that Na ions have penetrated the crystal region. However, no change in the crystal structure was observed as the temperature increased. The three sharp peaks at ~15, 17, and 18 nm^{-1} disappeared with increasing temperature, correspond to ice water. Fig 2-5 (b) shows the WAXS profiles obtained from the in situ WAXS measurements of the 10 wt% NaOH-soaked pulp paper. The ranges of q were different (Figs 2-5 (a) and (b)) because these measurements were performed at different beamlines. The cellulose I crystal peaks were broad, which is attributed to the lower crystallinity of the pulp paper than that of the cellulose powder. Similar to that observed for the cellulose powder, as the temperature increased, the intensity of the cellulose I crystal peak decreased, and the width at half maximum increased.

The in situ WAXS results are consistent with the C4 resonance line observed in the in situ solid-state ^{13}C CP/MAS NMR spectra, whose intensity decreased in the crystalline region and increased in the surface/amorphous region as the temperature was lowered. In summary, during the crystal transition induced by NaOH treatment at low temperatures, cellulose I crystals disappeared, alkali cellulose was formed as the temperature was decreased, and this amorphous structure remained unchanged as the temperature was increased, with no transition to cellulose II. Similar results were obtained in the experiment using pulp paper. This indicates that the behavior of the crystal morphology transition in low-concentration alkali treatment at low temperatures is consistent, regardless of the cellulose material.

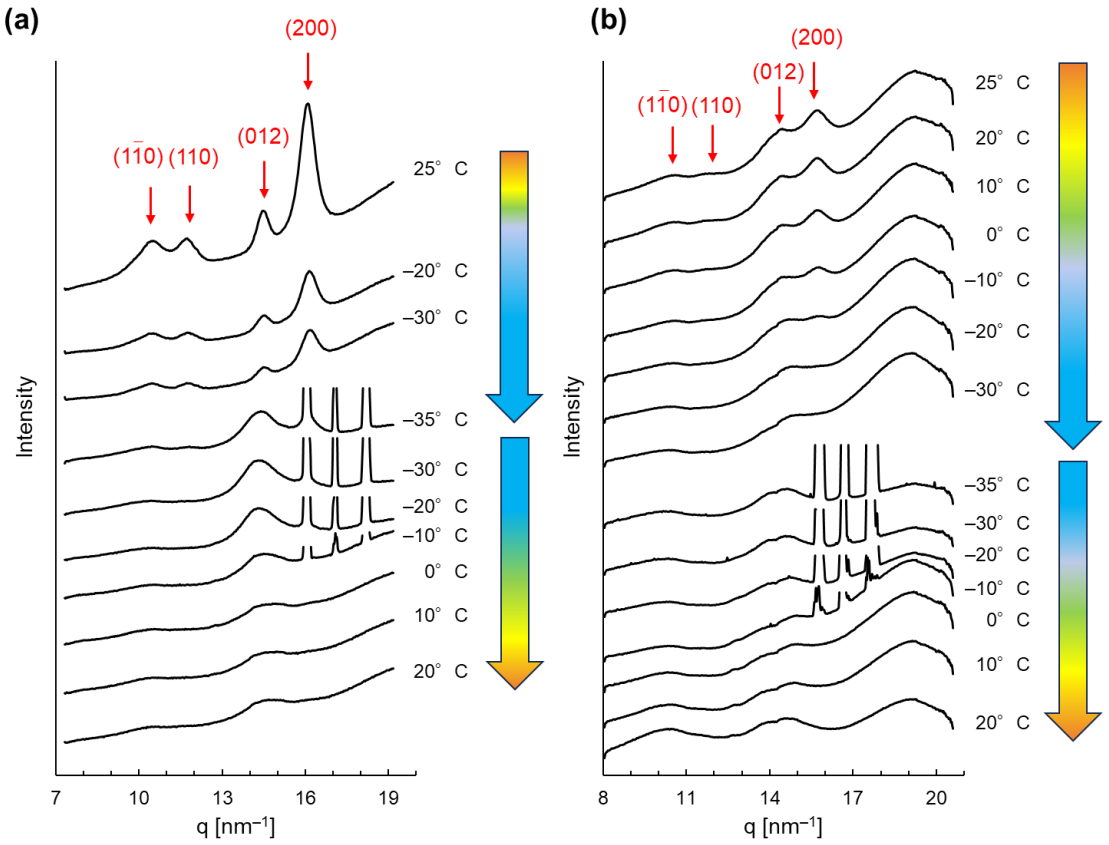

Fig. 2-5. Temperature-variable wide-angle X-ray scattering (WAXS) profiles of (a) the 10 wt% NaOH-soaked cellulose powder and (b) the 10 wt% NaOH-soaked pulp paper (25 °C > –35 °C > 20 °C).

Fig 2-6 shows the solid-state ^{13}C CP/MAS NMR spectra of the 10 wt% NaOH-soaked cellulose powder and pulp paper samples used in the in situ WAXS measurements before and after neutralization. In both cellulose materials, the samples before the neutralization were determined to be alkali cellulose, whereas the sample after the neutralization, washing, and drying was cellulose II. This confirms that regardless of cellulose material, cellulose I crystals disappeared, alkali cellulose was formed as the temperature decreased, and this amorphous structure remained unchanged as the temperature increased during the crystal transition induced by NaOH treatment at low temperatures.

Moreover, the transition from alkali cellulose to cellulose II occurred during neutralization, washing, and drying.

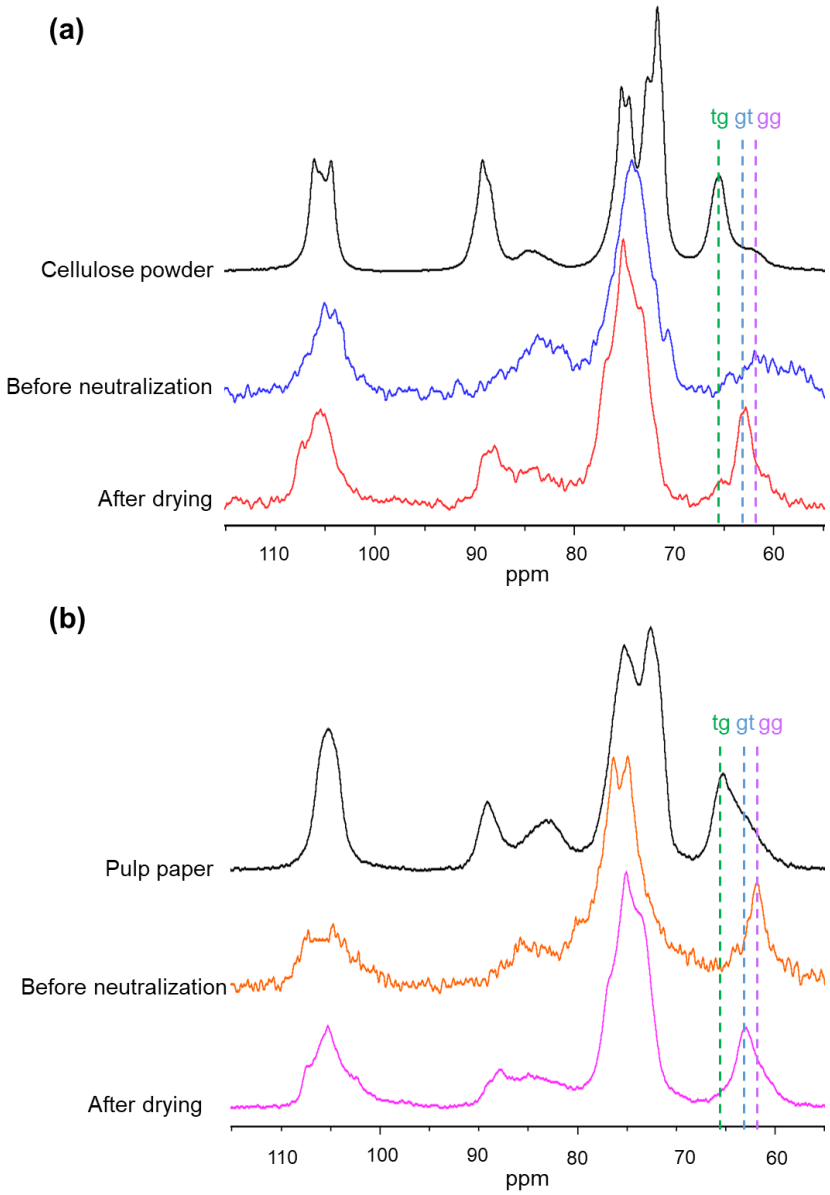

Fig. 2-6. Solid-state ^{13}C CP/MAS NMR spectra before neutralization and after drying of (a) the 10wt%-NaOH soaked cellulose powder samples and (b) 10 wt% NaOH-soaked pulp paper used for the temperature-variable WAXS measurements. *Color code:* (a) black line, cellulose powder; blue line, before neutralization; red line, after washing and drying, (b) black line, pulp paper; orange line, before neutralization; pink line, after washing. *Abbreviations*: *tg*, trans-gauche; *gt*, gauche-trans; and *gg*, gauche-gauche.

2.3.4. Prediction of Conformational Changes during Crystal Transition via the Calculation of Structural Optimization on Cello-oligomers

Fig 2-7 shows the ^{13}C CP/MAS NMR spectra of cellulose powder (cellulose I_β rich), the 10 wt% NaOH-soaked cellulose powder at –25 °C and 24 °C, and as-received cellobiose. The C6 line shift indicates that the O6 conformation changed from *tg* to *gg*, where the hydroxyl groups are perpendicular to the glucose residues and consequently do not form hydrogen bonds with neighboring glucose residues. Therefore, this C6 line shift suggests disruption of the intrachain O6-O2 hydrogen bonds. Kamide et al. reported that the disruption of the O3-O5 hydrogen bonds has a de-shielding effect on C4 and C5, which explains the large C4 line shift [4]. A similar upfield shift from 89 ppm to 80 ppm was observed for the C4 line in the in situ solid-state ^{13}C CP/MAS NMR measurement (shown in Fig 2-3) in this study, which suggests the disruption of the intrachain O5-O3 hydrogen bonds.

To confirm the conformation of the cellulose molecules after the intrachain hydrogen bonds were broken, the computational simulations were performed on the structures of cellobiose, cellotriose, and cellotetraose devoid of hydrogen bonds. The in situ ^{13}C NMR measurements show that the intrachain hydrogen bonds were broken during the crystal transition. The solid-state ^{13}C CP/MAS NMR spectrum of as-received cellobiose (Fig 2-7) revealed that the C4 lines of cellobiose appeared in the high magnetic field relative to the C4 crystalline line of cellulose, suggesting that as-received cellobiose has a similar structure to that of cellulose during crystal transition. I hypothesized that the optimized structure of cellobiose, cellotriose, and cellotetraose, a part of the cellulose molecular chain,

could predict the structure of cellulose during the crystalline transition. Fig 2-8 shows the optimized structures of cellobiose, cellotriose, and cellotetraose obtained by DFT calculations. No negative frequencies were observed in the optimized structures in the vibrational frequency calculations. The neighboring glucose residues are oriented in different directions in all optimized structures, suggesting the absence of a plane sheet structure. This suggests that the disruption of intrachain hydrogen bonds during the crystal transition results in a more stable structure. The absence of a plane sheet structure indicates weakened hydrophobic interactions between cellulose molecules, which would allow more water molecules to penetrate the crystal region and facilitate the presence of a higher number of NaOH in the vicinity of the cellulose molecule.

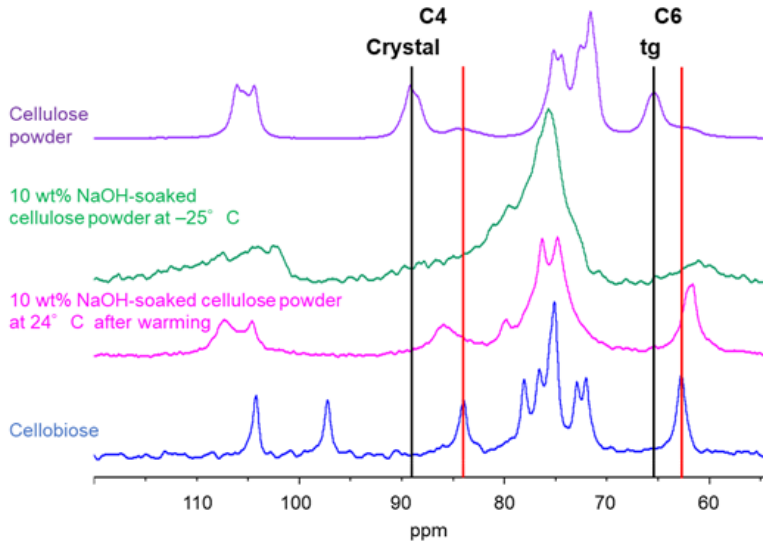

Fig. 2-7. Solid-state ^{13}C NMR CP/MAS NMR spectra. *Color code:* purple line, cellulose powder (cellulose I_β rich); green line, 10 wt% NaOH-soaked cellulose powder (the spectrum was recorded at –25 °C after cooling the sample from 24 °C to –25 °C); pink line, 10 wt% NaOH-soaked cellulose powder (the spectrum was recorded at 24 °C after cooling the sample from 24 °C to –25 °C, followed by warming to 24 °C); blue line, as-received cellobiose.

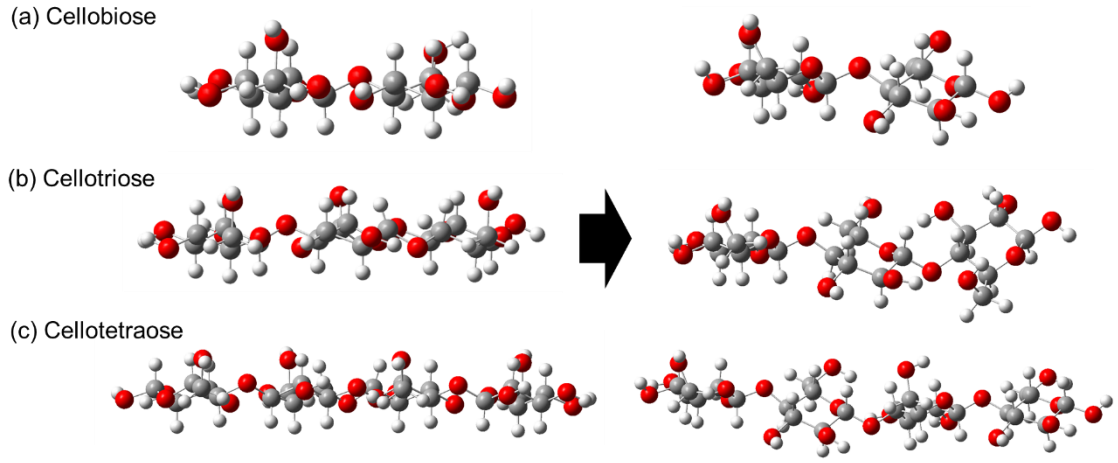

Fig. 2-8. Three-dimensional (3D) pre-computed and optimized structures of (a) cellobiose, (b) cellotriose, and (c) cellotetraose.

2.3.5. ^{23}Na NMR Relaxation Time Measurements

Fig 2-9 shows the solid-state ^{13}C CP/MAS NMR spectra of the 1 wt% to 10 wt% NaOH-soaked cellulose powder samples used in the ^{23}Na NMR relaxation time measurements. These ^{13}C NMR measurements were conducted to confirm the concentration of the NaOH solutions at which the crystal transition proceeded. The spectra of the samples soaked in 1 wt% and 5 wt% NaOH solutions were almost identical to those of the samples soaked in a 10 wt% NaOH solution before measurement (uncooled). However, C4 peaks were observed in both the amorphous and crystalline regions in the spectrum of the 8 wt% NaOH-soaked sample. The spectrum of the sample soaked in a 10 wt% NaOH solution showed that the C4 line completely disappeared in the crystal region. Moreover, the C6 line shifted upfield, confirming the conformational change from *tg* to *gg*. These results indicate that the crystal transition did not progress in the cellulose samples soaked in <5 wt% NaOH solution, partially progressed in an 8 wt% NaOH solution, and was completed in a 10 wt% NaOH solution. Thus, the

degree of crystal transition depends on the NaOH concentration. Dinand et al. (2002) previously reported that the crystal transition did not progress at <5 wt% NaOH concentration [1], which is consistent with the results of these ^{13}C NMR measurements.

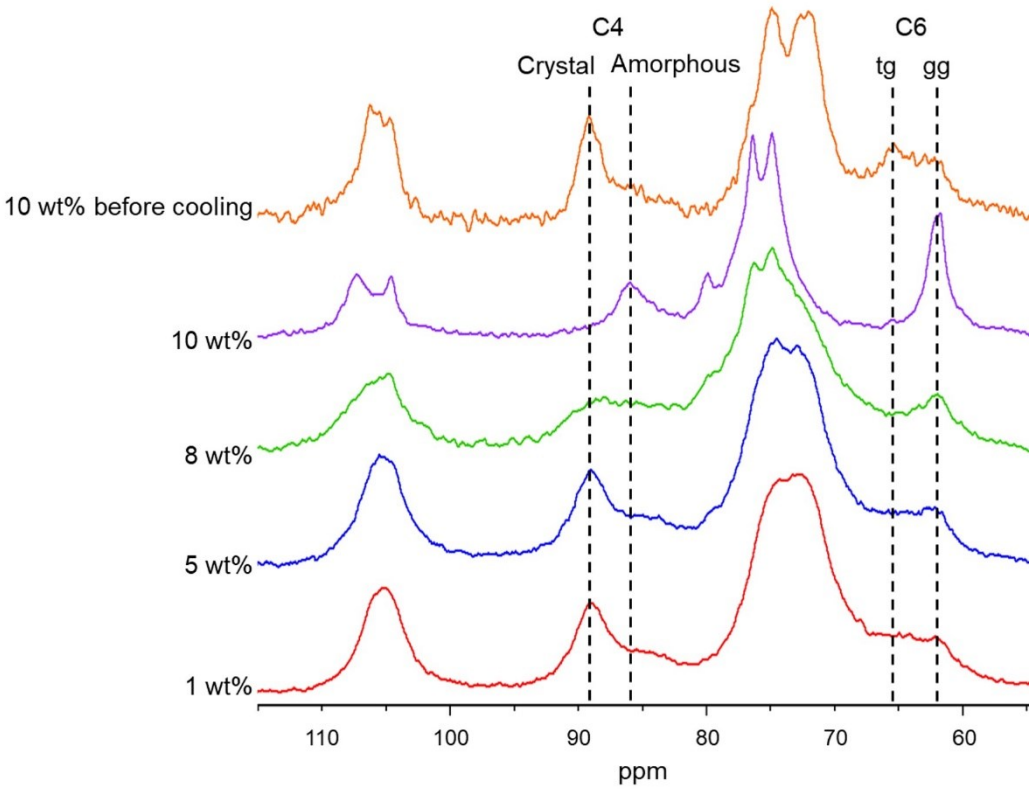

Fig. 2-9. Solid-state ^{13}C CP/MAS NMR spectra measured at room temperature (24 °C) of 1–10 wt% NaOH-soaked cellulose powders which were used for the ^{23}Na NMR relaxation measurements. The samples were cooled from room temperature to low temperatures and subsequently warmed back to room temperature. *Color code:* orange line, 10 wt% NaOH before cooling; purple line, 10 wt%; green line, 8 wt%; blue line, 5 wt%; red line, 1 wt%. *Abbreviations*: *tg*, trans-gauche; *gt*, gauche-trans; and *gg*, gauche-gauche.

The spin-lattice relaxation times (T_1) of the Na nuclei in 1 wt% to 10 wt% NaOH-soaked cellulose powder samples and 1 wt% and 10 wt% NaOH solutions without cellulose powder were

measured in the temperature range of 24 °C to –25 °C. Table 1 shows the T_1 of the Na nuclei in the 10 wt% NaOH-soaked cellulose powder while cooling. T_1 decreased with decreasing temperature, indicating that the Na-ion dynamics follow the Arrhenius law. Fig 2-10 shows the ^{23}Na NMR spectra of the 10 wt% NaOH-soaked cellulose powder, measured at 24 °C, 0 °C, and –15 °C. The width of the peak increased as temperature decreased, indicating T_1 was shorter as temperature decreased. Because the spin number of the Na nucleus is 3/2, it will have quadrupolar moments, and consequently, the main component of the spin-lattice relaxation mechanism is the interaction between the quadrupolar moment and the electric field gradient. Figs 2-11(a) and 2-11(b) show semi-logarithmic Arrhenius plots during cooling and heating, respectively, with the reciprocal of the absolute temperature (1/T) on the x-axis and the reciprocal of T_1 ($1/T_1$) on the y-axis. Although the observed temperature range is not sufficient, the changes in $1/T_1$ exhibit a roughly linear trend in this semi-logarithmic plot except around the lowest temperature end where the solution begins to freeze. The term $1/T_1$ is proportional to the term $\langle e^2qQ/h\rangle^2 \times J(\omega)$, where eq and eQ are the electric field gradient and the quadrupolar moment of ^{23}Na nuclei, respectively, $J(\omega)$ is the spectral density, and ω is the resonance frequency of the nucleus. The term, $\langle e^2qQ/h\rangle^2$ and ω were considered constants as only the ^{23}Na nuclei were experimentally measured. Therefore, $1/T_1$ becomes proportional to only $J(\omega)$, which is expressed as $\omega\tau_c/(1+\omega^2\tau_c^2)$, where τ_c is the correlation time. At the extreme narrowing condition such as $\omega\tau_c \ll 1$, and assuming that $\omega^2\tau_c^2 \approx 0$, $J(\omega)$ can be approximated as $J(\omega)=\omega\tau_c$ and the $1/T_1$ can directly represent

the correlation time. Generally, the correlation time for the motion of nuclei should increase with the decreasing temperature. In the case of the present study, the $1/T_1$ of the Na nuclei increases as temperature decreases. This indicates that the extremely narrowing condition can be adopted. Furthermore, J(ω) becomes proportional to τ_c, suggesting that $1/T_1$ is proportional to the correlation time. Notably, Na ions will have low mobility at long correlation times and high mobility at short correlation times. In addition, the slope of the semi-log plot is proportional to the activation energy for Na-ion mobility. However, this slope is not precise and provides only an approximate trend.

The term $1/T_1$ of the sample that underwent crystal transition increased with decreasing temperature (Fig 2-11(a)), indicating that the mobility of Na ions decreases with decreasing temperature. The 10 wt% NaOH-soaked sample, in which the crystal transition occurred, showed lower Na ions mobility than the 8 wt% NaOH-soaked sample. However, the mobilities of Na ions in the 1 wt% NaOH-soaked sample and the 1 wt% and 10 wt% NaOH solutions without cellulose powder were comparable. The Na ions in the 1 wt% and 10 wt% NaOH solutions without cellulose powder were expected to move freely. Notably, the Na ions in the 1 wt% NaOH-soaked sample moved freely, with no significant increase in the interaction between Na ions and cellulose. In addition, the slope of the semi-logarithmic plot was larger for the concentration at which crystal transition progressed than for the concentration that did not induce crystal transition. This indicates that the activation energy for

the motion of the Na ions was higher. Therefore, the interaction between Na ions and cellulose molecules is essential for the crystal transition.

The mobility of Na ions at Na concentrations that induced crystal transition and those that did not induce the crystal transition was different when the temperature was increased (Fig 2-11(b)). The $1/T_1$ of 1 wt% NaOH-soaked samples exhibited no significant changes, which is attributed to the absence of interactions between the Na ions and cellulose chains as the temperature increased. However, $1/T_1$ of the 8 wt% and 10 wt% NaOH-soaked samples at room temperature (24 °C) was larger than that before cooling. This is attributed to the penetration of NaOH into the crystalline region and subsequent interaction with the cellulose crystals, which facilitates the crystal transition to alkali cellulose.

In summary, the mobility of Na ions decreased significantly during the crystal transition. This suggests that the residence time of NaOH around the cellulose chain increased, facilitating crucial interactions between the cellulose chain and NaOH for the crystal transition of cellulose I to alkali cellulose.

Table. 2-1. Spin-lattice relaxation time (T_1) of Na ions in 10 wt% NaOH-soaked cellulose powder during cooling from 24 °C to –25 °C

Temperature (°C)	24	20	15	10	5	0	–5	–10	–15	–20	–25
T_1 (ms)	13.9	11.9	9.8	7.1	5.2	3.6	3.0	2.5	2.0	1.7	0.53

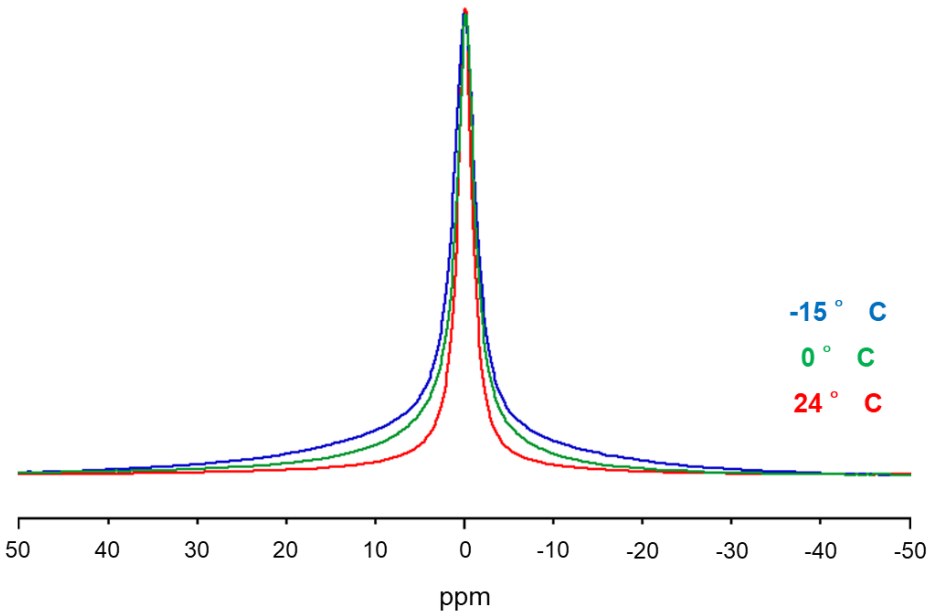

Fig. 2-10. The ^{23}Na NMR spectra of the 10 wt% NaOH-soaked cellulose powder, measured at 24 °C, 0 °C, and –15 °C.

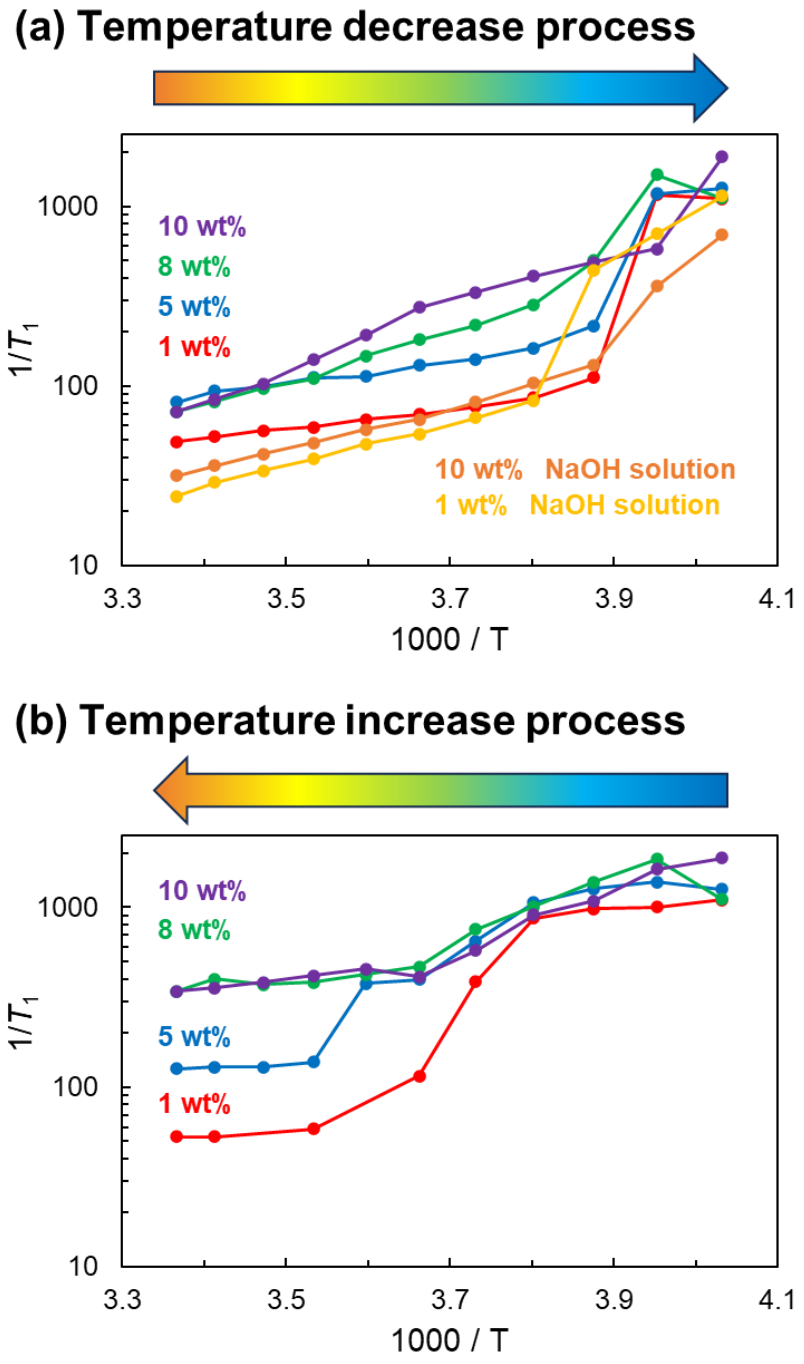

Fig. 2-11. Semi-logarithmic Arrhenius plots of the ^{23}Na-NMR relaxation time measurements of NaOH-soaked cellulose powder during (a) temperature-decrease and (b) temperature-increase processes. *Color code:* purple line, 10 wt%; green line, 8 wt%; blue line, 5 wt%; red line, 1 wt%; orange line, a 10 wt% NaOH solution without cellulose; yellow line, a 1 wt% NaOH solution without cellulose.

2.3.6. Mercerization Induced by a Concentrated NaOH Solution

Fig 2-12. Shows the in situ solid-state ^{13}C CP/MAS NMR spectra of 25 wt% NaOH-soaked cellulose powder at 24 °C. The C4 and C6 lines were similar to those observed in the spectrum of 10 wt% NaOH-soaked cellulose powder recorded at 24 °C after the in situ NMR measurements (Fig 2-4.), suggesting that the conformational changes in cellulose were the same in the cases of both mercerization with a high-concentration NaOH solution at room temperature and low-concentration alkali treatment at low temperatures.

In addition, the T_1 of Na ions in the 25 wt% NaOH-soaked cellulose powder at 24 °C was 1.40 ms, which is comparable to the T_1 value of Na ions in 10 wt% NaOH-soaked cellulose powder at low temperatures (Table 2-1). This also suggests that the Na-ion dynamics, which facilitate the crystal transition, in both cases were comparable. That is, the interactions between Na ions and cellulose decrease the mobility of Na ions because NaOH penetrates the crystal regions, resulting in a longer residence time. Table 2-2 shows the T_1 values of 1, 10, and 25 wt% NaOH solutions without cellulose powder measured at 24 °C. T_1 decreased with increasing NaOH concentration, which confirms a reduction in the mobility of the NaOH and an increase in their correlation time. This was attributed to the high alkali concentration, which suppresses the mobility of NaOH.

These results suggest that an elongated correlation time for Na ions is imperative for crystal transition. At high alkali concentrations or low alkali concentrations combined with low temperatures, NaOH penetrates the crystal and interacts with cellulose, disrupting intrachain hydrogen bonds. The

NaOH is removed by neutralization and washing, which completes the crystal transition to cellulose II.

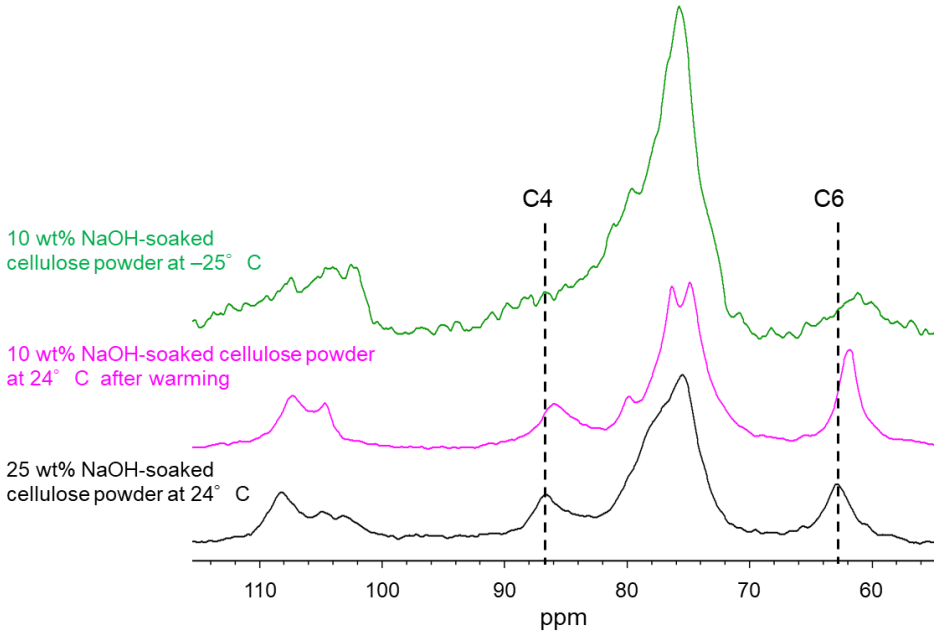

Fig. 2-12. In situ solid-state ^{13}C CP/MAS NMR spectra. *Color code:* green line, 10 wt% NaOH-soaked cellulose powder (the spectrum was recorded at –25 °C after cooling the sample from 24 °C to –25 °C); pink line, 10 wt% NaOH-soaked cellulose powder (the spectrum was recorded at 24 °C after cooling the sample from 24 °C to –25 °C, followed by warming to 24 °C); and black line, 25 wt% NaOH-soaked cellulose powder at 24 °C.

Table 2-2. T_1 values of 1, 10, and 25 wt% NaOH solutions without cellulose powder measured from the ^{23}Na NMR relaxation time measurements at 133 MHz

NaOH concentration (wt%)	T_1 (ms)
1	41.3
10	31.7
25	11.7

2.3.7. Crystal Transition Mechanism from Cellulose I to Cellulose II

Fig 2-13 shows the mechanism of the crystal transition from cellulose I to alkali cellulose during the temperature-decrease process. In this study, it was observed that the crystal transition in a

low-concentration alkali solution occurs only at low temperatures. This transition involves the disruption of intrachain hydrogen bonds and subsequent conformational changes in the cellulose molecular chains toward a more stable orientation. The disruption of hydrogen bonds is attributed to the penetration of NaOH in the crystal structure of cellulose, which also reduces their mobility.

NaOH cannot penetrate the cellulose crystals at room temperature. However, Na^+ ions adopt a solvated conformation in 7–10 wt% NaOH solutions at low temperatures [19]. Miyamoto et al. reported an increase in the density of water near cellulose at low temperatures based on computational simulations [20], which explains the facile penetration of NaOH into the crystals. Consequently, their mobility decreases and residence time around the cellulose molecular chains increases, facilitating interactions, such as the bulkiness of NaOH and electrophilic interactions, between them. When a 4–30% NaOD solution was used during mercerization, the dissociated form of C3-OH increased substantially with an increase in NaOD concentration, whereas that of C6-OH increased negligibly [21]. This suggests that the partial dissociation of the OH group at the C3 position of cellulose occurs only under the conditions in which mercerization proceeds. In other words, not only are the intrachain hydrogen bonds of O2-O6 associated with the conformation at the C6 position important, but the changes in the intrachain hydrogen bonds of O3-O5 also play a crucial role. The partial dissociation of the OH groups of cellulose is expected to produce cellulose-ONa-type structures. This is because NaOH solutions are commonly used to pretreat cellulose during the preparation of cellulose

derivatives, wherein OH ions withdraw protons to produce the cellulose-ONa-type structure. Furthermore, hydroxide ions are presumed to penetrate the cellulose crystal and be present in the vicinity of Na ions as counter ions. It is possible that hydroxide ions may influence the crystal transition; however, their specific role could not be determined in this study. Nevertheless, they may disrupt intramolecular hydrogen bonds by partially dissociating the OH groups of cellulose molecules in the vicinity of Na ions. These interactions disrupt the intrachain hydrogen bonds between glucose residues, contributing to conformational changes in the cellulose molecular chains from a plane-sheet structure toward a more stable orientation with a disrupted plane. This results in lower hydrophobic interactions among the cellulose molecular chains. This further facilitates the penetration of molecules, such as water, into the crystal, thereby increasing the mobility of the cellulose molecular chains. Finally, during neutralization, washing, and drying, new O6-O3 intrachain hydrogen bonds associated with the *gt* conformation are formed, completing the crystal transition to cellulose II. Through the results and discussion in this chapter, it is suggested that in the crystal transition of cellulose I to II, the dynamics of Na ions (NaOH), and slight conformational changes in the cellulose molecules due to the disruption of intrachain hydrogen bonds have a significant effect. The difference between cellulose I and II has traditionally been attributed to the orientation of cellulose molecular chains, which is considered to differ in direction. However, since the mobility of cellulose molecular chains is also expected to decrease under low-temperature conditions, it is unlikely that the orientation of molecular

chains shifts from parallel to antiparallel based on the results of this chapter. Instead, the progression of crystalline transition is implied to be driven by more subtle changes.

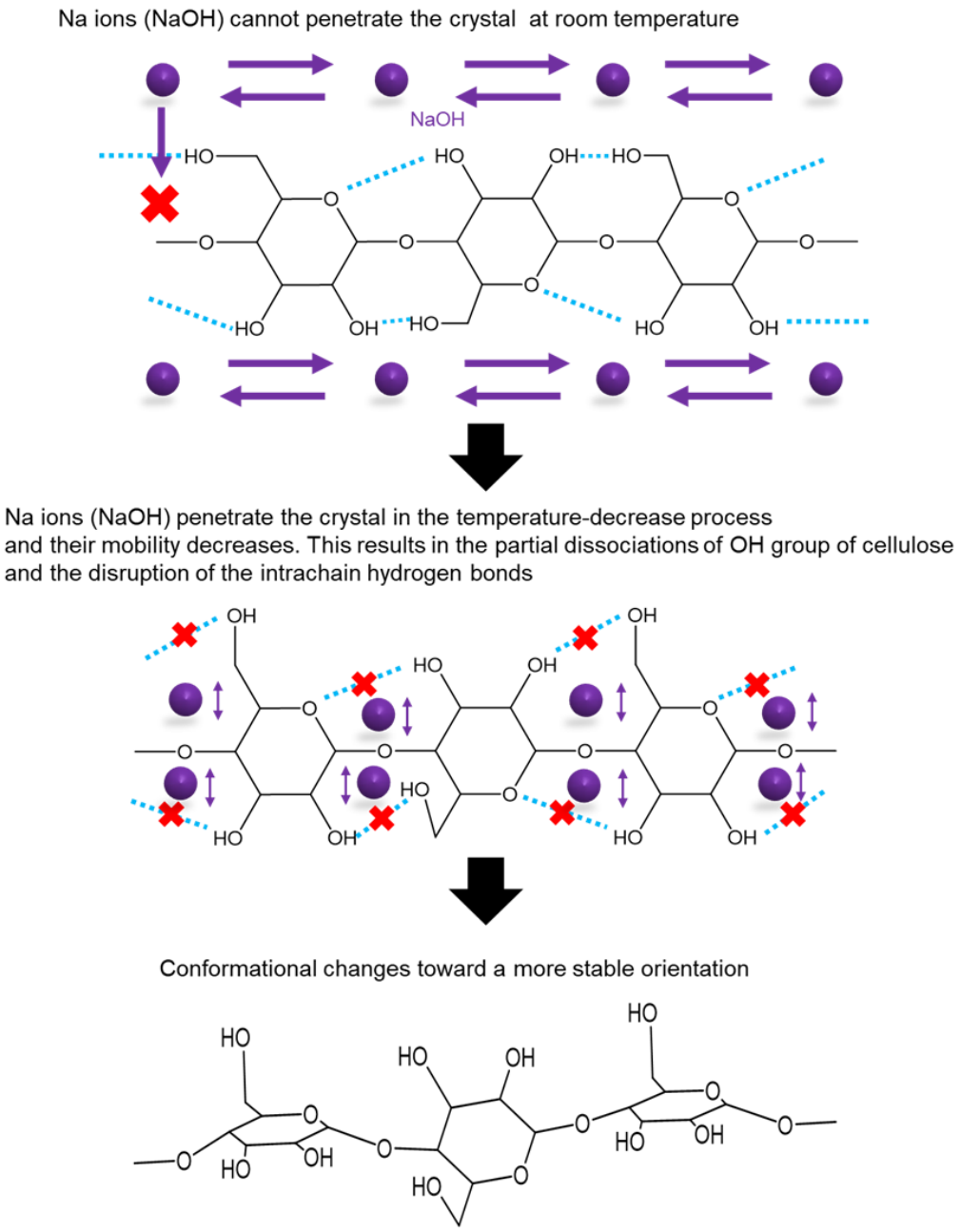

Fig. 2-13. Proposed mechanism for the defibrillation of the cellulose I molecular chains induced by alkali treatment at low temperatures.

2.4. Conclusion

In this chapter, the mechanism of the crystal transition from cellulose I to cellulose II during low-concentration NaOH treatment at low temperatures was traced, especially the transition behavior of the cellulose chains of cellulose I to alkali cellulose. The crystal transition was a non-Arrhenius reaction that proceeded in a shorter time at lower temperatures. Hence, the temperature condition is one of the crucial factors for the crystal transition. Subsequently, the conformational changes in the cellulose molecular chain and NaOH dynamics at low temperatures were traced. In situ solid-state ^{13}C NMR spectra revealed a shift in the C6 resonance line, indicating a conformational change from *trans-gauche* (*tg*) to *gauche-gauche* (*gg*), and an upfield shift in the C4 resonance line, indicating the disruption of the O6-O2 and O5-O3 intrachain hydrogen bonds. Computational simulations indicate that conformational changes in the cellulose molecular chains from a plane-sheet structure toward a more stable orientation with a disrupted plane occurred, resulting in lower hydrophobic interactions among the cellulose molecular chains. This could facilitate the penetration of molecules such as water into the crystal, thereby promoting the crystal transition. ^{23}Na NMR relaxation time measurements showed that the mobility of Na ions was significantly reduced at the alkali concentration at which the crystal transition progressed, suggesting that NaOH penetrates the crystal region and interacts with cellulose, resulting in sufficient residence times and longer correlation times for Na ions. These increased interactions could facilitate the disruption of the intrachain hydrogen bonds, thus contributing to the crystal transition. A similar increase in the correlation time of the Na ions was

observed during mercerization with a high-concentration NaOH solution. This indicates that NaOH dynamics play a crucial role in crystal transition.

The key condition for the crystal transition from cellulose I to II is the dynamics of the NaOH molecule, which is shown to decrease in mobility as the NaOH molecule penetrates the crystal as the temperature decreases. The decrease in mobility is due to the interaction with cellulose, and the crystal transition proceeds through the cleavage of hydrogen bonds. The clarification of the crystal transition mechanism suggests that the crystal transition from cellulose I to II can be controlled by adjusting the cooling temperature and the concentration of NaOH solution. In other words, it is possible to control the distribution and ratio of cellulose I and II by adjusting the cooling temperature in the low-concentration NaOH treatment, and to prepare all-cellulose composite materials containing cellulose I and II.

REFERENCES

[1] E. Dinand, M. Vignon, H. Chanzy, and L. Heux, "Mercerization of primary wall cellulose and its implication for the conversion of cellulose I → cellulose II," *Cellulose*, vol. 9, no. 1, pp. 7–18, 2002, doi: 10.1023/A:1015877021688.

[2] H. Wang, H. Kataoka, S. Tsuchikawa, and T. Inagaki, "Terahertz time-domain spectroscopy as a novel tool for crystallographic analysis in cellulose: Cellulose I to cellulose II, tracing the structural changes under chemical treatment," *Cellulose*, vol. 29, no. 6, pp. 3143–3151, 2022, doi: 10.1007/s10570-022-04493-x.

[3] A. Isogai and R. H. Atalla, "Dissolution of cellulose in aqueous NaOH solutions," *Cellulose*, vol. 5, no. 4, pp. 309–319, 1998, doi: 10.1023/A:1009272632367.

[4] K. Kamide, K. Okajima, T. Matsui, and K. Kowsaka, "Study on the solubility of cellulose in aqueous alkali solution by deuteration IR and 13C NMR," *Polym J*, vol. 16, no. 12, pp. 857–866, 1984, doi: 10.1295/polymj.16.857.

[5] K. Kamide, K. Kowsaka, and K. Okajima, "Determination of intramolecular hydrogen bonds and selective coordination of sodium cation in alkalicellulose by cp/mass 13C NMR," *Polym J*, vol. 17, no. 5, pp. 707–711, 1985, doi: 10.1295/polymj.17.707.

[6] B. Lindman, G. Karlström, and L. Stigsson, "On the mechanism of dissolution of cellulose," *J Mol Liq*, vol. 156, no. 1, pp. 76–81, 2010, doi: 10.1016/j.molliq.2010.04.016.

[7] W. G. Glasser *et al.*, "About the structure of cellulose: Debating the Lindman hypothesis," *Cellulose*, vol. 19, no. 3, pp. 589–598, 2012, doi: 10.1007/s10570-012-9691-7.

[8] Y. Nishiyama, G. P. Johnson, A. D. French, V. T. Forsyth, and P. Langan, "Neutron crystallography, molecular dynamics, and quantum mechanics studies of the nature of hydrogen bonding in cellulose Iβ," *Biomacromolecules*, vol. 9, no. 11, pp. 3133–3140, 2008, doi: 10.1021/bm800726v.

[9] P. Langan, Y. Nishiyama, and H. Chanzy, "A revised structure and hydrogen-bonding system in cellulose II from a neutron fiber diffraction analysis," J Am Chem Soc, vol. 121, no. 43, pp. 9940–9946, 1999, doi: 10.1021/ja9916254.

[10] S. Nomura, S. Sato, and T. Erata, "DFT approach to the pathway of conformational changes of cellulose C6-hydroxymethyl group with simple cellotetraose model involving the mechanism of mercerization process," *Chem Phys Lett*, vol. 742, no. October 2019, p. 137154, 2020, doi: 10.1016/j.cplett.2020.137154.

[11] D. Massiot *et al.*, "Modelling one- and two-dimensional solid-state NMR spectra," *Magnetic Resonance in Chemistry*, vol. 40, no. 1, pp. 70–76, 2002, doi: 10.1002/mrc.984.

[12] F. Horii, A. Hirai, and R. Kitamaru, “Solid-state 13C-NMR study of conformations of oligosaccharides and cellulose: Conformation of CH2OH group about the exo-cyclic C-C bond,” *Polymer Bulletin*, vol. 10, no. 7–8, pp. 357–361, 1983, doi: 10.1007/BF00281948.

[13] P. Phyo, T. Wang, Y. Yang, H. O’Neill, and M. Hong, “Direct determination of hydroxymethyl conformations of plant cell wall cellulose using 1 H polarization transfer solid-state NMR,” *Biomacromolecules*, vol. 19, no. 5, pp. 1485–1497, 2018, doi: 10.1021/acs.biomac.8b00039.

[14] A. Idström, S. Schantz, J. Sundberg, B. F. Chmelka, P. Gatenholm, and L. Nordstierna, “13C NMR assignments of regenerated cellulose from solid-state 2D NMR spectroscopy,” *Carbohydr Polym*, vol. 151, pp. 480–487, 2016, doi: 10.1016/j.carbpol.2016.05.107.

[15] G. Zuckerstätter, N. Terinte, H. Sixta, and K. C. Schuster, “Novel insight into cellulose supramolecular structure through 13C CP-MAS NMR spectroscopy and paramagnetic relaxation enhancement,” in *Carbohydrate Polymers*, 2013, pp. 122–128. Doi: 10.1016/j.carbpol.2012.05.019.

[16] S. Park, D. K. Johnson, C. I. Ishizawa, P. A. Parilla, and M. F. Davis, “Measuring the crystallinity index of cellulose by solid state 13C nuclear magnetic resonance,” *Cellulose*, vol. 16, no. 4, pp. 641–647, 2009, doi: 10.1007/s10570-009-9321-1.

[17] F. Porro, O. Bedue, H. Chanzy, and L. Heux, “Solid-state 13 C NMR study of Na -cellulose complexes,” *Biomacromolecules*, vol. 8, no. 8, pp. 2586–2593, 2007, doi: 10. 1021/bm0702657.

[18] N. Isobe, K. Noguchi, Y. Nishiyama, S. Kimura, M. Wada, and S. Kuga, “Role of urea in alkaline dissolution of cellulose,” *Cellulose*, vol. 20, no. 1, pp. 97–103, 2013, doi: 10.1007/s10570-012-9800-7.

[19] T. Yamashiki, K. Kamide, K. Okajima, K. Kowsaka, T. Matsui, and H. Fukase, “Some characteristic features of dilute aqueous alkali solutions of specific alkali concentration (2.5 mo11- 1) which possess maximum solubility power against cellulose,” *Polym J*, vol. 20, no. 6, pp. 447–457, 1988, doi: 10.1295/polymj.20.447.

[20] H. Miyamoto, U. Schnupf, K. Ueda, and C. Yamane, “Dissolution mechanism of cellulose in a solution of aqueous sodium hydroxide revealed by molecular dynamics simulations,” *Nord Pulp Paper Res J*, vol. 30, no. 1, pp. 67–77, 2015, doi: 10.3183/npprj-2015-30-01-p067-077.

[21] A. Isogai, “NMR analysis of cellulose dissolved in aqueous NaOH solutions,” *Cellulose*, vol. 4, no. 2, pp. 99–107, 1997, doi: 10.1023/A:1018471419692.

Chapter 3.

Crystallinity Improvement of Cellulose II by Multicycle Post-Treatment with Low-Concentration NaOH Treatments

3.1. Introduction

In this chapter, I aim to further improve the cellulose II crystallinity and fabricate high-strength cellulose II materials. Based on the obtained results, a detailed investigation of structural changes is conducted when NaOH does not penetrate the cellulose crystal regions. Cellulose II has excellent luster, dyeability, drape, and other properties; thus, it is applied as an indispensable and important material in various industrial fields, such as fibers and films. However, the crystallinity of cellulose II decreases during the crystal transition. The preparation of highly crystalline cellulose II using simpler methods could further expand the applications of cellulose. The post-treatment with low-concentration NaOH aqueous solutions [1]–[6] has long been used as a method to increase the crystallinity of cellulose II. Our group previously proposed a mechanism for improving the crystallinity of cellulose II via NaOH post-treatment [7]. As shown in Fig 1-3, the surface areas of cellulose II fibril can be classified as accessible surface and inaccessible surface, depending on whether solvent molecules, especially water, can access them [8], [9]. These surface regions could be distinguished by solid-state ^{13}C NMR spectroscopy [8], [9] and confirmed by dynamic nuclear polarization solid-state NMR spectroscopy [10]. Discussion of the post-treatment should consider the crystallization of the inaccessible surfaces because they are easily crystallized owing to their soft structure and high mobility. In our previous study, NaOH post-treatment was performed with aqueous NaOH solutions of various concentrations. It was found that the post-treatment with a 10 wt% NaOH solution resulted in maximum cellulose II crystallinity and that the proportion of inaccessible

surfaces/amorphous regions decreased as the crystallinity increased during post-treatment. In addition, the solid-state ^{13}C CP/MAS NMR spectrum of the cellulose II sample soaked in 10 wt% NaOH solution is a mixture of cellulose II and Na-Cellulose I. Based on these results, a crystallinity-improvement mechanism was proposed; the rearrangement of cellulose molecules in inaccessible surfaces occurs via the penetration of NaOH into these inaccessible surfaces, followed by the subsequent conversion of these inaccessible surfaces into crystalline regions. Furthermore, the crystallinity of cellulose II has been reported to be greater after repeated alkali post-treatments multiple times than after a single post-treatment [4]–[6]. This indicates that there is room to obtain more highly crystalline cellulose II by optimizing the post-treatment conditions. In addition, a detailed analysis of the compositional changes in the cellulose II fibrils over repeated post-treatment would aid in improving the understanding of the crystal structures of cellulose.

In this chapter, two post-treatment methods with a 10 wt% NaOH solution were examined to elucidate the mechanism for improvements in crystallinity and to further improve the crystallinity: long-term single-cycle post-treatment and multicycle post-treatment. In addition, controlling the mechanical properties of cellulose II fibers was attempted by employing the post-treatment. Fig 3-1 shows a schematic diagram of the expected crystallinity improvements achieved by long-term single-cycle post-treatment and multicycle post-treatment. The upper panel in Fig 3-1 shows the expected mechanism for the long-term single-cycle post-treatment. As crystallization proceeds from the

inaccessible surface, the crystalline regions spread toward the amorphous regions during the post-treatment. Therefore, if the post-treatment time is increased, crystallization may proceed over a wider surface area. However, once crystallization occurs on all inaccessible surfaces, further crystallinity improvement is not expected. On the other hand, during multicycle post-treatment, which is depicted in the lower panel in Fig 3-1, the crystallization is expected to proceed once more on the inaccessible surfaces expanded by previous post-treatment cycles. If our proposed mechanism is correct, multicycle post-treatment may be expected to lead to higher crystallinity improvements than a single post-treatment of a longer duration. In this chapter, two different post-treatment methods were implemented to compare the crystallinity, and the crystallinity improvement mechanism is discussed based on the observed proportion changes of crystalline regions, accessible surfaces, and inaccessible surfaces/amorphous regions during post-treatment. Furthermore, this post-treatment has the potential for the preparation of highly crystalline cellulose II material. Therefore, the post-treatments were conducted on cellulose II fiber, and the crystallinity and mechanical properties were analyzed.

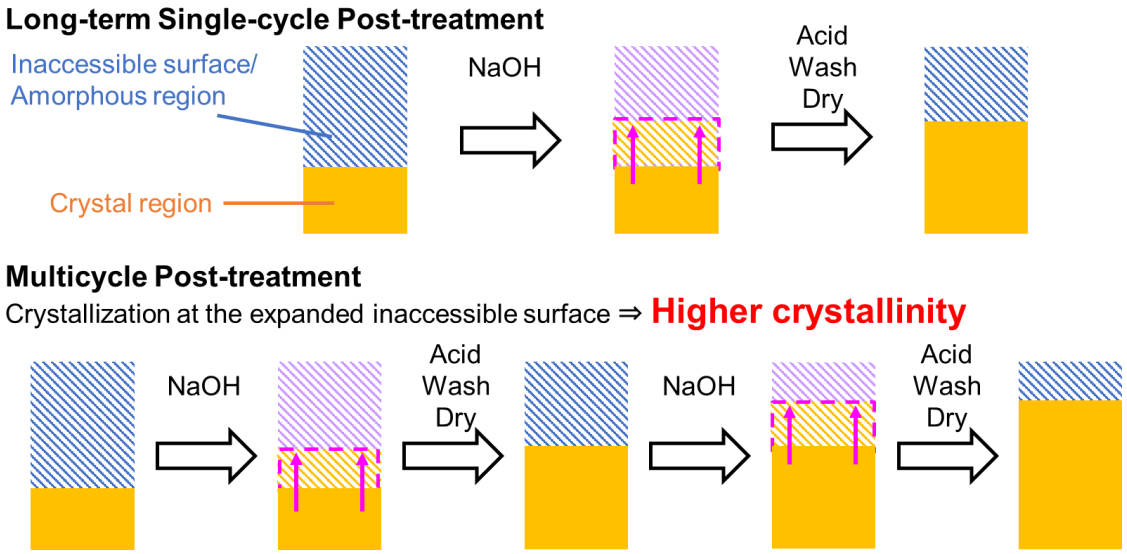

Fig. 3-1. Schematic images of the anticipated crystallinity improvement mechanisms for a long-term single-cycle post-treatment and multicycle post-treatment. In the long-term single-cycle post-treatment, the area that can be transformed into crystals (pink line) was limited. After the crystallinity was improved to some extent, further increases in the treatment time was not expected to lead to additional improvements in the crystallinity. During multicycle post-treatment, further crystallization was expected to progress from the expanded inaccessible surface regions in the previous cycle. Crystals were expected to accumulate with each post-treatment cycle, thereby enhancing the crystallinity compared to that achievable with a long-term single-cycle post-treatment.

3.2. Methods

3.2.1. Materials

Whatman CF11 cellulose powder (Whatman International Ltd., Kent, England) was used for the preparation of initial mercerized cellulose II powder. Cellulose II fibers, fortisan (Celanese Corp., Dallas, USA), polynosic (Teijin Limited, Tokyo, Japan), and a commercial rayon for handicrafts (Perugia Corp., Osaka, Japan) were used for the multicycle post-treatments. Fortisan is produced by the transition from cellulose acetate to cellulose II, and rayon and polynosic are produced by the regeneration from the dissolution of cellulose I. The fiber width of polynosic is narrower than that of rayon. Therefore, these cellulose II fibers differ in their fabrication methods and shapes. NaOH (>97.0%) and H_2SO_4 (>95.0%) were purchased from FUJIFILM Wako Pure Chemical Corporation (Osaka, Japan). Deionized water (Elix@Essential3, Merck KgaA, Darmstadt, Germany) was used to prepare NaOH and H_2SO_4 aqueous solutions and to wash cellulose II samples after the neutralization treatments.

3.2.2. Preparation of the Initial Cellulose II Powder

Cellulose powder was mercerized with a 25 wt% NaOH solution for 2 h at room temperature (24 °C). The mercerized sample was neutralized with a 20 vol% H_2SO_4 solution at room temperature (24 °C) to bring its pH below 7.0. The sample was washed with deionized water and air-dried at room temperature (24 °C).

3.2.3. Long-term Single Post-Treatments

The initial cellulose II powder was treated with a 10 wt% NaOH solution for 2–16 h at room temperature (24 °C) to observe the effect of the treatment time on the results of the low-concentration alkali post-treatment. A 10 vol% H_2SO_4 solution was used for neutralization. The samples were washed with deionized water, air-dried at room temperature (24 °C), and subsequently analyzed via solid-state ^{13}C CP/MAS NMR and X-ray diffraction (XRD).

3.2.4. Multicycle Post-Treatments

For each post-treatment cycle, the initial cellulose II powder was treated with a 10 wt% NaOH solution for 2 h at room temperature (24 °C). Neutralization treatment was performed with a 10 vol% H_2SO_4 solution at room temperature (24 °C) to bring the pH of the powder below 7.0. The sample was washed with deionized water and air-dried at room temperature (24 °C). The next post-treatment was performed after the sample was dried. The post-treatment process was repeated up to nine times with the same sample. After each cycle, the dried samples were analyzed by solid-state ^{13}C CP/MAS NMR and XRD.

To evaluate the effects of alkali treatments, multicycle post-treatments using water were performed. The initial cellulose II powder was treated with water for 2h at room temperature (24 °C). The sample was air-dried at room temperature (24 °C). The next treatment was performed after the sample was dried. The post-treatment process was repeated up to three times using the same samples.

After each cycle, the dried samples were analyzed by solid-state ^{13}C CP/MAS NMR measurements.

3.2.5. Multicycle Post-Treatments including the Neutralization Treatment using Various Concentration H_2SO_4 Solutions

In a series of multicycle post-treatments, the low-concentration NaOH treatment and neutralization treatment with an H_2SO_4 aqueous solution were repeated. Multicycle post-treatment cycles were performed with the initial cellulose II powder by changing the concentration of the H_2SO_4 aqueous solution used for neutralization to evaluate the effect of neutralization treatment on the crystallinities of the samples. Each multicycle post-treatment was performed for 2 h at room temperature (24 °C) with a 10 wt% NaOH solution. The neutralization treatments were performed with 0 (water), 5, and 20 vol% H_2SO_4 solutions at room temperature (24 °C) to bring the pH of the powder below 7.0. The samples were washed with deionized water and air-dried at room temperature (24 °C). After each subsequent post-treatment cycle, the samples were dried, and the process was repeated up to three times for the same sample. The dried samples were analyzed by solid-state ^{13}C CP/MAS NMR after each post-treatment cycle.

3.2.6. Multicycle Post-Treatments with Various durations

Multicycle post-treatment cycles were performed with the cellulose II powder for various durations ranging from 2 to 12 h during the second to fourth cycles with a 10 wt% NaOH solution at room temperature (24 °C) to evaluate the effect of the post-treatment time on the crystallinities of the

samples. The treatment time was set to 2 h in all cycles prior to that in which the treatment time was changed. For example, when the treatment time was changed in the fourth cycle after treatment, the treatment times for cycles 1–3 were 2 h.

Furthermore, the total post-treatment time was divided into several cycles of 6, 8, and 10 h to optimize the treatment time and number of post-treatment cycles. Each post-treatment cycle on the cellulose II powder was performed with a 10 wt% NaOH solution at room temperature (24 °C). The samples were neutralized with a 10 vol% H_2SO_4 solution at room temperature (24 °C) to bring their pHs below 7.0. The samples were washed with deionized water and air-dried at room temperature (24 °C). Each cycle was performed after the sample was dried. The dried samples were analyzed by solid-state ^{13}C CP/MAS NMR.

3.2.7. Multicycle Post-Treatments using a 10 wt% NaOH Solution on Cellulose II Fiber

Multicycle post-treatments to cellulose II fibers were performed in two ways: tension-free and tensioned. The tension-free multicycle post-treatment was performed on fortisan, rayon, and polynosic. The use of various cellulose II fibers was intended to investigate whether there are any changes in the improvement in crystallinity based on factors such as their fabrication methods, and shapes. In each post-treatment cycle, a 10 wt% NaOH solution treatment was performed at room temperature (24 °C) for 2 h in the vat. One side of the cellulose II fibers was taped to the bottom of the vat to stabilize it during the multicycle post-treatment. After neutralization with a 10 vol% H_2SO_4

solution, it was washed with deionized water and air-dried at room temperature (24 °C). All post-treatments were performed after the samples were dried. The multicycle treatments were repeated up to a maximum of the third cycle for the fortisan and rayon, and up to the fourth cycle for polynosic.

The tensioned multicycle post-treatments were performed on fortisan and rayon with the self-stretching instrument shown in Fig 3-2. The edge of the bundle of fiber was taped and fastened with metal fittings. The other edge was secured to the reel of the self-constructed instrument and tension was applied by reeling. In the tensioned multicycle post-treatments on fortisan, the tensions applied to a single strand were 250 g, 200 g, 100 g, and 50g. In the tensioned post-treatments on rayon, sufficient tension was applied to straighten the strands. This was necessary because the rayon strands tended to shrink and break when the rayon strands with subjected to a NaOH solution under large tension. The 40 cm length of these bundles was soaked in a 10 wt% NaOH solution in the vat at room temperature (24 °C) for 2 h. This vat was switched 2 h later with the container filled with a 10 vol% H_2SO_4 solution. This vat was also switched 10 minutes later with the vat filled with deionized water to wash the cellulose II fiber samples. The bundle was washed by replacing the water in the vat until it became neutral. The washed samples were dried at room temperature (24 °C) under tension. Each post-treatment was performed after these samples were dried. The series of post-treatment were repeated up to a maximum of the third cycle. These fiber samples were analyzed via the solid-state ^{13}C CP/MAS spectra, XRD, tensile test, Polarizing Optical Microscopy (POM), and Scanning Electron

Microscopy (SEM).

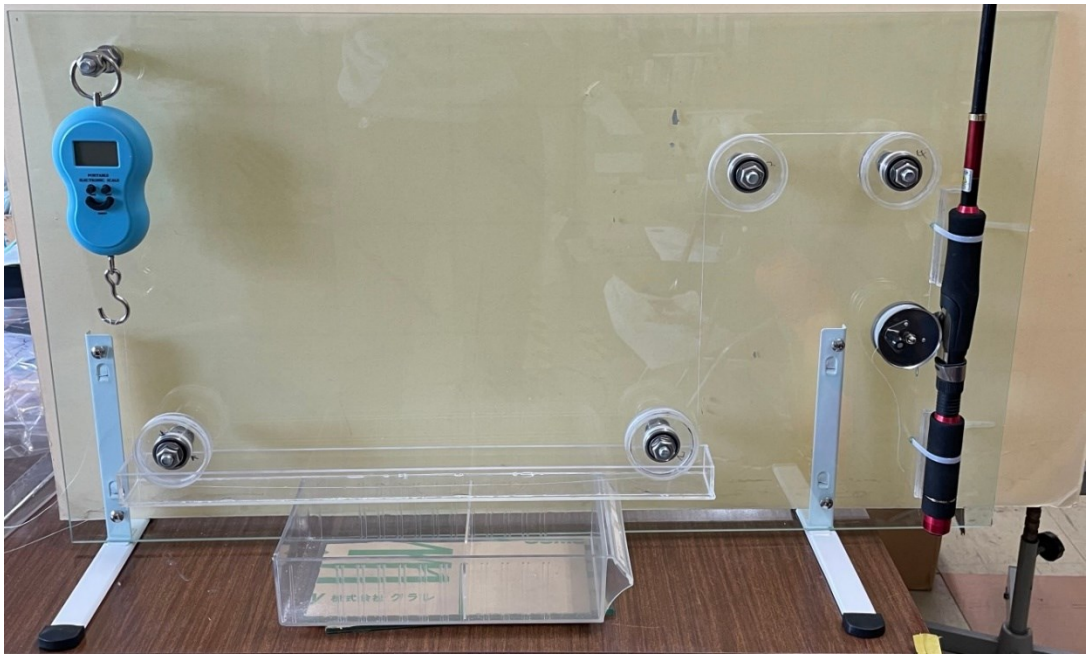

Fig.3-2. The self-stretching instrument for tensioned multicycle post-treatments on cellulose II fibers

3.2.8. Solid-State ^{13}C CP/MAS NMR Measurements

Solid-state ^{13}C CP/MAS NMR spectra were measured using a Bruker AVANCE NEO 500 spectrometer (Bruker, Germany) operating at 125 MHz with a 2.5 mm rotor and partly using a DSX300 spectrometer (Bruker, Germany) operating at 75 MHz with 4 mm rotor, at Instrumental Analysis Support Office, Frontier Chemistry Center, Faculty of Engineering, Hokkaido University, Japan. The frequency of MAS was 10 kHz. All spectra were obtained with a ^{1}H 90degree with a pulse length of 4.0us, a contact time of 1.5ms, and a repetition time of 4s. Spectra were calibrated with the carbonyl carbon peak of glycine (176.46 ppm). A ramp sequence was used for the contact pulse and a tppm-15 sequence for decoupling. Deconvolution of the C4 resonance lines was performed using the

Dmfit2017 line-fitting program [11]. A lorentz geometry was used for each line; C4 resonance lines were divided into crystalline regions, accessible surfaces, and inaccessible surface/amorphous lines, as shown in Fig 3-3 [7]. The chemical shifts for cellulose II crystal region are 88.9 and 87.8 ppm, for accessible surface are 86.9 and 85.9 ppm, and for inaccessible surfaces/amorphous is 84.2 ppm. The proportions of each region were calculated from the integrated area under these resonance lines.

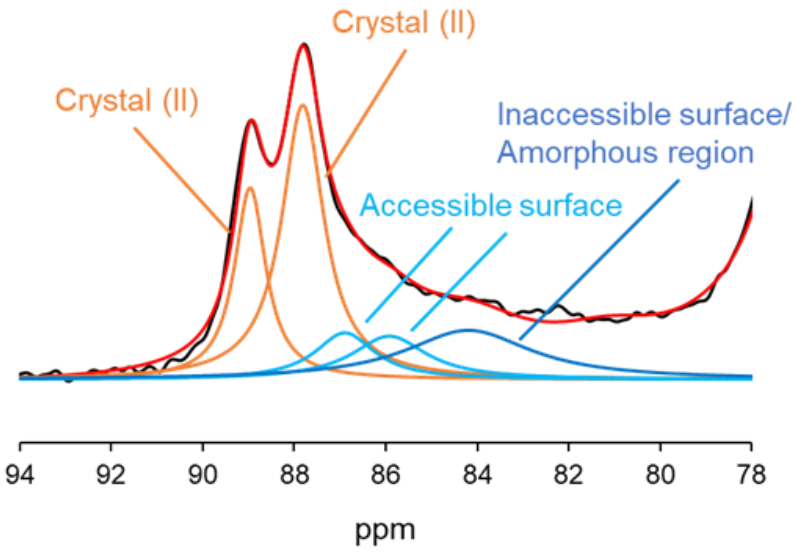

Fig. 3-3. Deconvolution of the solid-state ^{13}C CP/MAS NMR C4 resonance lines of dry cellulose II [7].

3.2.9. X-ray Diffraction (XRD) Analysis

XRD measurements were performed in transmission on SmartLab (Rigaku Co., Ltd., Tokyo, Japan), an X-ray diffractometer equipped with a CuKα anode (λ = 1.5418 Å) powered at 45kV. The scan range was 5° to 40° with a step value of 0.02°. The peak fitting was performed using the fitting software, SmartLab Studio II (Rigaku Co., Ltd., Tokyo, Japan) with three pseudo-Voigt functions to

obtain peak positions, peak heights, half-widths, and crystal sizes from ($1\bar{1}0$), (110), and (020) peaks.

3.2.10. Tensile Tests

Tensile tests were performed on the cotton fiber samples using an AG-100kNXplus (SHIMADZU CORPORATION, Kyoto, Japan). The samples were fixed using a pneumatic capstan-type yarn gripper (SHIMADZU CORPORATION, Kyoto, Japan) and pulled from a distance of 10 cm at a speed of 1 mm/s. A stress-strain curve (S-S curve) was drawn for each sample, with stress on the X-axis and strain on the Y-axis. The maximum stress, breaking strain, Young's moduli, and toughness of the cellulose II fiber samples obtained by the multicycle post-treatments on cellulose II fiber were determined. Young's moduli of the cellulose II fiber were calculated as the initial slope of the S-S curves. The toughness was calculated as the integral area under each S-S curve.

3.2.11. Polarizing Optical Microscopy (POM)

The as-prepared fortisan and rayon, and fortisan and rayon samples obtained by first-cycle post-treatment were fixed on glass slides with carbon tape, and observed using a polarizing microscope (BX40 DP70-WPCXP, OLYMPUS Corp., Tokyo, Japan). Observations were performed using an objective lens with a magnification of 10x.

3.2.12. Scanning Electron Microscopy (SEM)

The as-prepared fortisan and fortisan samples obtained by first-cycle post-treatment were

fixed to the sample stand with carbon tape, and gold deposition was conducted using a vacuum deposition instrument (E-1010, Hitachi, Ltd., Tokyo, Japan). Subsequently, microscopic observations were performed using Scanning Electron microscopy (JSM-70001FA, JEOL Ltd, Tokyo, Japan) at High-voltage Electron Microscope Laboratory, Faculty of Engineering, Hokkaido Univ, Sapporo, Japan, using an acceleration voltage of 30.0 kV. SEM images were acquired at 50x and 200x magnification.

3.3. Results and Discussions

3.3.1. Long-term Single-Cycle Post-Treatments

Fig 3-4 shows the proportions of the crystalline regions, accessible surfaces, and inaccessible surfaces/amorphous regions of the samples after the long-term single-cycle post-treatments; the data were calculated by deconvoluting the C4 resonance lines of each ^{13}C CP/MAS NMR spectrum. The crystallinities of the samples increased during post-treatment for up to 8 h but did not change with further treatment. This suggests that in the case of a long-term single-cycle post-treatment, the improvement in crystallinity was limited even with longer post-treatment times. The maximum crystallinity achieved was 59%, which was approximately 10% greater than the crystallinity of the initial cellulose II powder. In terms of surface area, the proportion of inaccessible surfaces/amorphous regions decreased with increasing crystallinity. This result confirmed our previously reported mechanism in which inaccessible surface regions are converted into crystalline regions by the rearrangement of the cellulose molecules, ultimately increasing their crystallinity. During the post-treatment process, the following changes were observed within the cellulose fibrils. First, the rearrangement of the cellulose molecules occurred on the inaccessible surfaces, and, as previously noted, crystallization and growth occurred from the boundaries between the crystalline and inaccessible surface regions. When all accessible surfaces were completely rearranged, the crystallinity of the fibrils did not increase further, even after longer post-treatment times. When the maximum crystallinity was achieved, the accessible and inaccessible surfaces expanded alternately.

This observation suggested that NaOH did not penetrate the crystalline regions during the post-treatment process; instead, it penetrated only the amorphous regions, thereby affecting the rearrangement of cellulose molecules only in these regions.

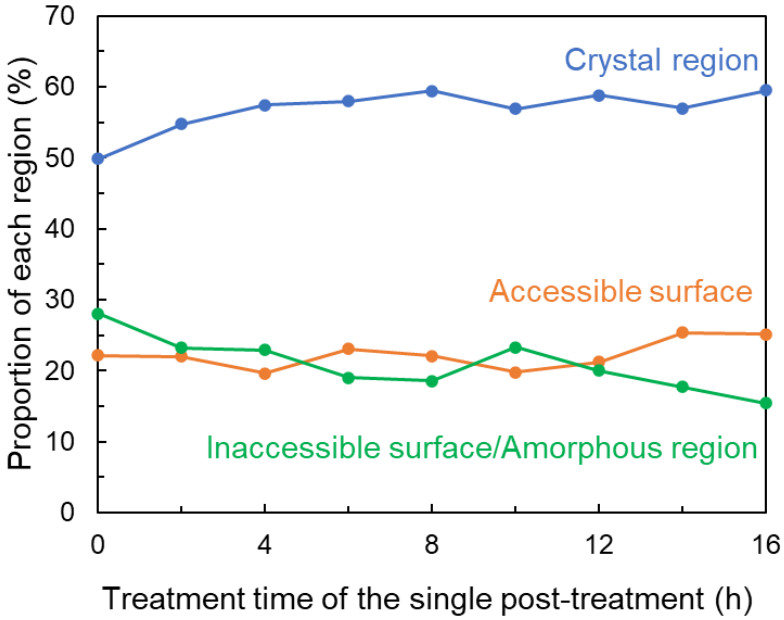

Fig. 3-4. Proportions of crystalline regions (blue line), accessible surfaces (orange line), and inaccessible surfaces/amorphous regions (green line) determined from the ^{13}C CP/MAS NMR spectra of cellulose fibrils subjected to a long-term single-cycle posttreatment.

Fig 3-5 shows the crystal sizes of the samples obtained after a long-term single-cycle post-treatment, as determined by XRD measurements. The crystal sizes of the samples increased by approximately 10%–20% for each plane over the course of 2–8 hours, but did not increase further during longer post-treatment. The NMR and XRD results were consistent, at least in terms of their trends.

In general, high concentrations (20%–25%) of the NaOH aqueous solution must be used for

mercerization at room temperature (24 °C); a 10% NaOH solution can hardly be used for this purpose. As shown by this behavior, the NaOH in a 10 wt% NaOH solution did not penetrate the crystalline regions but did penetrate the inaccessible surface regions. However, a certain amount of time is required for the NaOH to penetrate all areas of the inaccessible regions. The results also clearly show that the long-term single-cycle post-treatment increased the maximum crystallinity by no more than approximately 10%.

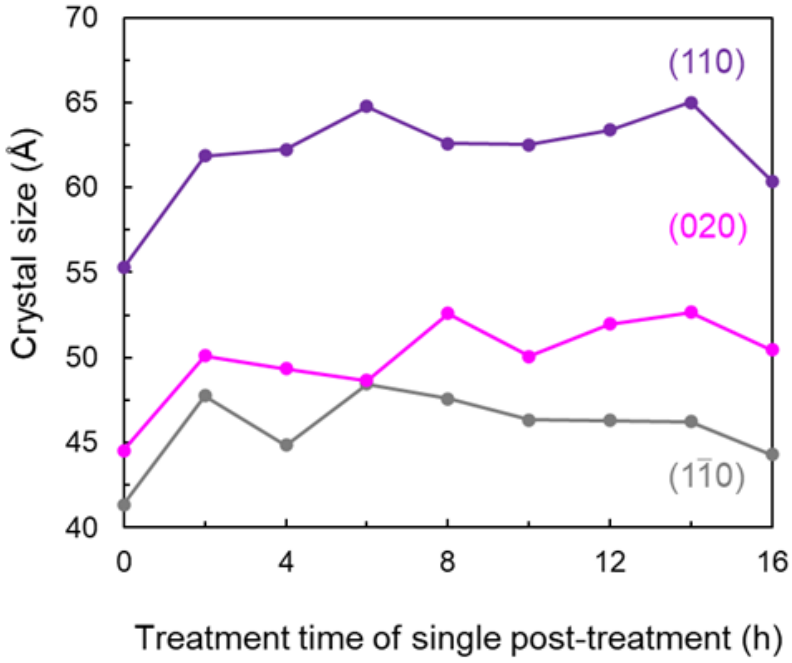

Fig. 3-5. Crystal sizes in the (1$\bar{1}$0) (gray line), (110) (purple line), and (020) (pink line) planes estimated from the X-ray diffraction profiles of cellulose II after a long-term single-cycle post-treatment.

3.3.2. Multicycle Post-Treatments

Fig 3-6 shows the proportions of crystalline regions, accessible surfaces, and inaccessible surfaces/amorphous regions determined by C4 resonance line-fitting of the ^{13}C CP/MAS NMR spectra

of the samples subjected to the multicycle post-treatments. The crystallinities of the samples increased over up to three cycles of post-treatment, reaching a maximum value of 69%. This value was 20% greater than that of the initial cellulose II powder and 10% greater than that of the long-term single-cycle post-treated sample. These findings confirmed the effectiveness of multicycle post-treatment in improving the crystallinity of cellulose II and verified the accuracy of our proposed crystallinity improvement mechanism. When the maximum crystallinity of cellulose II was achieved in the fourth to ninth cycles of post-treatment, no significant change in crystallinity was further observed. In terms of surface areas, the proportion of inaccessible surfaces/amorphous regions decreased with increasing crystallinity up to the third post-treatment cycle. This result also verified the accuracy of our proposed crystallinity improvement mechanism, where in the inaccessible surface penetrated by the NaOH underwent crystallization. After achieving the maximum crystallinity of cellulose II in the fourth to ninth post-treatment cycles, no further significant change in crystallinity was observed. This was attributed to the following characteristics. Crystallization on the inaccessible surfaces could only spread toward the amorphous regions. As the amorphous regions decreased by the multicycle post-treatment, the inaccessible surface regions in which crystallization could proceed gradually diminishes, and the improvement in crystallinity was saturated. After reaching saturation in crystallinity, a slight decrease in crystallinity occurred from the seventh cycle onwards, suggesting the possibility of minor crystallinity degradation.

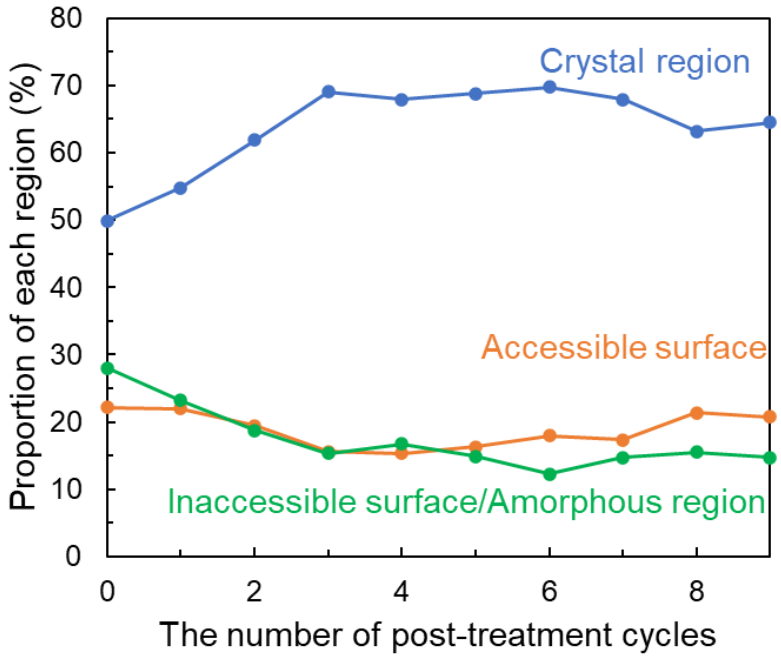

Fig. 3-6. Proportions of crystalline regions (blue line), accessible surfaces (orange line), and inaccessible surfaces/amorphous regions (green line) evaluated from the solid-state ^{13}C CP/MAS NMR spectra of cellulose II after multicycle post-treatment.

Fig 3-7 shows the crystal sizes obtained from the XRD measurements of the samples obtained after the multicycle post-treatment. When multicycle post-treatment was performed for up to three cycles, the crystal sizes increased in all planes as the number of post-treatment cycles increased. This finding indicates that the crystal size increases with increasing crystallinity, as estimated from the solid-state ^{13}C CP/MAS NMR spectra. The crystal sizes of the samples obtained after multicycle post-treatment were larger than those of the samples obtained after long-term single-cycle post-treatments. This was consistent with the fact that the crystallinities estimated from the solid-state ^{13}C CP/MAS NMR spectra were greater for samples subjected to multicycle post-treatment than for those subjected to long-term single-cycle post-treatment. After the seventh cycle, when the crystallinity decreased in

Fig 3-6, the hydrophobic (110) plane decreased slightly and the (020) and hydrophilic ($1\bar{1}0$) planes increased. This suggested that the orientations of the molecular chains may have changed slightly.

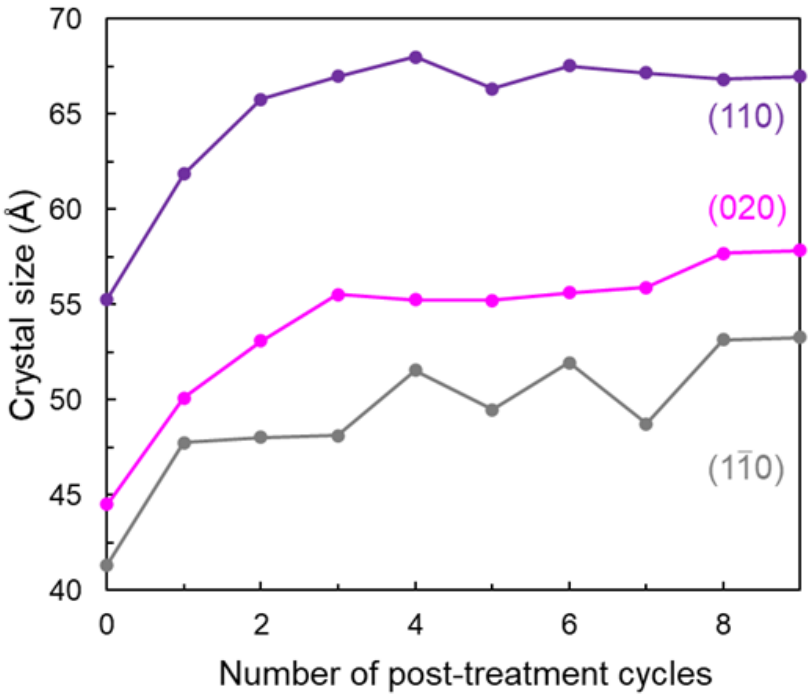

Fig. 3-7. Crystal sizes in the ($1\bar{1}0$) (gray line), (110) (purple line), and (020) (pink line) planes estimated from the XRD profiles of cellulose II after multicycle post-treatment.

Fig 3-8 shows the proportions of the crystalline regions, accessible surfaces, and inaccessible surfaces/amorphous regions determined by C4 resonance line-fitting of the ^{13}C CP/MAS NMR spectra of the samples subjected to the multicycle post-treatments using water. After the first cycle of post-treatment, the crystallinity was 52%, a 3% increase from the initial cellulose II. However, the value of the crystallinity was lower than that of the sample obtained by the first-cycle post-treatment with a 10 wt% NaOH solution. Furthermore, crystallinity did not improve even when the post-treatments were repeated for more second-cycle. Therefore, it was confirmed that the multicycle

post-treatments with a 10 wt% NaOH solution are more effective than multicycle post-treatments with water in the crystallinity improvement.

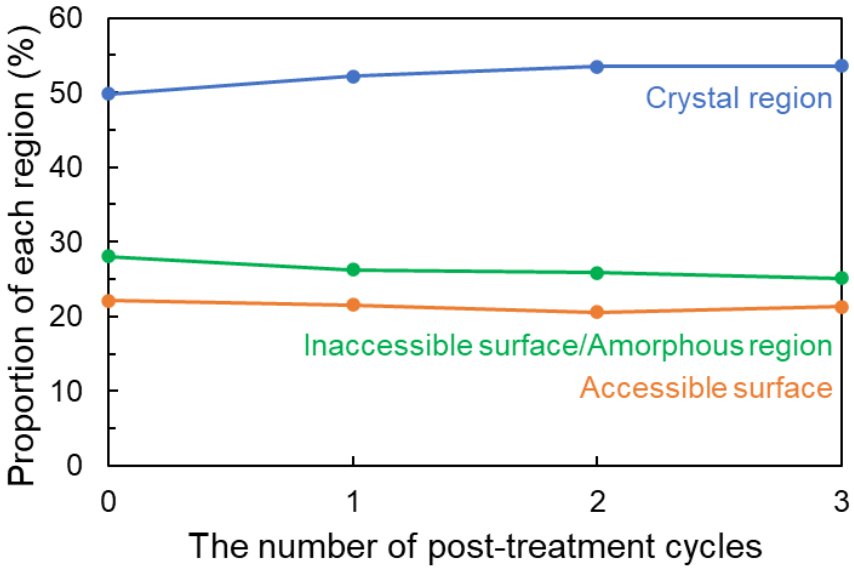

Fig. 3-8. Proportions of crystalline regions (blue line), accessible surfaces (orange line), and inaccessible surfaces/amorphous regions (green line) evaluated from the solid-state ^{13}C CP/MAS NMR spectra of cellulose II after multicycle post-treatments using water.

3.3.3. Multicycle Post-Treatments including the Neutralization Treatments using Various Concentration H_2SO_4 Solutions

In a series of multicycle post-treatments, the low-concentration alkali treatment and neutralization treatment with an H_2SO_4 aqueous solution were repeated. Repeated neutralization may have improved the crystallinity of cellulose II. Thus, to evaluate this effect, multicycle post-treatments including neutralization treatment with 0 (deionized water), 5, 10 (same as in Fig 3-6), and 20 vol% H_2SO_4 solutions were performed. As shown in Fig 3-6, the crystallinity of cellulose II continuously improved up to the third post-treatment cycle when a 10 vol% H_2SO_4 solution was used for

neutralization. Therefore, multicycle post-treatments with H_2SO_4 solutions of different concentrations were performed for up to three cycles. Fig 3-9. shows the proportions of the crystalline regions, accessible surfaces, and inaccessible surfaces/amorphous regions of the samples obtained following multicycle post-treatment. The crystallinity of the sample subjected to a single-cycle post-treatment was most improved when a 20 vol% H_2SO_4 solution was used, which was consistent with our previous report [7]. However, the crystallinity of the sample subjected to two-cycle post-treatment decreased and that of the sample subjected to three-cycle post-treatment was identical to that of the sample subjected to one cycle of post-treatment. The use of a 20 vol% H_2SO_4 solution for neutralization treatment led to the hydrolysis of the crystalline regions after two cycles of post-treatment, which suggested that some parts of the inaccessible surface were less crystallizable than others. On the other hand, multicycle post-treatment including neutralization treatment with 0, 5, or 10 vol% H_2SO_4 solution led to continuous improvements in the crystallinity for up to three post-treatment cycles. Furthermore, higher crystallinities were observed when 5 and 10 vol% H_2SO_4 solutions were used than when a 0% H_2SO_4 solution was used. This result suggested that the use of a low-concentration H_2SO_4 solution for neutralization treatment was effective in improving the crystallinity during multicycle post-treatment.

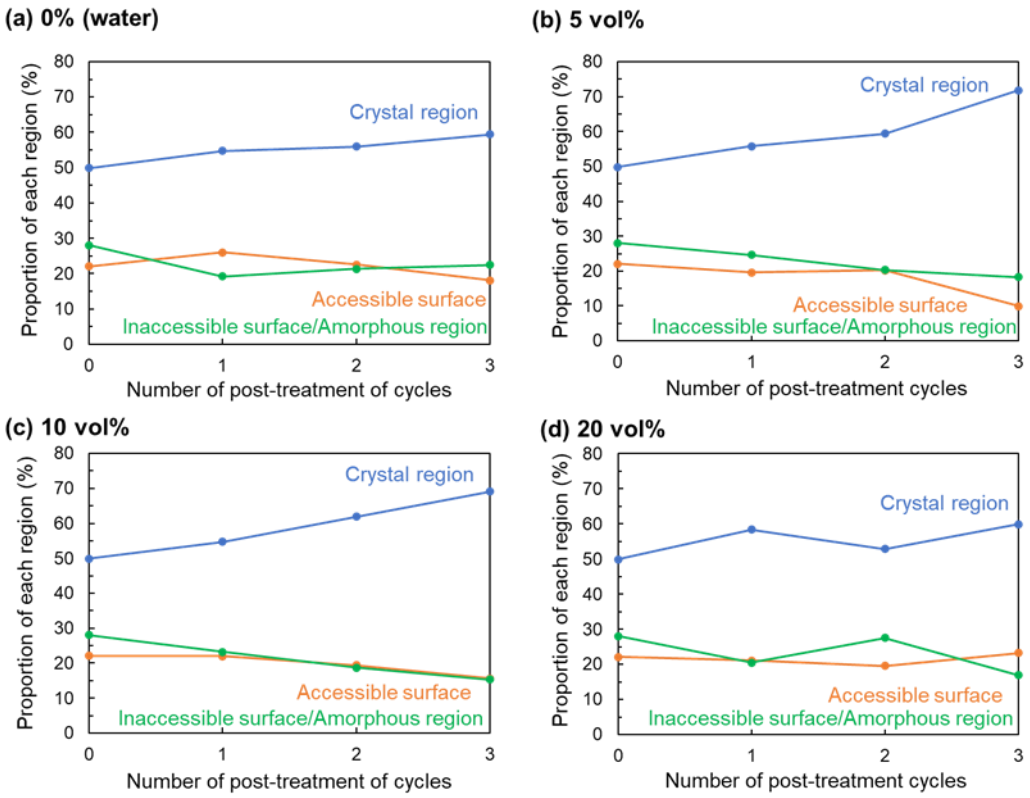

Fig. 3-9. Proportions of crystalline regions (blue line), accessible surfaces (orange line), and inaccessible surfaces/amorphous regions (green line) evaluated from the ^{13}C CP/MAS NMR spectra of samples obtained after multicycle post-treatment with neutralization using (a) 0% (water), (b) 5 vol%, (c) 10 vol%, and (d) 20 vol% H_2SO_4 solutions.

3.3.4. Multicycle Post-Treatments with Various Treatment Times in the Second to Fourth Cycles

Multicycle post-treatments of the cellulose II powder were performed with treatment times varying from 2 to 12 h in the second to fourth cycles to evaluate the effect of the post-treatment time in each cycle. Fig 3-10(a) shows the proportions of crystalline regions, accessible surfaces, and inaccessible surfaces/amorphous regions of samples that underwent the first post-treatment cycle for 2 h and the second post-treatment cycle for 2–12 h. The crystallinities of the samples increased up to 2 h but did not improve during subsequent post-treatments. The maximum crystallinity achieved was

63%, which was higher than that of the sample obtained after a single post-treatment cycle for 2 h. Figs 3-10(b) and 3-10(c) show the proportions of the crystalline regions, accessible surfaces, and inaccessible surfaces/amorphous regions of samples that underwent multicycle post-treatment for 2 h in the first and second cycles and 2–12 h in the third cycle, and samples that underwent multicycle post-treatment for 2 h in the first to third cycles and 2–12 h in the fourth cycle, respectively. As shown in Fig 3-10(b), during the three post-treatment cycles, the crystallinities of the samples increased up to 2 h, after which they were not affected by further post-treatment. The maximum crystallinity achieved was 69%, which was higher than those of the samples obtained after the one- and two-cycle post-treatments. The crystallinities of the samples subjected to four post-treatment cycles for varying treatment times differed from those of the previous samples. As shown in Fig 3-10(c), the crystallinities of the samples did not increase significantly over four cycles of post-treatment. The maximum crystallinity achieved was 69%, which was identical to those of the samples subjected to multicycle post-treatment shown in Fig 3-6, and those of the samples subjected to three cycles of post-treatment for varying treatment times shown in Fig 3-10(b). This indicated that there was an upper limit to the crystallinity improvement, and that once this limit was reached, further repeated or prolonged post-treatment did not lead to additional improvements. These findings suggested that there were surface regions that were difficult to crystallize or difficult to reach with NaOH. In addition, our previous report [7] showed that the crystallinity was greatly enhanced by post-treatment at higher

temperatures than a room temperature, and the most significant improvement in crystallinity was achieved by post-treatment at 80 °C for 2 h and subsequent neutralization at room temperature, with resulted in a crystallinity of 62.7%. In comparison, in this study, an upper limit of crystallinity improvement was observed for crystallinity improvement, and the crystallinity at this limit was 69%. The significant improvement in crystallinity was achieved by optimizing the post-treatment time even at room temperature.

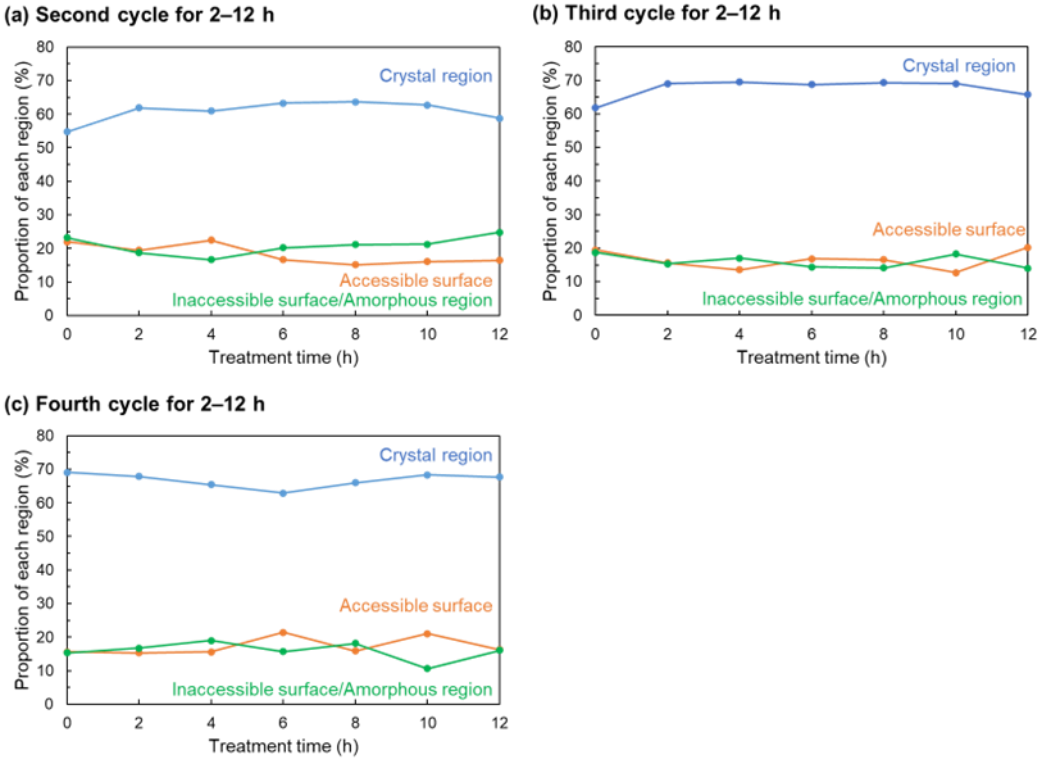

Fig. 3-10. Proportions of crystalline regions (blue line), accessible surfaces (orange line), and inaccessible surfaces/amorphous regions (green line) evaluated from the ^{13}C CP/MAS NMR spectra of samples that underwent (a) two-, (b) three- and (c) four-cycle post-treatments with treatment times varying from 2 to 12 h.

3.3.5. Crystallinity Improvement Mechanism of Multicycle Post-Treatment

The experimental results confirmed that the inaccessible surface regions were converted into crystalline regions after each post-treatment cycle. Fig 3-11 shows a schematic diagram showing the mechanism for crystallinity improvements during multicycle post-treatment, and the bottom part of Fig 3-11 shows the structural changes occurring a single-crystal region. In the first post-treatment cycle, NaOH penetrated only the inaccessible surfaces of the initial structure, and crystallization occurred on the inaccessible surfaces that NaOH penetrated. In the second and subsequent cycles of post-treatment, NaOH permeated only the inaccessible surfaces enlarged by the previous cycle of post-treatment and converted them into a crystalline region, resulting in improvements in crystal size following each cycle of post-treatment. However, since the crystallinity improvement was limited after a long-term single post-treatment as shown in Fig 3-5, it was also inferred that the crystallinity improvement per post-treatment cycle is restricted. These effects led to the conversion of amorphous regions, which are originally distant from the initial crystalline regions, into crystalline regions, resulting in higher crystallinity compared with that achieved via long-term single-cycle post-treatment. However, after two cycles of post-treatment using high-concentration H_2SO_4 solution for neutralization, the crystallinity of the sample decreased. Furthermore, an upper limit to the improvement in crystallinity was observed; once this limit was reached, further repeated or prolonged post-treatment did not improve the crystallinity of the sample. These results suggest that cellulose II contained some inaccessible surface regions that were difficult to crystallize or difficult for NaOH to

access.

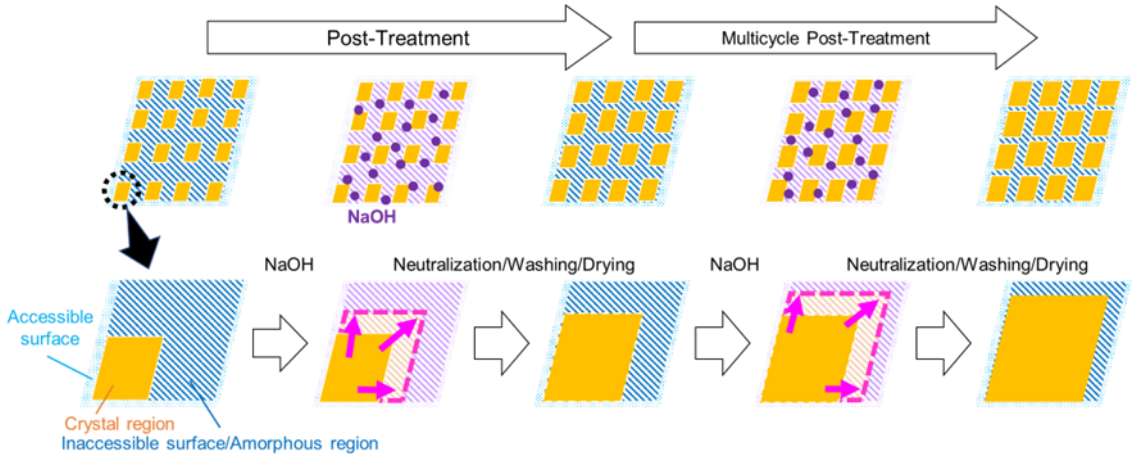

Fig. 3-11. Schematic diagram showing the mechanism of crystallinity improvement with multicycle posttreatment cycles of low-concentration NaOH. The bottom part of Fig 3-11 shows the structural changes focused on a single crystal. In subsequent post-treatments after the second post-treatment cycle, NaOH permeated only the inaccessible surface enlarged by the previous posttreatment cycle and converted it into a crystalline region. Consequently, the crystal size increased with each post-treatment cycle. The crystallinity continues to improve until reaching the upper limit.

3.3.6. Optimization of Treatment Times in Multicycle Post-Treatments

With more post-treatment cycles, more NaOH solution used for post-treatment and more deionized water was used for washing. Thus, reaching the upper limit for crystallinity with a smaller number of post-treatment cycles is important. The experimental results showed that both the three-cycle and the 8 h single-cycle post-treatments led to the greatest improvement in crystallinity. Based on these results, an ideal and efficient process for crystallinity improvement was realized by optimizing the treatment time and number of post-treatment cycles. For this purpose, the total post-treatment time was divided into several cycles of 6, 8, and 10 h. In the following discussion, the samples obtained after multicycle post-treatment for various treatment times were labeled according

to the treatment time for each cycle. For example, the sample obtained after three cycles of post-treatment for a total time of 6 h, with each cycle performed for 2 h, was denoted 6 h (2-2-2). Figs 3-11 (a), (b), and (c) show the proportions of crystalline regions, accessible surfaces, and inaccessible surfaces/amorphous regions of samples prepared with a total post-treatment time of 6, 8, and 10 h, respectively. Fig 3-12 (a) shows that the 6 h (4-2) sample had the highest crystallinity among the samples prepared with a total post-treatment time of 6 h. Fig 3-12(b) shows that the 8 h (4-4) sample had the highest crystallinity among the samples prepared with a total post-treatment time of 8 h. The 8 h (6-2) sample had higher crystallinity than the 8 h (2-6) sample. Fig 3-12(c) shows that the 10 h (6-4) sample had the highest crystallinity among the four samples obtained after two cycles of post-treatment for various treatment times. Furthermore, the 10 h (8-2) sample had higher crystallinity than the 10 h (2-8) and 10 h (4-6) samples. These results confirmed that when the post-treatment time for the first cycle was sufficiently long and the post-treatment time for the second cycle was relatively short, the crystallinity of the sample tended to increase with fewer post-treatment cycles. The conversion of inaccessible surface regions during the first cycle of post-treatment is believed to play a crucial role in obtaining highly crystalline samples. A possible explanation for this tendency is that the longer first post-treatment cycle enabled the conversion of a wider area of the inaccessible surface into the crystalline region while the second post-treatment cycle further converted this enlarged inaccessible region into a crystalline region.

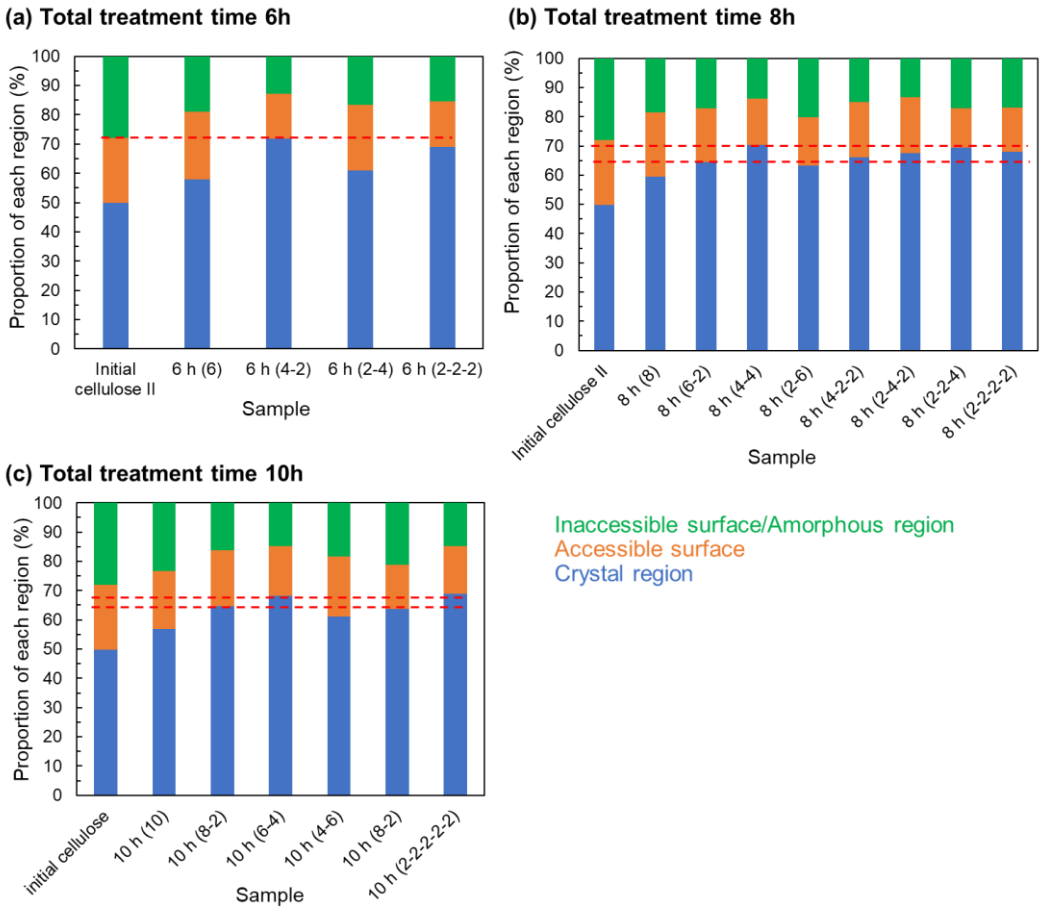

Fig. 3-12. Proportions of crystalline regions (blue bars), accessible surfaces (orange bars), and inaccessible surfaces/amorphous regions (green bars) as evaluated from the solid-state ^{13}C CP/MAS NMR spectra of samples obtained via multicycle post-treatment with a total post-treatment time of (a) 6 h, (b) 8 h, and (c) 10 h. When the post-treatment time for the first cycle was sufficiently long and the post-treatment time for the second cycle was relatively short, the crystallinity tended to increase with fewer post-treatment cycles.

3.3.7. Crystallinity and Crystal Size of Cellulose II Fiber Obtained by Multicycle Post-Treatment

For cellulose II powder, multicycle post-treatment has been demonstrated to be effective in crystallinity improvement based on previous experiments. If this post-treatment proves effective in the crystallinity improvement of cellulose II fibers, it opens up the possibility of fabrication of high-strength cellulose II materials. The multicycle post-treatments were conducted on cellulose II fiber,

fortisan, rayon, and polynosic, to confirm the crystallinity improvement. Fig 3-13 shows a photograph of the prepared fortisan, the prepared rayon, and the samples obtained by first cycle post-treatments. Regarding the shape of the post-treated samples, the fibers were twisted in the tension-free post-treatment and straightened in the tensile post-treatment.

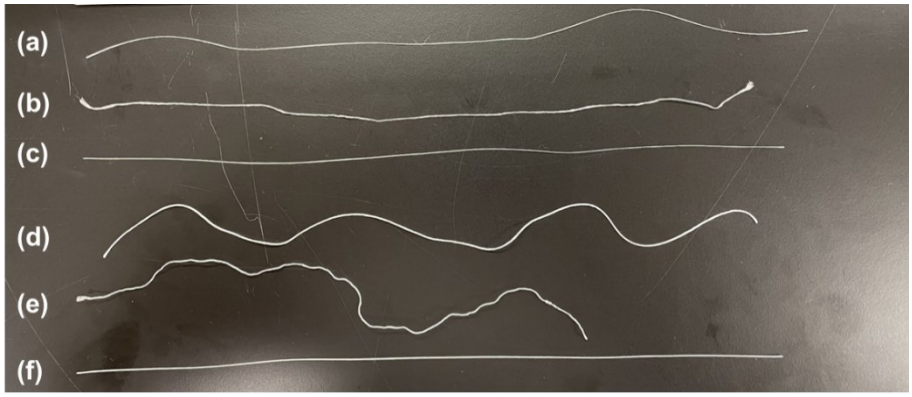

Fig. 3-13. The photograph of (a) the prepared fortisan, (b) the fortisan sample obtained by tension-free first-cycle post-treated, (c) the fortisan sample obtained by tensioned at 100 g on single strand first-cycle post-treated, (d) the prepared rayon, (e) the rayon sample obtained by the tension-free first-cycle post-treatment, and (f) the rayon sample obtained by the tensioned first-cycle post-treatment.

Fig 3-14 shows the proportion of each region of the samples, which were obtained by the post-treatments on fortisan, rayon, and polynosic, determined by C4 line fitting of ^{13}C CP/MAS NMR spectra. The crystallinity was improved in all cellulose II fiber resources regardless presence of tension. In the case of fortisan, both tension-free and tensioned at 100 g on single strand post-treatment result in an approximately 15% increase in crystallinity. In the case of rayon, both tension-free and tensioned post-treatment led to an increase in crystallinity, approximately 25 % and 20 %, respectively, with a slightly higher improvement in crystallinity observed in the tension-free post-treatment. The

crystallinity of these polynosic samples was also improved up to the fourth post-treatment cycle, upon about 36%. These results show that the multicycle post-treatment is effective in the improvement of cellulose II fiber. In all post-treatments, the proportion of inaccessible surface/amorphous was decreased as the crystallinity was improved. Those behaviors are similar to the case of mercerized cellulose II powder. In other words, the mechanisms of crystallinity improvement through the multicycle post-treatments seem to be the same, irrespective of the shape of cellulose II samples.

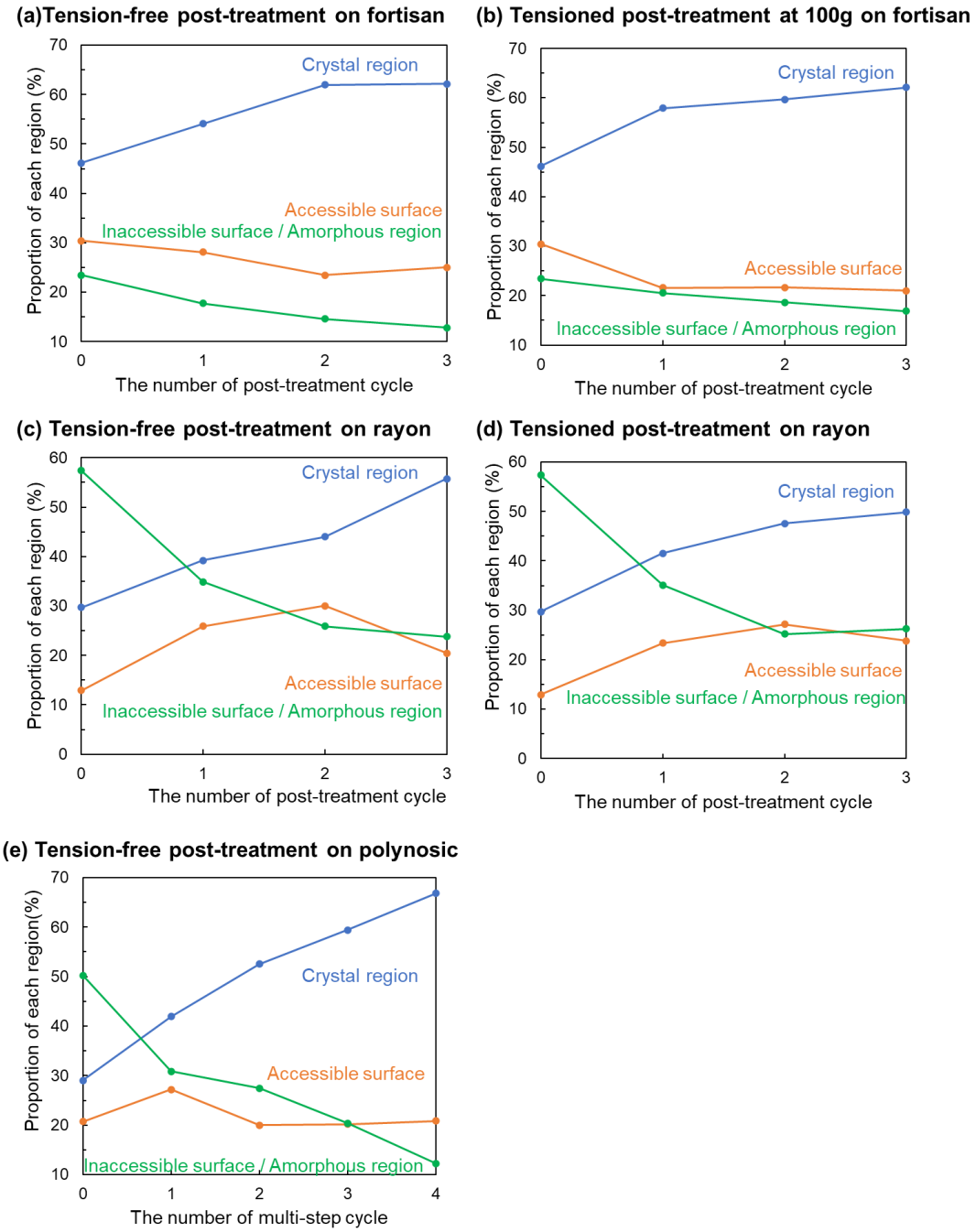

Fig. 3-14. Proportions of crystalline regions (blue line), accessible surfaces (orange line), and inaccessible surfaces/amorphous regions (green line) evaluated from the ^{13}C CP/MAS NMR spectra of the fortisan samples that underwent (a) tension-free multicycle post-treatment, (b) tensioned at 100 g on single strand multicycle post-treatment, the rayon samples that underwent (c) tension-free multicycle post-treatment, (d) tensioned multicycle post-treatment, (e) the polynosic samples that underwent tension-free post-treatment.

Fig 3-15 shows the crystallinity of post-treated fortisan samples obtained by the tension-free multicycle post-treatments and the tensioned multicycle post-treatments applied various magnitudes of tension. The crystallinity was improved regardless of the magnitude of applied tension. There was no significant crystallinity improvement among the tension-free and the tensioned multicycle post-treatments with small tensions, however, the crystallinity of the tensioned multicycle post-treatment with large tensions was lower than those of other methods. Similar to the fortisan samples, Figs 3-13(c) and (d) show the crystallinities of the rayon samples obtained by the tensioned multicycle post-treatments were lower than the tension-free multicycle post-treatment. These results suggested that the large tension narrows the amorphous region sufficient for NaOH to penetrate. The reduction in NaOH penetration is thought to inhibit their growth from amorphous to crystal. Fig 3-16 shows the crystal size of the fortisan and rayon samples obtained by the tension-free and the tensioned multicycle post-treatments, determined by XRD measurements. It was observed that the crystal size of the hydrophobic (110) plane significantly increased. It was reported that the hydrophobic interaction plays an important role in sheet stacking in the crystal structure of cellulose II [12], [13]. While the crystal size increased for all planes in the multicycle post-treatment of cellulose II powder as shown in Fig 3-7, it increased in a specific direction, particularly along the hydrophobic plane direction, in the case of cellulose II materials with high orientation, such as fiber.

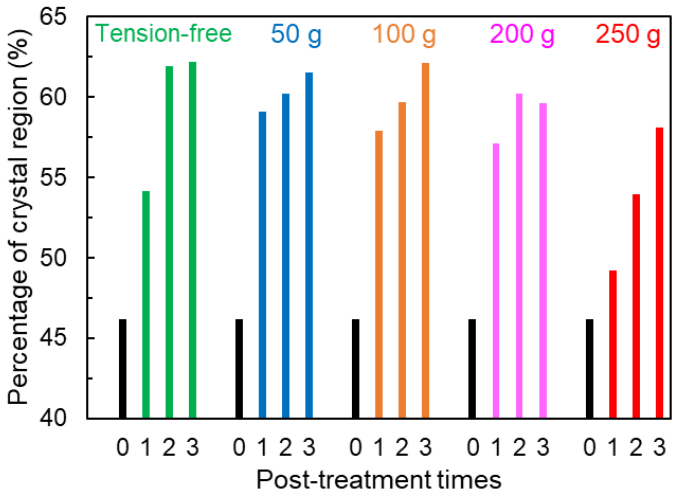

Fig. 3-15. The crystallinities of the fortisan samples obtained by the multicycle post-treatment, determined by C4 lines fitting of solid-state ^{13}C CP/MAS NMR spectra. *Color code*; black bar, fortisan; green bars, tension-free multicycle post-treatments, blue bars, applied tension at 50 g on the single strand; orange bars, applied tension at 100 g on the single strand; pink bars, applied tension at 200 g on the single strand; red bars, tension at 250 g on a single strand.

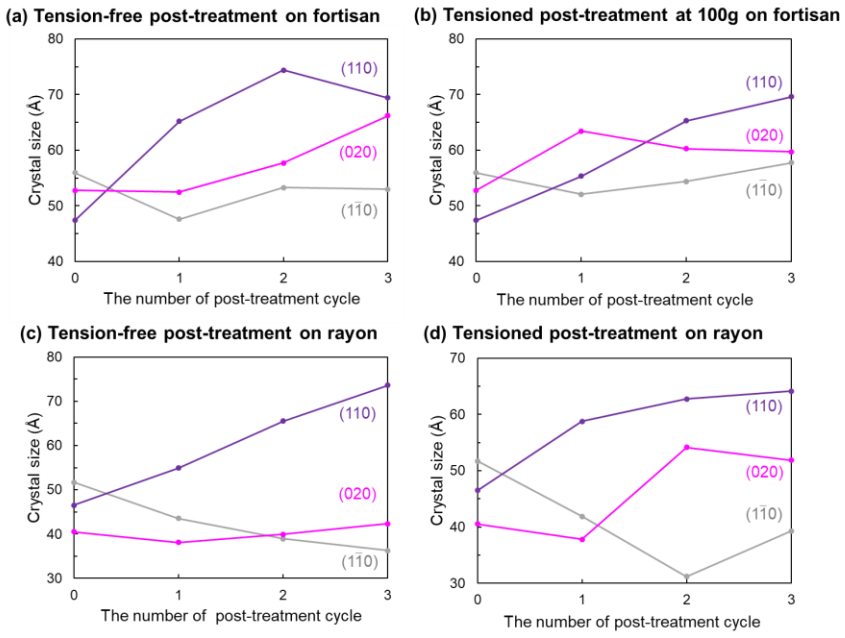

Fig. 3-16. The crystal size of (1$\bar{1}$0) plane (gray line), (110) plane (purple line), and (020) plane (pink line) estimated from XRD profiles in (a) the tension-free multicycle post-treatment on foritsan, (b) the tensioned multicycle post-treatment on fortisan applied tension at 100 g on single strand, (c) the tension-free multicycle post-treatment on rayon and (d) the tensioned multicycle post-treatment on rayon.

3.3.8. Tensile Tests

Fig 3-17 shows the stress-strain (S-S) curves of as-prepared fortisan and the fortisan samples obtained by the multicycle post-treatments. Table. 3-1 shows the maximum stress, breaking strain, Young's moduli, and toughness of as-prepared fortisan and the fortisan samples obtained by the multicycle post-treatments. The mechanical properties varied depending on the magnitude of tension applied during post-treatment. In high-tensioned post-treatments (red, deep red, light blue, and blue lines in Fig 3-17), Young's modulus increased and the breaking strain reduced. The effect of repeating the post-treatment was observed as Young's modulus increased a bit and the breaking strain decreased after the second high-tensioned post-treatment cycle. Conversely, in cases of tension-free and low-tensioned post-treatments (orange, yellow, pink, purple, light green, and green lines in Fig 3-17), Young's modulus decreased, and breaking strain increased. Additionally, these post-treatments suggested that repetition treatment improved breaking strain, indicating potential improvements in toughness. However, in most cases, the toughness of the samples obtained by post-treatments was smaller than that of the as-prepared fortisan.

Fig 3-18 shows the S-S curve of the as-prepared rayon and the rayon samples obtained by multicycle post-treatments. Table. 3-2 shows the maximum stress, breaking strain, Young's moduli, and toughness of the as-prepared rayon and the samples obtained by multicycle post-treatments. The toughness of the sample obtained by post-treatments was smaller than that of the as-prepared rayon. In tensioned post-treatments, Young's modulus increased, conversely, in tension-free post-treatments,

Young's modulus decreased and the breaking increased. The effect of repeating the post-treatment was observed as Young's modulus and the breaking strain decreased regardless application of tension, unlike the case of the fortisan sample. Thus, it was demonstrated that the magnitude of tension influences the mechanical properties, especially Young's moduli and breaking strain, however, the repeating treatment effect varied depending on the cellulose resources, suggesting it is likely difficult to control the mechanical properties of cellulose II fibers using multicycle post-treatment. Generally, in polymer fibers, an increase in crystallinity tends to improve Young's modulus and decrease the breaking strain. However, despite an improvement in crystallinity in tension-free post-treatment, Young's moduli decreased and the breaking strain increased. The cellulose II fibers used in this experiment are composed of multiple filaments, suggesting that factors beyond crystallinity, such as filament interactions and twist pitch, may also impact mechanical strength.

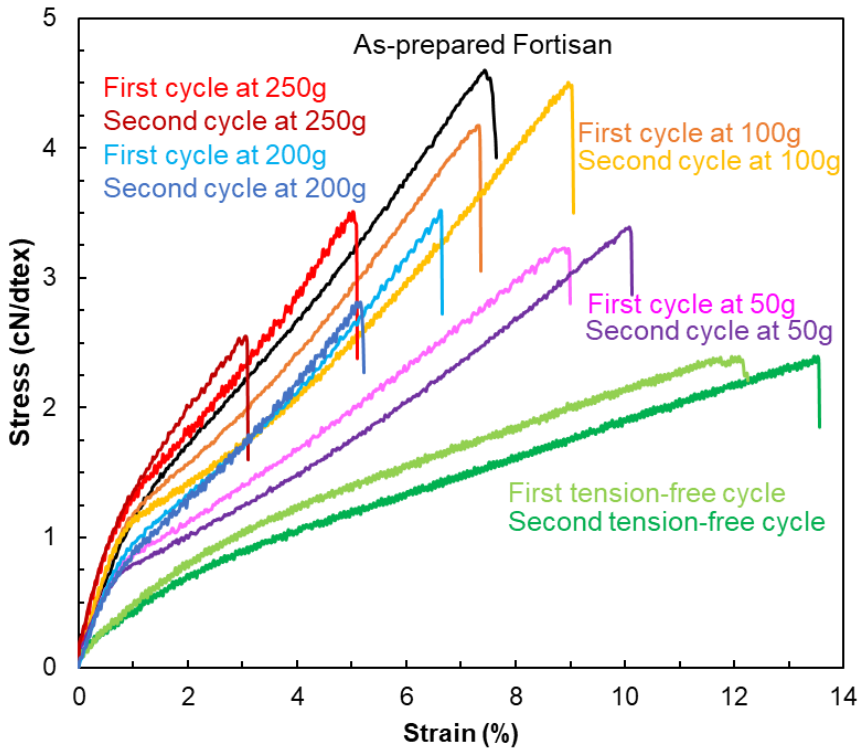

Fig. 3-17. The stress-strain (S-S) curves of the as-prepared fortisan and the fortisan samples that underwent the multicycle post-treatments; black line, the as-prepared fortisan; redline, first cycle tensioned at 250 g on single strain; deep red line, second cycle tensioned at 250 g on single strain; light blue line, first cycle tensioned at 200 g on single strain; blue line, second cycle tensioned at 200 g on single strain; orange line, first cycle tensioned at 100 g on single strain; yellow line, second cycle tensioned at 100 g on a single strain, pink line, first cycle tensioned at 50 g on single strain; purple line, second cycle tensioned at 50 g on single strain; light green line, first tension-free cycle; green line, second tension-free cycle.

Table. 3-1. The maximum stress, breaking strain, Young's moduli, and toughness of fortisan samples.

Tension (g/strand)	Cycle	Maximum stress (cN/dtex)	Breaking strain (%)	Young' moduli (cN/dtex)	Toughness (cN/dtex) × 100^{-2}
as-prepared fortisan	-	4.6 ± 0.2	7.4 ± 0.5	120.7 ± 2.0	19.0 ± 2.3
Tension-free	1	2.2 ± 0.5	12.4 ± 2.5	39.3 ± 4.3	18.7 ± 7.2
Tension-free	2	2.4 ± 0.3	13.5 ± 1.0	30.1 ± 3.8	19.0 ± 2.4
50	1	3.2 ± 0.4	9.0 ± 1.5	99.5 ± 6.3	16.6 ± 3.2
50	2	3.4 ± 0.3	10.1 ± 1.3	99.3 ± 10.4	18.5 ± 3.3
100	1	4.2 ± 0.3	7.3 ± 1.1	127.8 ± 7.0	17.1 ± 4.3
100	2	4.5 ± 0.3	9.0 ± 0.5	128.4 ± 8.0	21.7 ± 1.2
200	1	3.5 ± 0.7	6.7 ± 1.2	113.7 ± 10.4	12.5 ± 5.4
200	2	2.8 ± 0.8	5.2 ± 1.0	109.7 ± 7.0	8.0 ± 2.7
250	1	3.5 ± 1.2	5.0 ± 2.3	135.3 ± 6.2	10.2 ± 7.0
250	2	2.6 ± 0.9	3.1 ± 0.7	136.2 ± 12.0	4.9 ± 2.6

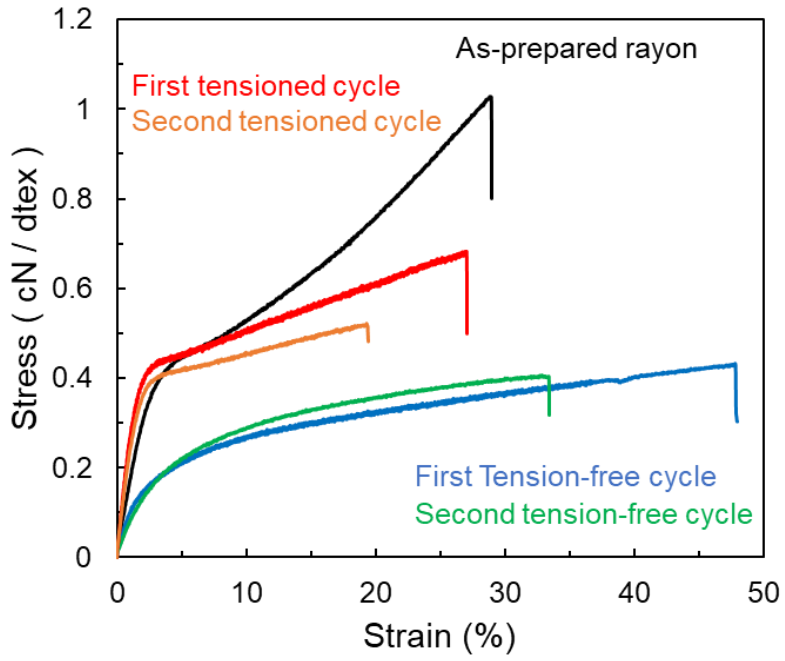

Fig. 3-18. The S-S curves of the as-prepared rayon and post-treated rayon samples. *Color code*: black line, the as-prepared rayon; blue line, the sample obtained by the first tension-free post-treatment cycle; green line, the sample obtained by the second tension-free post-treatment cycles; red line, the sample obtained by the first tensioned post-treatment cycle; orange line, the sample obtained by the second tensioned post-treatment cycle.

Table. 3-2. The maximum stress, breaking strain, Young's moduli, and toughness of the rayon samples.

Methods	Cycle	Maximum stress (cN/dtex)	Breaking strain (%)	Young' moduli (cN/dtex)	Toughness (cN/dtex) × 100^{-2}
as-prepared rayon	-	1.03 ± 0.02	28.9 ± 0.9	14.1 ± 0.6	18.3 ± 0.9
Tension-free	1	0.29 ± 0.05	49.0 ± 2.8	8.7 ± 1.9	15.8 ± 3.7
Tension-free	2	0.40 ± 0.21	33.4 ± 5.7	6.3 ± 0.7	10.4 ± 2.2
Tensioned	1	0.68 ± 0.08	27.0 ± 4.2	26.2 ± 0.7	14.3 ± 3.6
Tensioned	2	0.44 ± 0.23	20.3 ± 6.4	22.4 ± 1.6	8.8 ± 4.8

3.3.9. POM and SEM Observation

In order to examine the cause of the differences in mechanical property behavior due to the magnitude of tension, morphological observations of the samples were conducted using POM and SEM. Fig 3-19 shows POM images of the as-prepared fortisan, rayon, and the samples obtained by first-cycle post-treatment. Fiber width of fortisan increased in the tension-free post-treatment, and decreased in the tensioned post-treatment. In the case of rayon, even in tension-free post-treatment, the fiber width has slightly decreased, and filament breakages were observed intermittently in tensioned post-treatment. These results suggest that the morphology of the samples changed during post-treatment, and the way of morphology changes varies depending on the cellulose II resources. Fig 3-13 shows SEM images of the as-prepared fortisan, and the fortisan samples obtained by first-cycle post-treatment. The filaments were likely to be straight in the sample obtained by the tensioned post-treatment, however, those of the sample obtained by tension-free post-treatment were twisted. This twisting is considered to be related to the thickening of the fiber observed in the POM image shown in Fig 3-20. Because the filaments are twisted, it is possible that these filaments are stretched

in a bellows-like manner when tensile testing is performed. This may have resulted in a decrease in Young's modulus and an increase in breaking strain in the no-tension treatment. In addition, the twisting of fiber obtained by tension-free post-treatment shown in Fig 3-13 also may affect to their mechanical properties. Thus, it was suggested that although multi-cycle post-treatment can improve the crystallinity of cellulose II fibers, its mechanical properties are also closely related to the morphology of the cellulose II fiber material, including fibril thickness, twist, orientation, and stretching. Therefore, the high crystallization process by low-concentration NaOH post-treatment may be more effective if it is performed during the fiber formation process rather than after the cellulose II fiber preparation.

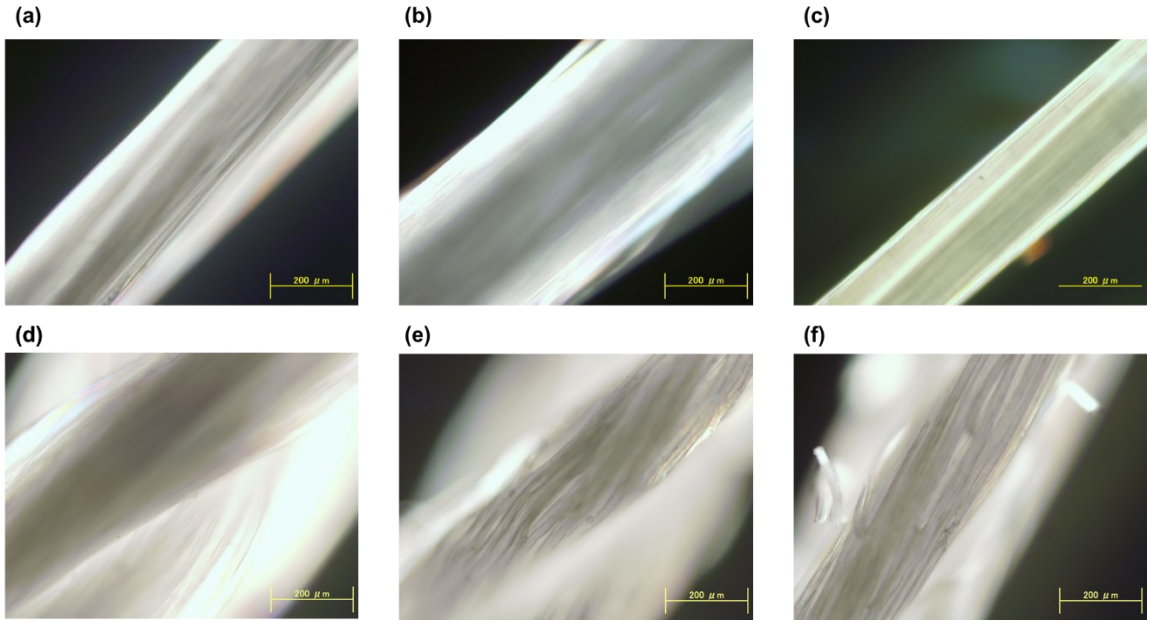

Fig. 3-19. The polarizing optical microscopy (POM) images of (a) the as-prepared fortisan, (b) the fortisan samples obtained by (b) tension-free and (c) tensioned at 100 g on single strand first-cycle post-treatment, (d) the as-prepared rayon, and the rayon samples obtained by (e) tension-free and (f) the rayon sample obtained tensioned first-cycle post-treatment.

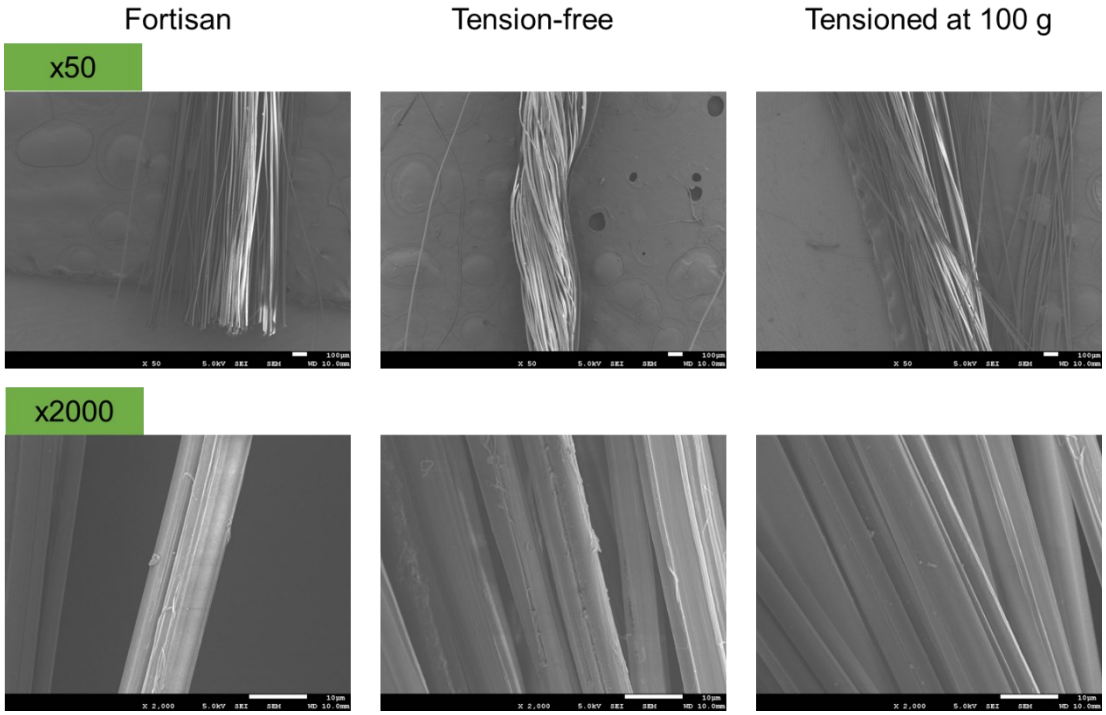

Fig. 3-20. The 50x and 2000x Scanning Electron Microscopy (SEM) images of the as-prepared fortisan, and the fortisan samples obtained by tension-free and tensioned at 100 g on single strand first-cycle post-treatment.

3.4. Conclusions

In this chapter, the crystallinity of cellulose II was improved by low-concentration NaOH post-treatment, and the mechanism of crystallinity improvement by multicycle post-treatment was proposed. The crystallinity of cellulose II was improved by up to approximately 10% during a long-term single-cycle post-treatment and up to approximately 20% during multicycle post-treatment. Thus, multicycle post-treatment was more effective than single-cycle post-treatment in improving the crystallinity of cellulose II. During multicycle post-treatment, the crystallinities and crystal sizes were improved after each cycle and the proportion of inaccessible surfaces/amorphous regions decreased as the crystallinity increased. This was explained by the model we previously proposed: in the second and subsequent cycles of post-treatment, the rearrangement of cellulose occurred only at the inaccessible surface expanded by the previous cycle of post-treatment, and crystallization proceeded toward amorphous regions far from the initial crystalline regions. Moreover, I confirmed that when the treatment time for the first cycle of post-treatment was relatively long and that for the second cycle of post-treatment was somewhat short, the crystallinity tended to increase even with fewer post-treatment cycles. A possible explanation for this tendency is that the longer first post-treatment cycle converted a wider area of the inaccessible surface into a crystalline region while the second cycle further converted this enlarged region into a crystalline region. The important points obtained from results in this chapter and in the proposed mechanism for improving crystallinity include that the NaOH, which did not penetrate cellulose crystals, selectively permeated only the amorphous and

inaccessible surface regions, and the NaOH acted only on structural changes resulting from the rearrangement of cellulose molecular chains on the inaccessible surfaces surrounding the crystalline region.

The multicycle post-treatments were also effective in improving the crystallinity of cellulose II fibers. The mechanical properties of the cellulose II fiber samples, especially Young's modulus and breaking strain, were dependent on the magnitude of tension applied. The results of tensile tests and morphological observations of the post-treated samples under various conditions suggest that the multi-cycle post-treatment improves the crystallinity of cellulose II fibers, but that the mechanical properties are also closely related to the morphology of the cellulose II fiber material, including fibril thickness, twist, orientation, and stretching. These results suggest that the high crystallization treatment by low concentration NaOH post-treatment may be more effective when performed during the fiber formation process rather than after the preparation of cellulose II fibers.

REFERENCES

[1] P. Langan, Y. Nishiyama, and H. Chanzy, "X-ray structure of mercerized cellulose II at 1 Å resolution," *Biomacromolecules*, vol. 2, no. 2, pp. 410–416, 2001, doi: 10.1021/bm005612q.

[2] X. Colom and F. Carrillo, "Crystallinity changes in lyocell and viscose-type fibres by caustic treatment," *Eur Polym J*, vol. 38, no. 11, pp. 2225–2230, 2002, doi: 10.1016/S0014-3057(02)00132-5.

[3] J. Široký, R. S. Blackburn, T. Bechtold, J. Taylor, and P. White, "Attenuated total reflectance Fourier-transform Infrared spectroscopy analysis of crystallinity changes in lyocell following continuous treatment with sodium hydroxide," *Cellulose*, vol. 17, no. 1, pp. 103–115, Feb. 2010, doi: 10.1007/s10570-009-9378-x.

[4] B. R. Manjunath and A. Venkataraman, "Fibrillar aggregation in cotton cellulose subjected to multiple swelling treatments with alkali," *Journal of Polymer Science: Polymer Chemistry Edition*, vol. 18, pp. 1407–1424, 1980, doi: 10.1002/pol.1980.170180424.

[5] M. Hirota, N. Tamura, T. Saito, and A. Isogai, "Cellulose II nanoelements prepared from fully mercerized, partially mercerized and regenerated celluloses by 4-acetamido-TEMPO/NaClO/NaClO2 oxidation," *Cellulose*, vol. 19, no. 2, pp. 435–442, 2012, doi: 10.1007/s10570-011-9642-8.

[6] K. Daicho, S. Fujisawa, and T. Saito, "Linear correlation between True density and crystallinity of regenerated and mercerized celluloses," *Biomacromolecules*, vol. 24, no. 2, pp. 661–666, 2023, doi: 10.1021/acs.biomac.2c01067.

[7] S. Nomura, Y. Kugo, and T. Erata, "13C NMR and XRD studies on the enhancement of cellulose II crystallinity with low concentration NaOH post-treatments," *Cellulose*, vol. 27, no. 7, pp. 3553–3563, May 2020, doi: 10.1007/s10570-020-03036-6.

[8] P. T. Larsson, K. Wickholm, and T. Iversen, "A CP/MAS 13C NMR investigation of molecular ordering in celluloses," *Carbohydr Res*, vol. 302, no. 1–2, pp. 19–25, 1997, doi: 10.1016/S0008-6215(97)00130-4.

[9] G. Zuckerstätter, N. Terinte, H. Sixta, and K. C. Schuster, "Novel insight into cellulose supramolecular structure through 13C CP-MAS NMR spectroscopy and paramagnetic relaxation enhancement," in *Carbohydrate Polymers*, 2013, pp. 122–128. doi: 10.1016/j.carbpol.2012.05.019.

[10] A. Kirui *et al.*, "Atomic resolution of cotton cellulose structure enabled by dynamic nuclear polarization solid-state NMR," *Cellulose*, vol. 26, no. 1, pp. 329–339, Jan. 2019, doi: 10.1007/s10570-018-2095-6.

[11] D. Massiot *et al.*, “Modelling one- and two-dimensional solid-state NMR spectra,” *Magnetic Resonance in Chemistry*, vol. 40, no. 1, pp. 70–76, Jan. 2002, doi: 10.1002/mrc.984.

[12] N. Isobe, U. J. Kim, S. Kimura, M. Wada, and S. Kuga, “Internal surface polarity of regenerated cellulose gel depends on the species used as coagulant,” *J Colloid Interface Sci*, vol. 359, no. 1, pp. 194–201, 2011, doi: 10.1016/j.jcis.2011.03.038.

[13] K. Kobayashi, S. Kimura, E. Togawa, and M. Wada, “Crystal transition from Na-cellulose IV to cellulose II monitored using synchrotron X-ray diffraction,” *Carbohydr Polym*, vol. 83, no. 2, pp. 483–488, 2011, doi: 10.1016/j.carbpol.2010.08.006.

Chapter. 4.

Control of Mechanical Properties of Composite Materials by Control of Crystal Transition

4.1. Introduction

The enhancement of the mechanical strength of cellulose II materials will contribute to the development of a wide range of cellulose applications. In Chapter 3, I attempted to fabricate the desired material by improving the crystallinity of cellulose II. In this chapter, I aim to achieve this objective by controlling the percentage and distribution of cellulose I and II crystals. Hints for developing a novel method were obtained from the results of Chapter 2. The temperature conditions and the dynamics of Na ions were shown to be important factors in the crystal transition from cellulose I to II in low-concentration NaOH treatment. This indicates the possibility of preparing composite materials of cellulose I and II by controlling treatment conditions such as temperature and treatment time. Therefore, I focused on a method to fabricate cellulose-base composite materials including cellulose I and II crystals by controlling the distribution of these crystals. It has been reported that cellulose sheets containing cellulose I and II were prepared by alkali treatment with a 7 wt% NaOH/12 wt% urea solution using the surface dissolution method [1], [2]. In other words, composite materials can be prepared using NaOH-based solvents. On the other hand, the solubility of cellulose in low-concentration NaOH solutions is limited by the degree of polymerization and NaOH concentration [3]–[5]. In other words, if I could establish a novel approach to selectively induce the crystal transition from cellulose I to II at the surface of the cellulose material, rather than partially dissolving the surface, it would be possible to prepare cellulose-based composite materials on a larger scale and more freely without the above-mentioned limitations.

The purpose of this chapter is to establish a new methodology to control the percentage and distribution of cellulose I and II crystals by using dilute alkali treatment, thereby controlling the mechanical properties of composite materials including cellulose I and II. In cellulose I and II composites, it has been reported that composites with a higher percentage of cellulose I have higher mechanical strength than those with a lower percentage of cellulose I [6], [7]. This suggests that mechanical properties can be controlled by adjusting the percentage of cellulose crystals. When cellulose powder immersed in an 8 wt% NaOH solution is quenched with liquid nitrogen, the crystal transition from cellulose I to II proceeds quickly from the outside to the inside. From this result, I hypothesized that the distribution of cellulose I and II could be controlled by controlling the quenching treatment time. In this study, I followed the progression of crystal transition during quenching treatment with liquid nitrogen. Using the quench treatment, I attempted to prepare a composite fiber material with cellulose I as the core and cellulose II as the surface. The resulting samples were analyzed by solid-state ^{13}C CP/MAS NMR measurements and tensile testing. In addition, the mechanical properties of the composite samples and the mercerized cellulose II fiber were compared.

4.2. Methods

4.2.1. Materials

100-200 mesh filter paper pulp powder of wood and commercial organic cotton yarn for handicrafts were purchased from Advantech Co., Ltd. (Tokyo, Japan) and MOTOHIRO & Co., Ltd. (Kyoto, Japan), respectively. NaOH (>97.0%) and H_2SO_4 (>95.0%) were purchased from FUJIFILM Wako Pure Chemical Corporation (Osaka, Japan). Deionized water (Elix®Essential3, Merck KGaA, Darmstadt, Germany) was used to prepare NaOH and H_2SO_4 aqueous solutions and to wash the cellulose samples.

4.2.2. Quenching Treatments with Liquid Nitrogen on Cellulose Powder

The cellulose powder was soaked in an 8 wt% NaOH solution at room temperature (24 °C) in a 50 mL centrifuge tube with a diameter of 2.8 cm. The samples were centrifuged at 1,000 × g for 5 min. The supernatant was removed, and the precipitate was used for the quenching treatments. The precipitate was divided into the 2mL microtube. The quenching treatments were performed including chilling the 2 mL microtube containing 8 wt% NaOH-soaked cellulose in a container filled with liquid nitrogen for up to 90 s. In addition, the quenching treatments were conducted by chilling the centrifuge tube containing 8 wt% NaOH-soaked cellulose powder that was not divided into microtubes for up to 120 s. The reason for quenching treatments with different containers is to confirm the effect of the heat capacities of the container. The samples were then thawed by immediately adding a sufficient amount of a 10 vol% H_2SO_4 solution to bring the pH below 7.0 at room temperature (24 °C). The samples

were washed with deionized water and air-dried at room temperature (24 °C). The dried samples were analyzed using solid-state ^{13}C CP/MAS NMR measurements. The cellulose II proportion was determined by the C6 line fitting of the ^{13}C NMR spectra. The mechanical properties were analyzed by tensile tests.

4.2.3. Quenching Treatments with Liquid Nitrogen on Cotton Fiber

The cotton fibers were cut to a length of 40 cm. The fiber was soaked in an 8 wt% NaOH solution in a beaker at room temperature (24 °C) for 10 min. The samples were wrapped after being taken out from a beaker and chilled in a container filled with liquid nitrogen. The treatment durations were 5, 10, 15, 30, 60, and 90 s. The samples were then thawed by immediately adding a sufficient amount of a 10 vol% H_2SO_4 solution to bring the pH below 7.0 at room temperature (24 °C). The samples were then washed with deionized water and air-dried at room temperature (24 °C). The dried samples were analyzed using solid-state ^{13}C CP/MAS NMR spectroscopy and tensile tests. The cellulose II proportion was determined by the C6 line fitting of the ^{13}C NMR spectra.

To compare the effect of temperature and alkali concentrations, the room-temperature treatments using an 8 wt% NaOH solution, and the mercerization treatment using a high-concentration NaOH solution were conducted. The cotton fibers were soaked in an 8 wt% NaOH solution for 10 min at room temperature (24 °C). These fiber samples were neutralized in a vat filled with a 10 vol% H_2SO_4 solution. After neutralization, the samples were washed with deionized water and air-dried at

room temperature (24 °C). For mercerization, the cotton fibers were soaked in a 25 wt% NaOH solution at room temperature (24 °C) for 2 h. These fiber samples were neutralized in a vat filled with a 20 vol% H_2SO_4 solution. After neutralization, the samples were washed with deionized water and air-dried at room temperature (24 °C). The dried samples were analyzed using solid-state ^{13}C CP/MAS NMR measurements and tensile tests.

4.2.4. Solid-State ^{13}C CP/MAS NMR Measurements

Solid-state ^{13}C CP/MAS NMR measurements were performed using a Bruker AVANCE NEO 500 spectrometer (Bruker, Germany) at Instrumental Analysis Support Office, Frontier Chemistry Center, Faculty of Engineering, Hokkaido University, Japan. The dried samples were packed in a 3.2 mm rotor. Solid-state ^{13}C CP/MAS NMR spectra were recorded at 125 MHz. The MAS frequency was set to 10 kHz. All solid-state ^{13}C CP/MAS high-resolution spectra were recorded with a ^{1}H 90° pulse length of 4.0 μs, a contact time of 1.5 ms, and a repetition time of 4 s. Ramp and tppm-15 sequences were used for the contact pulse and decoupling, respectively. The chemical shifts were calibrated using the carbonyl carbon of glycine at 176.46 ppm. The crystalline form was identified based on the chemical shift of the C6 resonance lines. The C6 lines were deconvoluted using the DMfit2017 line-fitting program [8]. A Lorentzian shape was used for each line. Deconvolution of the C6 resonance lines was based on the chemical shifts of the *tg* (65–66 ppm), *gt* (62–63 ppm), and *gg* (60–62 ppm) conformations [9], as described in Section 2.2.3 and Fig 2-1. The proportion of each

region was calculated using the integrated areas of the *tg* lines at 66.0, 65.5, and 65.2 ppm, *gt* lines at 63.3 ppm and 62.6 ppm, and *gg* lines at 61.9, 61.5, and 61.0 ppm. In addition, the cellulose II proportion in the crystal region was calculated using the following equation:

$$\text{Cellulose II proportion in the crystal region} = \frac{A_{gt}}{A_{tg} + A_{gt}} \times 100$$

where A_{tg} is the integrated area of *tg* lines, and A_{gt} is the integrated area of *gt* lines.

4.2.5. Tensile Tests

Tensile tests were performed on the cotton fiber samples using an AG-100kNXplus (SHIMADZU CORPORATION, Kyoto, Japan). The samples were fixed using a pneumatic capstan-type yarn gripper (SHIMADZU CORPORATION, Kyoto, Japan) and pulled from a distance of 10 cm at a speed of 1 mm/s. A stress-strain curve (S-S curve) was drawn for each sample, with stress on the X-axis and strain on the Y-axis. The J-shaped S-S curves are observed in all samples. The maximum stress, breaking strain, elastic moduli, and toughness were determined. The toughness was calculated as the integral area under each S-S curve. The J-shaped S-S curve is a behavior commonly observed in the tensile tests of biomacromolecules, such as silk and spider silk [10]. In the initial region at low stress level and the subsequent region at higher stress, the slopes of the curve differ. In the initial region, factors such as crimping and unfolding of molecules play a significant role, while in the region at higher stress, the stretches of the polymer backbone and crystalline regions are considered to have a substantial impact [10]. In this study, elastic moduli in initial and higher stress regions are noted as E_I

and E_H, respectively. E_I was determined from the initial slope of the S-S curves. E_H was calculated as the slope of S-S curves within the range of 40% to 80% of the maximum stress, where the slopes of the S-S curves are relatively constant, as follows:

$$E_H\ [cN/dtex] = (\sigma_{80} - \sigma_{40})/(\frac{\varepsilon_{80} - \varepsilon_{40}}{100})$$

where σ_{40} is 40 % of the maximum stress, σ_{80} is 80 % of the maximum stress, ε_{40} is the strain at 40 % of the maximum stress, and ε_{80} is the strain at 80 % of the maximum stress.

4.3. Results and Discussions

4.3.1. Quenching Treatments with Liquid Nitrogen on Cellulose Powder

Fig 4-1 shows the solid-state ^{13}C CP/MAS NMR spectra of 8 wt% NaOH-soaked cellulose in the 2 mL microtube after quenching treatments with liquid nitrogen at different time intervals. As the treatment time increased, the C6 tg line decreased while the C6 gt line increased. The samples froze when cooled in liquid nitrogen for ~30 seconds, and the samples soaked for a longer duration completely transitioned to cellulose II after neutralization treatment. This suggests that the proportion of cellulose II increased with treatment time, and the crystal transition was completed in an extremely short time at an extremely low temperature.

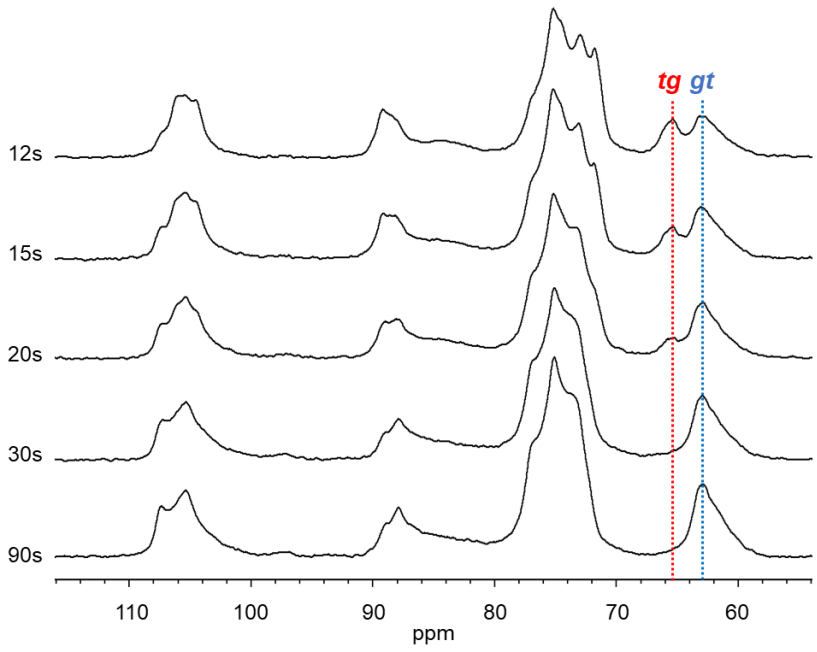

Fig. 4-1. Solid-state ^{13}C CP/MAS NMR spectra of 8 wt% NaOH-soaked cellulose in the 2 mL microtube after quenching treatments with liquid nitrogen at different time intervals. *Abbreviations*: *tg*, trans-gauche and *gt*, gauche-trans.

Fig 4-2 shows the solid-state ^{13}C CP/MAS NMR spectra of the 8 wt% NaOH-soaked cellulose powder obtained by quenching treatments in the centrifuge tubes. Similar to the treatments in the microtube, the C6 *tg* line decreased and the C6 *gt* line increased as treatment time increased. This indicates that the cellulose II proportion increased with prolonged treatment time, suggesting the coexistence of cellulose I and II. Therefore, if the cellulose resources can be precisely soaked in a NaOH solution, the crystal transition of cellulose I to II progresses through a quenching treatment. Fig 4-3 shows the proportion of cellulose I crystal, cellulose II crystal, and surface/amorphous regions, and Fig 4-4 shows the cellulose II proportion in crystal region determined by the C6 line fitting of the solid-state ^{13}C CP/MAS NMR spectra shown in Fig 4-2, respectively. Fig 4-3 shows that the proportion of cellulose II increased as that of cellulose I decreased, while the proportion of surface/amorphous region remained nearly constant, with some minor fluctuations. The proportion of cellulose II increased as that of the surface/amorphous region decreased during the first 30 s. Subsequently, the proportions of the cellulose II crystal and the surface/amorphous region increased as that of cellulose I decreased. This suggests that the transition from the surface/amorphous region to cellulose II occurs initially, followed by the transition from cellulose I to cellulose II. The reason why the surface/amorphous regions were initially converted to the cellulose II crystal is thought to be because NaOH penetrated the surface/amorphous regions more easily than cellulose I crystals. Fig 4-4 shows that the proportion of cellulose II in crystal regions reached 94% within 120 seconds under the

quenching treatment. As shown in Fig 2-3 in Chapter 2, crystal transition was completed in 30 minutes at –20°C, 20 minutes at –25°C, and 15 minutes at –30°C. This indicates that quenching treatments facilitate rapid crystal transition within a very brief timeframe. Furthermore, the cellulose II proportion increased proportionally over periods of 30 and 90 s, suggesting that the cellulose II proportion can be controlled by adjusting the quenching treatment times.

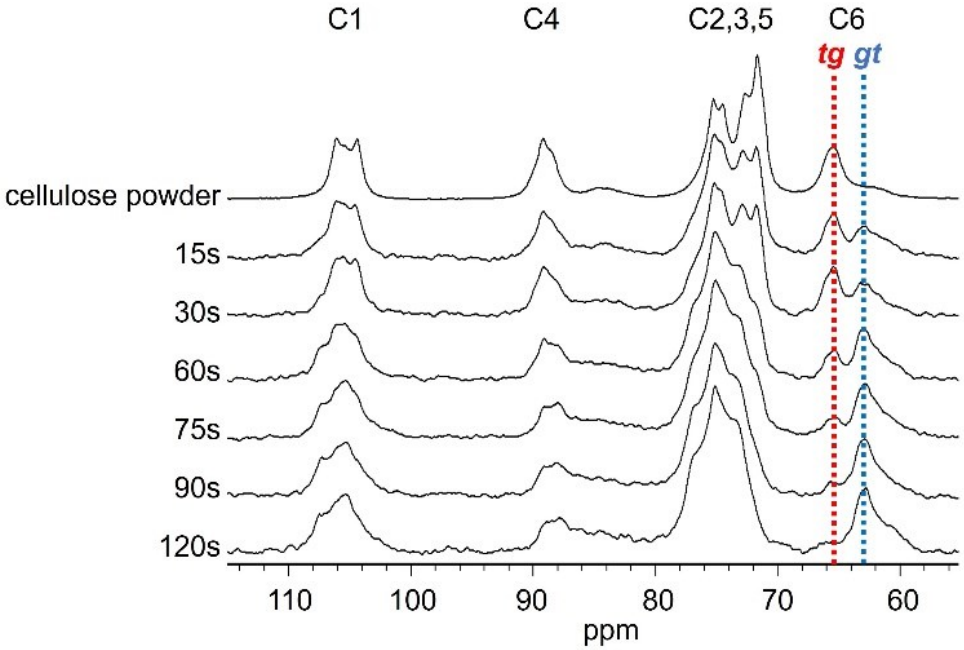

Fig. 4-2. Solid-state ^{13}C CP/MAS NMR spectra of the cellulose powder samples obtained by the quenching treatments. *Abbreviations*: *tg*, trans-gauche and *gt*, gauche-trans.

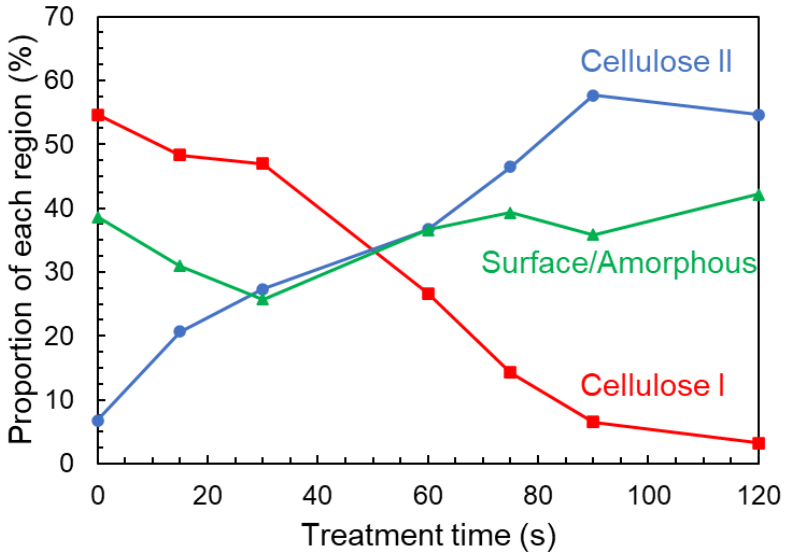

Fig. 4-3. Time-course changes for the proportion of cellulose I crystal (red line), cellulose II crystal (blue line), and surface/amorphous regions (green line) of cellulose powder samples obtained by the quenching treatments, determined by the line fitting of C6 resonance lines of solid-state ^{13}C CP/MAS NMR spectra shown in Fig. 4-2.

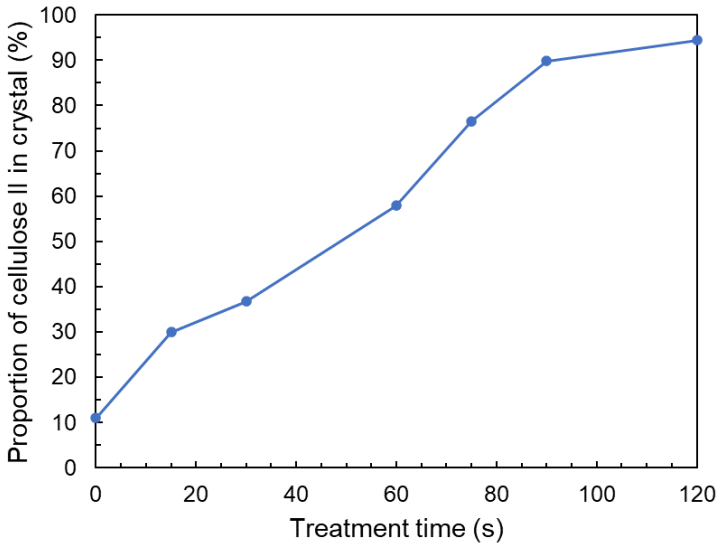

Fig. 4-4. Time-course changes for the cellulose II proportion of cellulose powder samples obtained by the quenching treatments, determined by the line fitting of C6 resonance lines of solid-state ^{13}C CP/MAS NMR spectra shown in Fig. 4-2.

During these quenching treatments in the centrifuge tubes, the cellulose powder froze from the outside to the inside of the sample, and the frozen portion gradually increased with increasing treatment time. The freezing behavior of these samples is thought to be related to the increasing trend in the cellulose II proportion. Therefore, it is necessary to consider the relationship between these behaviors. Celluloses I and II were present in the sample cooled for 30 seconds. The frozen and unfrozen portions were present when this sample was immediately transferred from liquid nitrogen temperature to room temperature (24 °C). The outer portions of the samples were frozen, and the central portions remained unfrozen. Individual portions were separated and subjected to neutralization, water washing, and drying. Fig 4-5 shows the solid-state ^{13}C CP/MAS NMR spectra of the dried samples. The frozen portion contained cellulose I and II, whereas the unfrozen portion contained only cellulose I, indicating that the crystal transition proceeded from outside the sample. This is thought to be because NaOH penetrated the cellulose crystals only in the outer part of the sample, where the temperature dropped sharply, and the mobility of NaOH decreased accordingly. As the mobility of Na ions decreases, interactions between cellulose and NaOH are more likely to occur, and the molecular chain of cellulose changes into a more stable structure. Hence, by adjusting the treatment time of this quenching treatment to create a temperature difference between the central and outer portions, it is expected that the distribution of cellulose I and II can be controlled such that the outer portion of the sample is cellulose II and the central portion is cellulose I. If this quenching treatment is applied to

cellulose I fibers, composite fibers with a cellulose II surface and a cellulose I core can be produced.

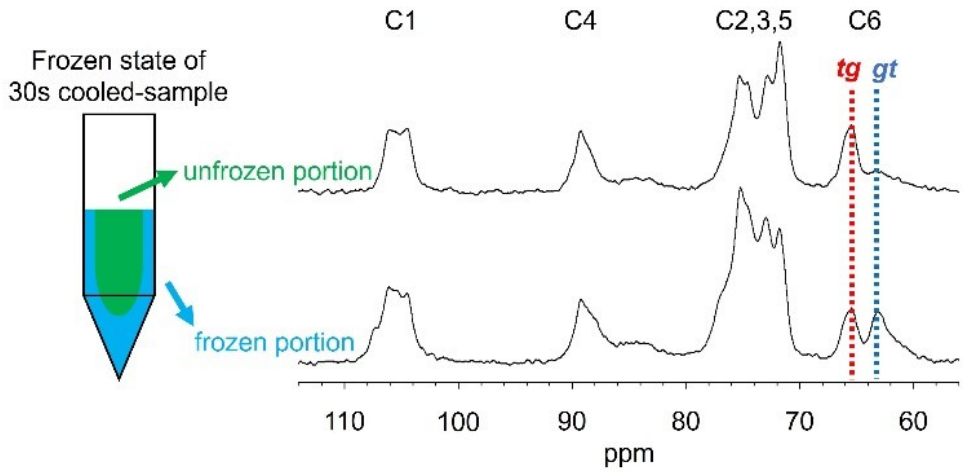

Fig. 4-5. Solid-state ^{13}C CP/MAS NMR spectra of the frozen and unfrozen portion of the samples obtained by quenching treatment at the centrifuge tube for 30 s. *Abbreviations*: *tg*, trans-gauche and *gt*, gauche-trans.

4.3.2. Quenching Treatments with Liquid Nitrogen on Cotton Fiber

Fig 4-6 shows the prepared cotton fiber, the sample obtained after cooling in liquid nitrogen for 90 s with an 8 wt% NaOH solution, and the sample obtained through a mercerization treatment with a 25 wt% NaOH solution at room temperature (24 °C) for 2 h. Although the mercerized sample shrank from 40 to 28 cm, the length of the quenched sample decreased from 40 to 38 cm. This indicates that the quenching treatment resulted in less sample deformation compared to the mercerization treatment.

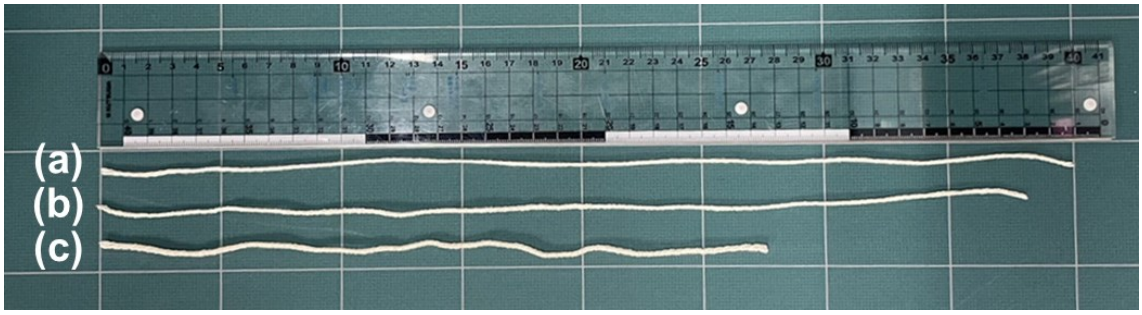

Fig. 4-6. The morphology of the samples of (a) the prepared cotton fiber, (b) the obtained sample after quenching treatment for 90 s, and (c) the sample after mercerization treatment with a 25 wt% NaOH solution at room temperature (24 °C).

Fig 4-7 shows the solid-state ^{13}C CP/MAS NMR spectra of the cotton fiber samples, including the prepared sample and the samples obtained through room-temperature treatment using an 8 wt% NaOH solution and mercerization treatment using a 25wt% NaOH solution. The sample soaked in an 8 wt% NaOH solution contained cellulose I, confirming that the crystal transition did not progress. The mercerized sample contained cellulose II, indicating that the crystal transition progressed completely.

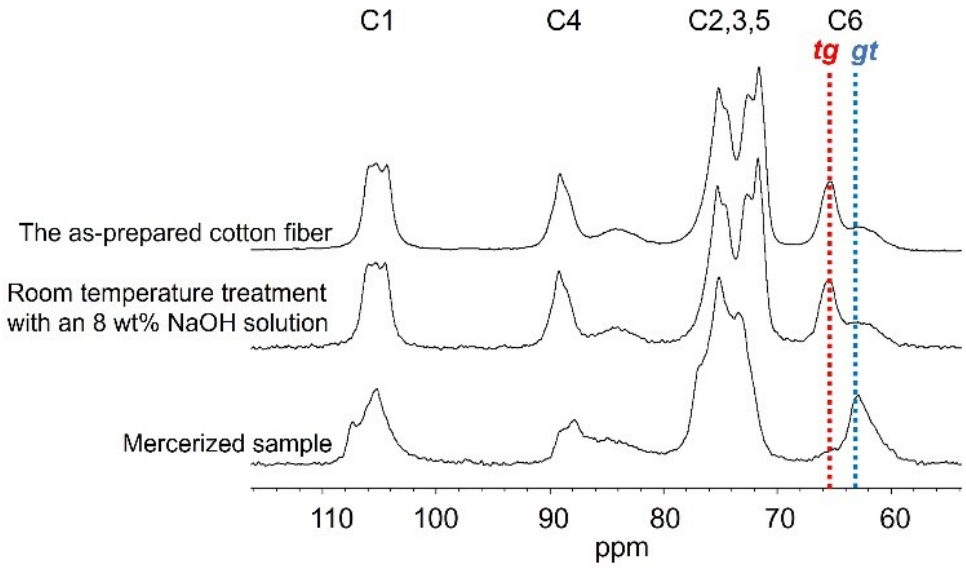

Fig. 4-7. Solid-state ^{13}C CP/MAS NMR spectra of the as-prepared cotton fiber and the samples obtained by the room-temperature treatments using 8 and 25 wt% NaOH solutions. *Abbreviations*: *tg*, trans-gauche and *gt*, gauche-trans.

Fig 4-8 shows the solid-state ^{13}C CP/MAS NMR spectra of the cotton fiber samples obtained by the quenching treatments. Like the quenching treatments on the cellulose powder, the C6 *tg* line decreased, and the C6 *gt* line increased as the treatment time increased. This indicates that quenching treatments can produce composite fibers of cellulose I and II. Fig 4-9 shows the proportion of each region, and Fig 4-10 shows the proportion of cellulose II in crystal region in cotton fiber samples obtained by the quenching treatments determined by C6 line fitting of the solid-state ^{13}C CP/MAS NMR spectra, respectively. Fig 4-9 shows that the proportion of cellulose II increased as that of cellulose I decreased, while the proportion of surface/amorphous region remained nearly constant, with some minor fluctuations. The proportion of cellulose II increased as that of surface/amorphous region decreased during the first 10 s. Subsequently, the proportions of cellulose II and

surface/amorphous region increased as that of cellulose I decreased. This behavior is similar to the crystal transition observed in Fig 4-3. This suggests that the transition from the surface/amorphous region to cellulose II occurs initially, followed by the transition from cellulose I to cellulose II. The reason why the surface/amorphous regions were initially converted to the cellulose II crystal is thought to be because NaOH penetrated the surface/amorphous regions more easily than cellulose I crystals. Fig 4-10 shows that the cellulose II proportion increased proportionally with the treatment time from 10 to 30 seconds, similar to the cellulose powder treatments shown in Fig 4-4. This suggests that the cellulose II proportion can be controlled by adjusting the quenching treatment time.

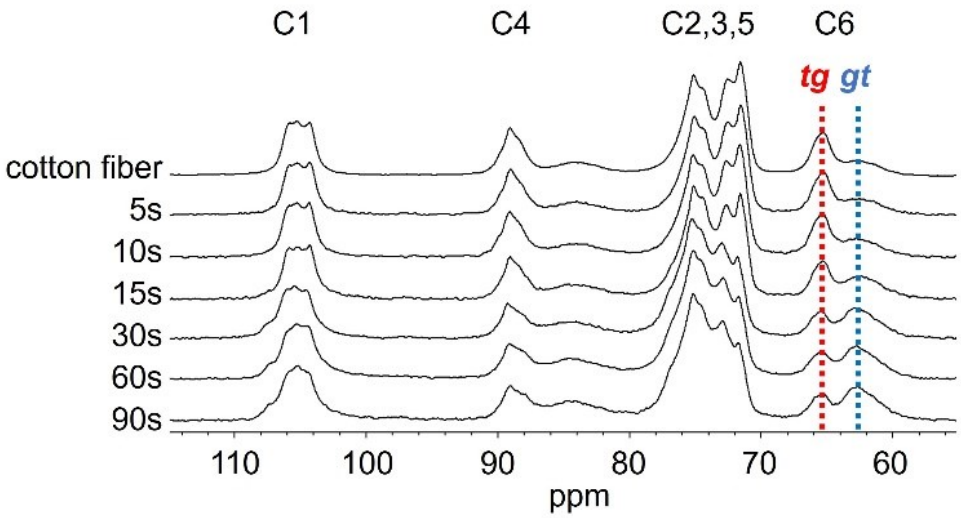

Fig. 4-8. Solid-state ^{13}C CP/MAS NMR spectra of the cotton fiber samples obtained by the quenching treatments. *Abbreviations*: *tg*, trans-gauche and *gt*, gauche-trans.

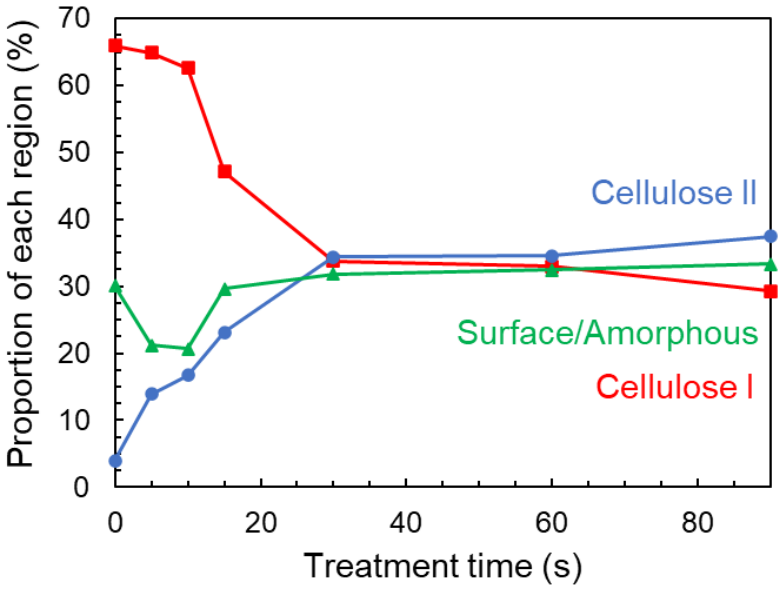

Fig. 4-9. Time-course changes for the proportion of cellulose I crystal (red line), cellulose II crystal (blue line), and surface/amorphous regions (green line) of cellulose powder samples obtained by the quenching treatments, determined by the C6 line fitting of solid-state ^{13}C CP/MAS NMR spectra shown in Fig 4-8.

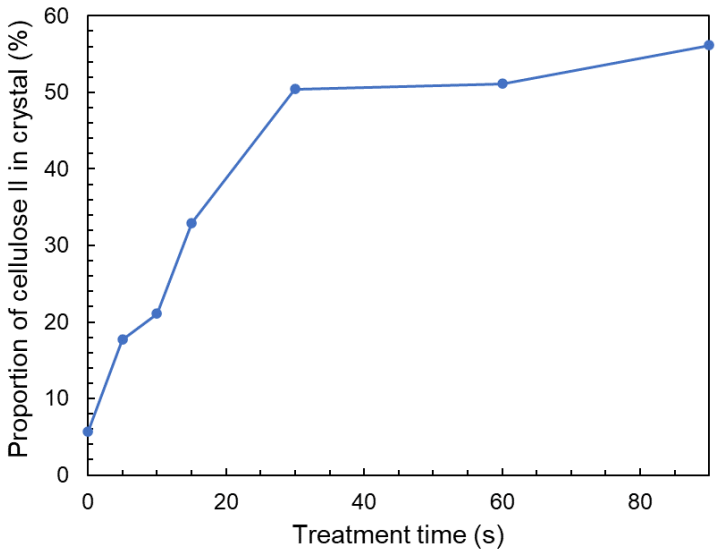

Fig. 4-10. Time-course change for the cellulose II proportion in the crystal region of cotton fiber samples obtained by the quenching treatments, determined by the C6 line fitting of solid-state ^{13}C CP/MAS NMR spectra shown in Fig 4-8.

4.3.3. Crystal Distribution of Cellulose I and II on Composite Fiber

In this section, the crystal distribution of the cotton fiber samples obtained by quenching treatments is discussed. In these samples, which contain both cellulose I and II, it is expected that cellulose II is present in the surface region and cellulose I in the core region, similar to the model shown in Fig 4-11. In this method, which is similar to the surface dissolution approach, the reinforcement and outer matrix are composed of the same material. Furthermore, by using the solvent necessary to soak the cellulose materials and inducing crystal transition from the surface while maintaining a solid state, this method makes it possible to produce all-cellulose composite materials. This composite fiber is expected to exhibit the characteristics of cellulose I, such as high mechanical strength, and the characteristics of cellulose II, including luster and dyeability. This model is expected to exhibit superior mechanical strength compared with cellulose II materials because the cellulose I core acts as a reinforcement. Therefore, the mechanical properties of the composite samples were evaluated by tensile testing.

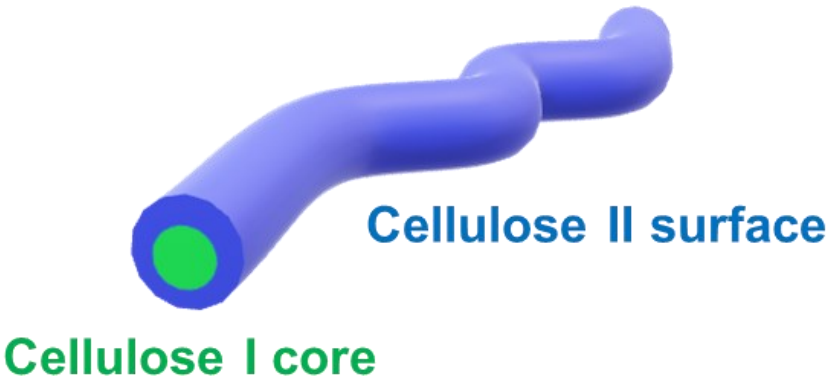

Fig. 4-11. The schematic image of the estimated distribution of cellulose I and II in the composite fiber obtained by the quenching treatment.

4.3.4. Tensile Tests

Fig 4-12 shows the stress-strain curve (S-S curve) of the prepared cotton fiber and the samples obtained by quenching treatments for 15 and 30 s and mercerization treatment using a 25 wt% NaOH solution at room temperature (24 °C) for 2 h. The S-S curves of the composite samples were intermediate between those of the cotton fiber and mercerized fiber sample. This indicates that these composite fibers had the mechanical properties of both cellulose I and II. Table. 4-1 summarizes the maximum stress, breaking strain, elastic moduli, and toughness of the samples. The maximum stress and elastic moduli at higher stress revel (E_H) of the samples obtained by quenching treatment were greater than those of the mercerized fiber sample. This indicates that the cellulose I core serves as a reinforcement, resolving the low mechanical strength of cellulose II. Therefore, this composite material may have the potential for use as alternative materials to plastics. The breaking strain and toughness of the composite fiber samples were higher than those of the cotton fibers and lower than

those of the mercerized fibers. Furthermore, elastic moduli at the initial region (Ei) were nearly the same for the fiber sample obtained by quenching treatment for 15 s and the mercerized fiber sample, however, it was smaller for the sample obtained by the quenching treatment for 30s. The breaking strain of the sample obtained by quenching treatment for 30 s was larger compared to that of the sample obtained by quenching treatment for 15 s. These results suggest that it is inferred that while the quenching treatment allows for easy deformation even at low stress, it can produce materials with minimal stress deformation under higher stress. The shape of the S-S curve, which is known as the J-shaped S-S curve, for this composite is similar to that observed in the skin [10], [11], and this mechanical property is also similar to the skin [11], [12]. Therefore, this composite material has potential applications in medical materials. The ease of initial deformation is believed to be adjusted by quenching time due to, in part, the changes in the proportion of cellulose II. There is potential to prepare composite materials with more diverse mechanical properties by selecting cellulose resources because their characteristics, such as their orientation, affect the mechanical properties of the all-cellulose composite [13], [14]. This result indicates that by adjusting the treatment time, not only can the proportion of cellulose I and II be controlled, but the mechanical properties can also be altered.

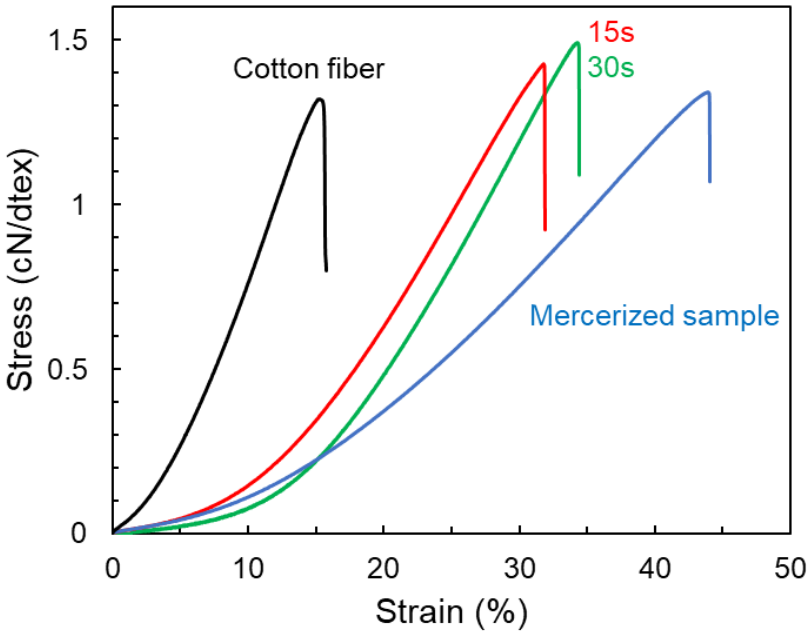

Fig. 4-12. Stress-strain curve of the cotton fiber samples. *Color code:* black line, cotton fiber; red line, the quenching treatment for 15s; green line, the quenching treatment for 30 s; blue line, mercerization treatment for 2 h with a 25 wt% NaOH solution at room temperature (24 °C).

Table. 4-1. Maximum stress, breaking strain, elastic moduli, and toughness of cotton fiber, the cotton fiber samples obtained by the quenching treatments cooled for 15 s and 30 s and by the mercerization treatment for 2 h with a 25 wt% NaOH solution at room temperature (24 °C).

sample	Maximum stress (cN/dtex)	Breaking strain (%)	Elastic moduli (E_I) (cN/dtex)	Elastic moduli (E_H) (cN/dtex)	Toughness (cN/dtex) × 100^{-2}
Cotton fiber	1.32 ± 0.06	15.3 ± 1.1	3.01 ± 0.34	11.28 ± 0.03	8.8 ± 1.2
Quenched sample for 15 s	1.43 ± 0.17	31.8 ± 2.9	0.68 ± 0.18	6.90 ± 0.12	16.4 ± 2.8
Quenched sample for 30 s	1.49 ± 0.15	34.3 ± 1.4	0.39 ± 0.05	7.27 ± 0.26	16.8 ± 1.8
Mercerized sample	1.34 ± 0.05	43.9 ± 1.5	0.70 ± 0.24	4.26 ± 0.21	23.1 ± 2.2

4.4. Conclusions

In this chapter, I developed a novel method to fabricate composite materials with cellulose I as the core and cellulose II as the surface, and succeeded in controlling the mechanical properties by adjusting the proportion of cellulose II. Quenching treatment with liquid nitrogen accelerates the crystal transition from cellulose I to II in a shorter time than the treatment at –20°C to –30°C described in Chapter 2. The crystal transition progressed from the periphery to the center, and the percentage of cellulose II increased with increasing treatment time. The crystal transition also progresses in cotton fiber as in cellulose powder, which is considered to have a cellulose I core and a cellulose II surface. The maximum stress and elastic moduli at higher stress of the composite fiber material are greater than that of the mercerized cellulose II fiber, which may be attributed to the strengthening of the cellulose I core. This composite fiber material may have the potential for use as alternative materials to plastics. Furthermore, the mechanical properties of the composite fiber materials were altered by varying the treatment time. In particular, the initial elastic moduli are similar to the properties of the skin. Therefore, this composite material may have potential applications in medical materials. In summary in this chapter, it was possible to control the crystal transition of cellulose by adjusting the treatment conditions in the quenching process, thereby producing a composite material of cellulose I and II with the superior mechanical properties.

REFERENCES

[1] P. Piltonen, N. C. Hildebrandt, B. Westerlind, J. P. Valkama, T. Tervahartiala, and M. Illikainen, "Green and efficient method for preparing all-cellulose composites with NaOH/urea solvent," *Compos Sci Technol*, vol. 135, pp. 153–158, 2016, doi: 10.1016/j.compscitech.2016.09.022.

[2] N. C. Hildebrandt, P. Piltonen, J. P. Valkama, and M. Illikainen, "Self-reinforcing composites from commercial chemical pulps via partial dissolution with NaOH/urea," *Ind Crops Prod*, vol. 109, no. March, pp. 79–84, 2017, doi: 10.1016/j.indcrop.2017.08.014.

[3] O. Korhonen, D. Sawada, and T. Budtova, "All-cellulose composites via short-fiber dispersion approach using NaOH–water solvent," *Cellulose*, vol. 26, no. 8, pp. 4881–4893, 2019, doi: 10.1007/s10570-019-02422-z.

[4] M. Egal, T. Budtova, and P. Navard, "Structure of aqueous solutions of microcrystalline cellulose/sodium hydroxide below 0 °C and the limit of cellulose dissolution," *Biomacromolecules*, vol. 8, no. 7, pp. 2282–2287, 2007, doi: 10.1021/bm0702399.

[5] Y. Wang and Y. Deng, "The kinetics of cellulose dissolution in sodium hydroxide solution at low temperatures," *Biotechnol Bioeng*, vol. 102, no. 5, pp. 1398–1405, 2009, doi: 10.1002/bit.22160.

[6] W. Gindl and J. Keckes, "All-cellulose nanocomposite," *Polymer (Guildf)*, vol. 46, no. 23, pp. 10221–10225, 2005, doi: 10.1016/j.polymer.2005.08.040.

[7] N. Soykeabkaew, N. Arimoto, T. Nishino, and T. Peijs, "All-cellulose composites by surface selective dissolution of aligned ligno-cellulosic fibres," *Compos Sci Technol*, vol. 68, no. 10–11, pp. 2201–2207, 2008, doi: 10.1016/j.compscitech.2008.03.023.

[8] D. Massiot *et al.*, "Modelling one- and two-dimensional solid-state NMR spectra," *Magnetic Resonance in Chemistry*, vol. 40, no. 1, pp. 70–76, 2002, doi: 10.1002/mrc.984.

[9] F. Horii, A. Hirai, and R. Kitamaru, "Solid-state 13C-NMR study of conformations of oligosaccharides and cellulose: Conformation of CH2OH group about the exo-cyclic C-C bond," *Polymer Bulletin*, vol. 10, no. 7–8, pp. 357–361, 1983, doi: 10.1007/BF00281948.

[10] M. A. Meyers, J. McKittrick, and P.-Y. Chen, "Structural biological materials: Critical mechanics-materials connections," *Sciences*, vol. 339, no. 6121, pp. 773–779, 2013.

[11] A. Ní Annaidh, K. Bruyère, M. Destrade, M. D. Gilchrist, and M. Otténio, "Characterization of the anisotropic mechanical properties of excised human skin," J Mech Behav Biomed Mater, vol. 5, no. 1, pp. 139–148, 2012, doi: 10.1016/j.jmbbm.2011.08.016.

[12] W. Yang et al., "On the tear resistance of skin," Nat Commun, vol. 6, pp. 1–10, 2015, doi: 10.1038/ncomms7649.

[13] W. Gindl and J. Keckes, “Drawing of self-reinforced cellulose films,” *J Appl Polym Sci*, vol. 103, no. 4, pp. 2703–2708, Feb. 2007, doi: 10.1002/app.25434.

[14] S. Fujisawa, E. Togawa, and N. Hayashi, “Orientation control of cellulose nanofibrils in all-cellulose composites and mechanical properties of the films,” *Journal of Wood Science*, vol. 62, no. 2, pp. 174–180, 2016, doi: 10.1007/s10086-015-1533-4.

Chapter 5.

Concluding Remarks

The objective of this study is to create new cellulose-based materials that combine the properties of cellulose II with controllable and excellent mechanical properties. I focused on alkali treatments using low-concentration NaOH solutions. The mechanisms involved in the crystal transition from cellulose I to II at low temperatures, and the improvement of crystallinity in cellulose II during multicycle alkali post-treatment were elucidated. Based on the findings, I developed a new method to produce cellulose-based materials by controlling the ratio and distribution of cellulose I and II. Here, the conclusions derived from each chapter are summarized.

Chapter 2

In Chapter 2, the structural changes of cellulose molecules and the dynamics of Na ions during the low-concentration NaOH treatments at low temperatures were evaluated mainly by NMR and WAXS measurements. The completion of crystal transition in a shorter time at lower processing temperatures indicated that temperature conditions are one of the crucial factors in this crystal transition. It was suggested that the C6 conformation changes, a reduction of crystallinity, disruption of intrachain hydrogen bonds, and penetration of NaOH into the cellulose crystal region occur in the temperature decrease process through in situ solid-state ^{13}C CP/MAS NMR and in situ WAXS measurements. Structural optimization calculations of cello-oligomers lacking hydrogen bonds between glucose residues suggested that during crystal transition, cellulose molecular shift from a

planar structure to more a stable one when the intrachain hydrogen bonds are disrupted. Furthermore, at alkali concentrations where crystal transition progresses, a decrease in the mobility of Na ions compared to concentrations where no crystal transition occurs was demonstrated by ^{23}Na NMR relaxation time measurements. This implies the occurrence of interactions between NaOH and cellulose. The reduction of their mobility is believed to be due to their penetration into cellulose crystals. The mobility of Na ions at concentrations where crystal transition does not occur was found to be nearly the same as that of Na ions in NaOH aqueous solutions without cellulose. In this case, the interactions between NaOH and cellulose did not occur, suggesting that these interactions are essential for crystal transition. Furthermore, a decrease in the mobility of Na ions was also observed in the mercerization treatment using a high concentration of NaOH solution.

In the crystal transition occurred by the NaOH treatments, the mobility of Na ions is considered a crucial factor, and it is believed to be controlled by temperature and alkali conditions. This indicates that the progression of crystal transition could be controlled by adjusting the condition of low-concentration NaOH treatments, such as temperatures and treatment times. Therefore, it has been found that it is possible to control of mechanical properties of cellulose materials by controlling the proportion and distribution of cellulose crystals using a low-temperature NaOH treatment.

Chapter 3

In Chapter 3, further crystallinity improvement of cellulose II in low-concentration NaOH post-treatment and clarification of this mechanism were addressed. In addition, the preparation of highly crystalline cellulose II fibers and the control of their mechanical properties using this post-treatment. The further crystallinity improvement of cellulose II is achieved by the multicycle post-treatment using a 10 wt% NaOH solution. The proportion of the inaccessible surface decreases as the crystallinity is improved and the crystal size is improved at each cycle. These results support the mechanism of the crystallinity improvement during the multicycle post-treatment; in the second and subsequent post-treatment cycle, NaOH does not permeate crystal regions, but only the inaccessible surface regions enlarged by the previous cycle of the post-treatments, and these inaccessible surface regions convert into the crystal regions by the rearrangement of cellulose molecules. This leads to the conversion of amorphous regions, originally distant from the initial crystalline regions, into crystalline regions. This multicycle post-treatment is also effective in the crystallinity improvement of cellulose II fibers, however, the control of their mechanical properties is difficult because they depend on the characteristics of cellulose resources. Applying this post-treatment during the preparation process of cellulose II fiber is expected to enable the production of cellulose II fibers with high strength and controllable mechanical properties.

Chapter 4

In Chapter 4, the fabrication of a novel cellulose-base composite of cellulose I and cellulose II, and the control of their mechanical properties were addressed by controlling the crystal transition in the solid state. The quenching treatments with liquid nitrogen have the potential for a novel fabrication method of an all-cellulose composite with a cellulose I core and a cellulose II surface in a single step. In this treatment, the crystal transition from cellulose I to cellulose II proceeds from an outer to a central portion of cellulose material, and the proportion of cellulose II increases as treatment times are longer. Therefore, the quenching on cellulose I fiber can prepare the composite material with a cellulose I core and a cellulose II surface. The maximum stress and elastic moduli of composite fibers are higher than those of mercerized cellulose II fiber. In addition, the mechanical properties of composite fibers are controlled by adjusting treatment times, thereby controlling the proportion of cellulose II.

As summarized above, I gave insights into the crystal cellulose and the fabrication of novel cellulose materials. NaOH that does not penetrate the crystal regions affects only the amorphous regions around the crystal regions. On the other hand, the NaOH that penetrates the crystal regions generates interactions with cellulose molecules, promoting conformational changes in the cellulose molecules of the crustal regions. The clarification of the dynamics of NaOH when they penetrate the

crystal regions is expected to contribute to the elucidation of the entire mechanism of crystal transition. Furthermore, it has been revealed that by controlling the proportion of cellulose II through the quenching with liquid nitrogen, the mechanical properties of composite materials can be easily controlled. To increase the utilization of environmentally friendly cellulose, it is crucial to efficiently produce cellulose materials with various properties. The methods developed in this study serve as a contribution towards achieving this goal.

I believe that the insights gained from this thesis not only form the basis for the research on cellulose crystal structures but also hold the potential for practical applications in the development of novel cellulose materials.

Acknowledgments

I would like to express my sincere appreciation to Associate Professor Kenji Tajima, Faculty of Engineering, Hokkaido University, for his unwavering support and guidance in the entire work of this study. I would like to express my heartfelt thanks to Dr. Tomoki Erata, Faculty of Engineering, Hokkaido University, for his continuous support and guidance in the entire work of this study. I would like to acknowledge Dr. Mutsumi Takagi, Associate Professor Hirofumi Tani, Faculty of Engineering, Hokkaido University, and Associate Professor Masashi Fujiwara, Institute for Chemical Reaction Design and Discovery (ICReDD), Hokkaido University, for their valuable advice and encouragement.

I am deeply thankful to Dr. Toshifumi Hiraoki and Mr. Naoki Nakagawa, Instrumental Analysis Support Office, The Frontier Chemistry Center, Faculty of Engineering, Hokkaido University, for their cooperation and variable advice in NMR measurements. I would like to express my great appreciation to Professor Chihiro Yamane, Kobe Women's University, for the variable discussion and advice. I would like to thank Associate Professor Takuya Isono, Faculty of Engineering, Hokkaido University, for his cooperation with WAXS measurements and his variable advice. I would like to thank Associate Professor Shin-ichiro Sato, Faculty of Engineering, Hokkaido University, for his cooperation in computational calculations. I would like to thank Mr. Shuichiro Seno, Industrial Research Institute, Industrial Technology and Environment Research Department, Hokkaido Research Organization, for his cooperation in the tensile test of fiber samples. I would like to express special

thanks to Dr. Nomura Satoshi for his variable advice and guidance on the methods of experiments and data analysis.

I would like to thank the High-1energy Accelerator Research Organization for their help with the WAXS measurements at the Photon Factory, KEK, Tsukuba, Japan. I would like to thank The High Brilliance X-ray Laboratory, Hokkaido University, for allowing the utilization of their X-ray diffractometer. I would like to thank the Information Initiative Center, Hokkaido University, for using a supercomputer system for DFT calculation. I would like to thank High-voltage Electron Microscope Laboratory, Faculty of Engineering, Hokkaido University, for performing the observation of the fiber samples using a Scanning Electron microscopy.

I would like to thank Mr. Minami Ebe, Mr. Chaehun Lee, and Mr. Taiki Nishimura for their support in WAXS measurements. I would also like to thank to members of this laboratory for their assistance.